A CFD Investigation of Balcony Spill Plumes

by

Cameron John McCartney

A thesis
presented to the University of Waterloo
in fulfillment of the
thesis requirement for the degree of
Master of Applied Science
in
Mechanical Engineering

Waterloo, Ontario, Canada, 2006

I hereby declare that I am the sole author of this thesis. This is a true copy of the thesis, including any required final revisions, as accepted by my examiners.

I understand that my thesis may be made electronically available to the public.

Signature

Abstract

A series of numerical modeling studies were conducted to characterize the mass flow rates in balcony spill plumes (BSP), a type of buoyant fire plume occurring in atria. The variation of BSP mass flow rate as a function of elevation, fire size and fire compartment geometry was examined both numerically and experimentally. A new method for estimation of BSP mass flow rates, appropriate for design of smoke management systems in high-elevation atria, was developed based on simulations of BSP mass flow rate.

An experimental program conducted in a 12 m high atrium measured BSP mass flow rates as well as temperatures in the fire compartment and atrium. This data was used to evaluate CFD models of the fire compartment and atrium in the experimental facility. These were implemented using the Fire Dynamics Simulator (FDS) software. The models were extended to investigate BSP behaviour at elevations up to 50 m. The removal of atrium walls in the model to allow free development of the BSP is a unique approach among published numerical modeling studies of BSP behaviour.

The high-elevation CFD model was used to perform a parametric study of BSP mass flow rate as a function of elevation, fire size and fire compartment geometry. Predictions of BSP mass flow rate from this study extend to 50 m above the atrium floor, extending the range of elevations represented in the published experimental data ($\leq$ 9 m). Data from the parametric study was used to develop a new method for estimation of BSP mass flow rates at high elevations. BSP mass flow rates estimated using the new method are shown to be bounded by values estimated using existing methods based on low-elevation experimental data.

Acknowledgements

The author wishes to acknowledge his advisors, Dr. Elizabeth Weckman and Dr. Gary Lougheed, for their guidance and support, the Natural Sciences and Engineering Research Council of Canada for financial support and the staff at the National Research Council Canada for their efforts in the design, construction and implementation of the full-scale experimental program.

Table of Contents

List of Figures

List of Tables

Nomenclature

A_{burner}	area of experimental facility burner (m^2)
C	proportionality constant in plume mass flow expressions (kg/s-m)
C_m	proportionality constant in BSP mass flow expressions ($kg/s\text{-}kW^n\text{-}m^{m+1}$)
$C_{m,ave}$	average value of proportionality constant C_m ($kg/s\text{-}kW^n\text{-}m^{m+1}$)
C_{McC}	proportionality constant in new BSP mass flow rate expression ($kg/s\text{-}kW^n\text{-}m^{m+1}$)
C_s	Smagorinsky coefficient
c	heat capacity (kJ/kg-K)
d_{balc}	depth of approach flow under balcony (m)
h_{atr}	height of the atrium (m)
h_{comp}	height of the fire compartment (m)
h_{draft}	draft curtain depth (m)
h_{fasc}	fire compartment opening fascia depth (m)
k	thermal conductivity (W/m-K)
m, n	exponents in expression for BSP mass flow rate
m_0	mass flow rate in balcony spill plume at edge of balcony (kg/s)
m_{axi}	mass flow rate in axisymmetric plume (kg/s)
m_{balc}	mass flow rate of approach flow under balcony (kg/s)
m_{BSP}	mass flow rate of balcony spill plume (kg/s)
m_{exh}	mass flow rate of atrium exhaust system (kg/s)
m_{mol}	molecular weight of fuel (g/mol)
m_o	mass flow rate of approach flow at the compartment opening (kg/s)
Q	heat release rate of fire (kW)
Q_c	convective heat release rate of fire (kW)
Q_{rad}	radiative heat release rate of fire (kW)

T	temperature (ºC, K)
T_{av}	average temperature (ºC, K)
T_{ign}	ignition temperature (K)
$T_{s,ave}$	average temperature of atrium smoke layer (K)
T_{surf}	surface temperature (K)
V_{exh}	volumetric flow rate of atrium exhaust system (m^3/s)
V_{sim}	simulated volumetric flow rate of atrium exhaust system (m^3/s)
W	fire compartment opening width (m)
z	elevation above atrium floor (m)
z_0	virtual origin elevation (m)
z_{balc}	elevation of the balcony above the floor (m)
z_l	atrium smoke layer elevation (m)
Δ	thermal thickness, isometric control volume size (m)
Δ_{opt}	optimized isometric control volume size (m)
$\Delta x, \Delta y, \Delta z$	control volume dimensions (m)
χ	radiative fraction
ρ	density (kg/m^3)
ρ_∞	ambient air density (kg/m^3)
σ_{Cm}	standard deviation of proportionality constant C_m ($kg/s\text{-}kW^n\text{-}m^{m+1}$)

Chapter 1 Introduction

The design of effective atrium smoke management systems requires methods by which to accurately estimate the amount of smoke produced by a given fire in the atrium. The advent of performance-based building and fire codes requires designers of such systems to give increased consideration to the behaviour and development of balcony spill plumes (BSPs), a type of buoyant line plume particular to atria. Although methods exist to estimate the mass flow rate in unobstructed axisymmetric fire plumes and in BSPs at elevations up to 9 m above the atrium floor, the accuracy of these methods for estimation of BSP mass flow rate at higher elevations in tall atria is unknown due to a lack of relevant experimental data against which to verify any calculated values. Given the continuing trend towards the construction of higher elevation atria in shopping malls, office buildings and high-rise hotels, a new method to accurately estimate BSP mass flow rates at high elevations is needed to ensure the effectiveness of smoke management systems designed for such applications.

Atria are large enclosed volumes within a building which span more than one storey and typically connect to a number of adjacent compartments [37]. Traditionally, for smoke management system design, atrium fires have been assumed to occur in the center of the atrium at floor level, as illustrated schematically in Figure 1. In this scenario, the hot combustion products produced by the fire rise through the atrium as an unobstructed, axisymmetric plume. Cooler ambient air entrained into the plume via turbulent mixing increases the plume mass flow rate as it rises. If the fire remains uncontrolled, the atrium will gradually fill with smoke, posing a life safety hazard to occupants of the atrium and any interconnected spaces. Atrium smoke management systems in North America typically take the form of mechanical exhaust systems located near the atrium ceiling. They are designed with the objective of preventing the atrium smoke layer from expanding below a certain elevation in order to maintain smoke-free egress routes for building occupants in the event of a fire. The critical design parameter for the atrium exhaust system is the estimated mass flow rate in the buoyant fire plume at the desired atrium smoke layer elevation. Well-established methods are available to estimate the mass flow rate of an axisymmetric plume as a function of fire size and elevation [37], allowing designers of atrium smoke management systems to effectively control smoke produced by a fire on the atrium floor.

In addition to axisymmetric plumes, a second important type of buoyant smoke plume that can be produced during an atrium fire is the balcony spill plume, or BSP (Figure 2). In this case, a fire in a compartment adjacent to the atrium produces a hot buoyant layer of smoke along the ceiling of the compartment. This layer exits the compartment through an opening, flowing underneath a balcony and spilling out into the atrium as a BSP. BSPs are generally assumed, for modeling purposes, to be a type of

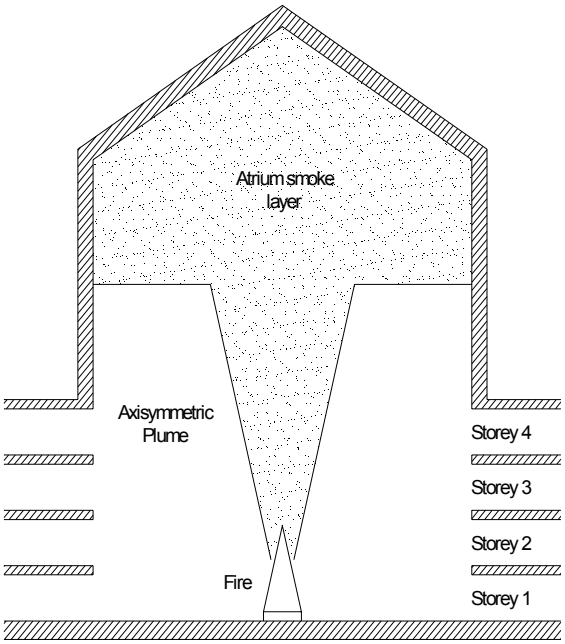

Figure 1. Schematic of an example axisymmetric plume and atrium smoke layer produced by a fire on an atrium floor.

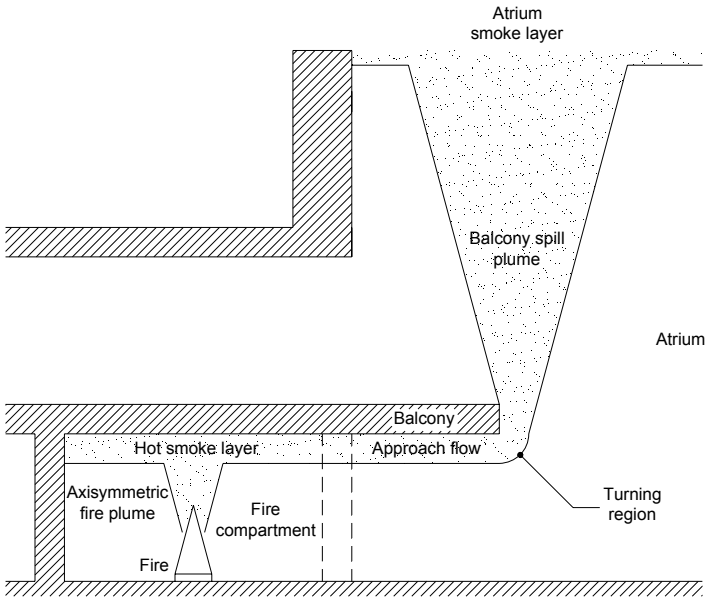

Figure 2. Balcony spill plume from a fire in a compartment adjacent to an atrium.

buoyant line plume. Therefore, they exhibit substantially different behaviour than axisymmetric plumes, particularly with respect to variation in plume mass flow rate with elevation. In the last ten years, BSP have drawn increased attention by designers of atrium smoke management systems since they are seen to pose an as great, or greater, hazard to the life safety of atrium occupants as axisymmetric fire plumes. Comparison of the mass flow rates of BSPs and axisymmetric plumes using existing estimation methods [15, 49] shows that, in many cases, the quantity of smoke produced by a BSP is greater than that produced by an axisymmetric plume for the same fire size and elevation. Further, BSPs produced by small fires may contain as much smoke as axisymmetric plumes produced by much larger fires. Given the importance of BSPs in determining the optimal design and effectiveness of atrium smoke management systems, a number of experimental programs have been conducted to characterize BSP behaviour and to provide data for the development of methods to estimate BSP mass flow rates for different fire scenarios. None of the published experimental data, however, provides BSP mass flow rate data at elevations greater than 9 m above the atrium floor. Since modern atria extend to elevations over 30 m, additional data and validated methods for estimating BSP mass flow rates at these higher elevations are necessary.

1.1 Literature Review

This section summarizes the current state of research into BSP behaviour with a focus on the existing methods for estimation of their mass flow rate for use in designing atrium smoke management systems. Over the past thirty years, five main methods to estimate BSP mass flow rates at low elevations have been developed: BRE [40], Law [22, 24], Thomas [51], Poreh et al. [45] and Thomas et al. [54]. All are based on buoyant line plume models and were developed using data from a series of experimental programs conducted at one-tenth scale [42, 43, 18, 33, 32, 19]. Over the last ten years, limited attempts to model BSP behaviour using computational fluid dynamics (CFD) have not successfully extrapolated the experimental data, nor extended the analytical methods, to estimate BSP mass flow rates at higher elevations [36, 4, 3, 26, 19].

1.1.1 BSPs and Buoyant Line Plumes

All existing methods used to estimate BSP mass flow rates assume that, since the BSP flow at the balcony edge resembles the flow above a rectangular buoyancy source, the BSP can be accurately modeled as a buoyant line plume above the balcony elevation [42, 51, 17]. Most are based on modifications of the original work by Lee and Emmons [25] who developed a theoretical model to characterize the velocity and temperature distributions in buoyant line plumes based on a series of experiments in which they investigated the development of plumes above 0.014 m by 1.98 m rectangular fires. In an accompanying mathematical analysis, the plumes produced by these rectangular fires were shown to be equivalent to

those produced by theoretical line buoyancy sources located at an elevation below that of the actual fire, defined as the 'virtual origin elevation'. The results inferred that the mass flow rate of buoyant line plumes increases linearly with elevation above the source. Based on small-scale experimental data, Yokoi [58] extended a similar analysis of buoyant line plumes to the characterization of window plumes. These window plumes resembled BSPs except for that they lacked a balcony above the compartment opening. Comparison with data from full-scale building fires showed that these window plumes could be modelled as buoyant line plumes emitted from a theoretical line source located within the fire compartment, near the compartment ceiling [58]. Neither Lee and Emmons' line plume model nor Yokoi's window plume model could be directly applied for characterization of BSP behaviour since they did not account for the impact of the balcony on the developing plume.

The current model of BSP behaviour was first proposed by Morgan and Marshall in 1975 [42]. They divided the BSP into three conceptual flow regions: an approach flow, a turning region and a buoyant line plume region (Figure 3). The approach flow is located underneath the balcony, and extends from the compartment opening to a vertical plane aligned with the edge of the balcony. The turning region then

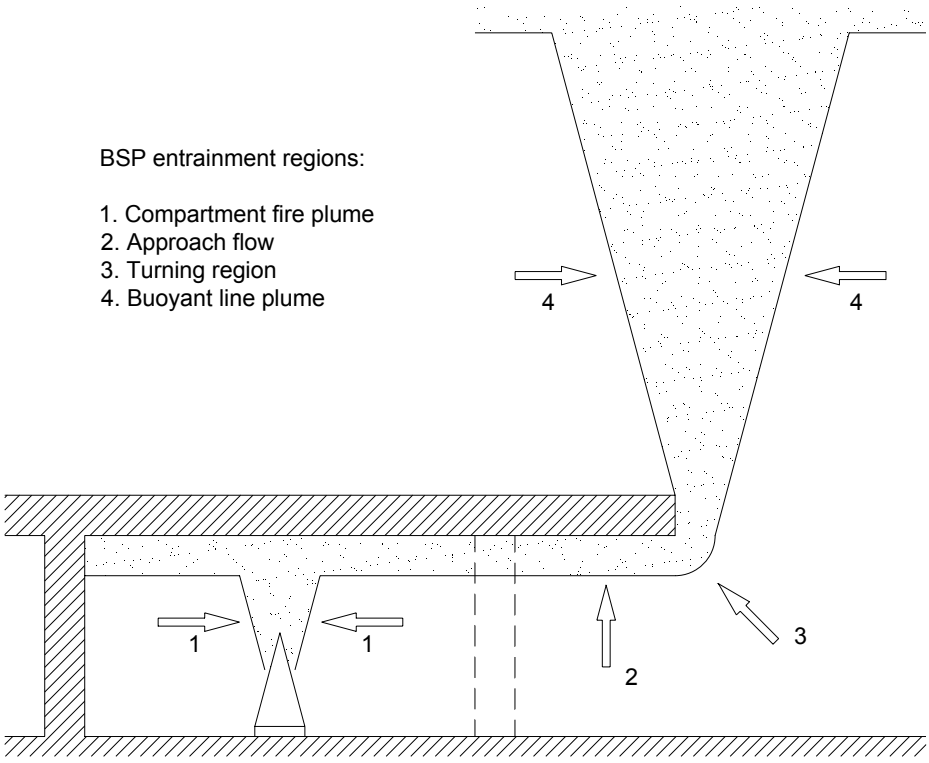

Figure 3. Schematic of balcony spill plume entrainment regions.

spans from this vertical plane, where the plume begins to rise vertically, to a horizontal plane some distance above the elevation of the balcony. Finally, the line plume region extends from the top of the turning region to the atrium smoke layer elevation. These three regions relate directly to formation of the hot gas plume from the fire. First, the fire in the compartment produces an axisymmetric plume which entrains air as it rises due to buoyancy and forms a layer of hot gases (i.e. smoke) along the compartment ceiling. This hot gas layer exits the compartment through a vertical opening and flows under the balcony forming the approach flow. Starting at the balcony edge, momentum transfer from the heated gases in the approach flow to the stagnant atrium air reduces the horizontal velocity of the BSP while buoyancy forces cause its vertical velocity to increase. The BSP trajectory gradually turns upwards until the top of the turning region where it is assumed to have predominantly vertical velocity. The BSP then rises through the atrium as a buoyant line plume, entraining additional air and increasing in mass flow rate until entering the atrium smoke layer. If the atrium is wide enough to allow the BSP to develop without impacting the atrium walls, additional ambient air will be entrained into the ends of the BSP. In any case, the mass flow rate in the BSP increases due to air entrainment along the path from the fire, through the approach flow and turning regions and into the line plume region. In terms of modeling the BSP, the final line plume region is disconnected from the compartment fire plume since the line plume is assumed to emanate either from an independent rectangular buoyancy source located at the balcony elevation or a theoretical line buoyancy source located some distance below the balcony elevation. Furthermore, the mass flow rate in the line plume region of the BSP is assumed to vary linearly with elevation in accordance with Lee and Emmons' model of buoyant line plume behaviour [25].

1.1.2 Methods to Estimate BSP Mass Flow Rates

The first generation of methods to estimate BSP mass flow rates were developed based on data from two sets of experiments conducted at one-tenth scale [42, 43]. This relatively small scale was adopted due to the prohibitively high cost of constructing a full-scale experimental facility. Scaling of the experimental data was based on scaling principles advanced by Thomas et al. [53]. These followed a modified Froude number modeling where the Froude numbers of the full- and model-scale flows were preserved by scaling the full-scale fire size by the five-halves power of the physical scale factor: $Q_{model} = Q_{full}/(L_{full}/L_{model})^{5/2}$ [9]. The accuracy of Thomas et al.'s scaling laws may be adversely affected by the presence of significant radiative heat transfer [19], but this effect has never been evaluated for BSP flow due to a lack of full-scale experimental data against which to verify the scale-model data. Fire compartments 0.5 m in height with opening widths of 0.7 and 1.4 were located at floor level in a two-storey atrium. BSPs were produced by fires between 2.8 and 16 kW (0.9 and 5.0 MW full-scale) in size. The mass flow rate of the mechanical exhaust system located at the top of the atrium was varied to achieve various equilibrium

atrium smoke layer elevations. Once the atrium smoke layer attained an equilibrium position, the exhaust flow rate from the top of the smoke layer was used to infer the BSP mass flow rate into the bottom of the smoke layer. Atrium smoke layer elevations were determined based on temperatures measured using a vertical array of thermocouples in the atrium. The facility design and procedure used in these first two experimental programs have been repeated in all subsequent experimental programs investigating BSP behaviour, including the reliance on one-tenth scale model testing and the inference of BSP mass flow rate from an equilibrium with the exhaust system mass flow rate [18, 33, 32, 19].

The BRE method developed by Morgan and Marshall was the first systematic method to estimate BSP mass flow rate [40]. Measured values of BSP mass flow rate and temperature [42, 43] were used to develop a multistep, partially iterative algorithm to calculate BSP mass flow rate as a function of elevation, fire size, compartment opening width, compartment area and other parameters. Simple expressions for entrainment into the ends of the BSP were derived to facilitate application of Lee and Emmons' model for infinite line plumes to BSPs with finite length [42, 43]. The BSP mass flow rate and temperature calculated at the top of the turning region were used to characterize an equivalent rectangular source for the BSP line plume region located at the balcony elevation, after Lee and Emmons' [25] line plume model. Entrainment into the BSP turning and line plume regions were modeled separately with the line plume entrainment calculated assuming the same entrainment coefficient as measured by Lee and Emmons for their buoyant line plumes [25]. This assumption required that a much higher entrainment coefficient be assumed for the BSP turning region in order to match the experimental mass flow rate data [42, 43]. Subsequent numerical modeling by Miles et al. [36] and salt water scale modeling by Yii [57] showed that plume entrainment in the BSP turning region was not significantly greater than that in the line plume region, calling into question the requirement in the BRE method for using high entrainment coefficients to model plume flow in the BSP turning region.

Two new methods for estimation of BSP mass flow rate were developed in 1986 based on a desire to provide designers of atrium smoke management systems with simpler estimation methods than the BRE method. These methods expressed BSP mass flow rate as a function of elevation, fire size and fire compartment geometry using a single expression rather than a multistep, iterative algorithm. Law's method [22] was based on Yokoi's [58] window plume model with an entrainment coefficient for the BSP line plume region calculated from the experimental data of Morgan and Marshall [43]. Law modeled the BSP line plume region as emanating from a virtual line source below the balcony rather than as a rectangular source at the balcony elevation. This treatment obviated the need for a separate calculation of entrainment in the turning region, in effect incorporating it into the line plume region entrainment calculation. Law chose to express the virtual origin elevation in terms of the fire compartment height based on the experimental data [43]. Law's method demonstrated that the variation

of BSP mass flow rate with elevation could be expressed as a function of elevation (z), fire size (Q) and compartment opening width (W) with a reasonable degree of accuracy. The entrainment coefficient in Law's method was reduced by ≈ 8% in 1995 [24] based on data from experiments conducted by Hansell et al. [18]. It formed the basis of similar methods listed in North American (NFPA) [14] and United Kingdom (CIBSE) [7] design guides for atrium smoke management systems. Concurrent with Law, Thomas [51] developed a method for estimating BSP mass flow rate based on Lee and Emmons' line plume model [25]. Thomas also modeled the BSP line plume region as emanating from a line source located below the balcony, but did not make Law's simplifying assumption that the approach flow mass flow rate was equal to the BSP mass flow rate at the balcony elevation. Relaxing this constraint allowed Thomas to correlate his model to the experimental data of Morgan and Marshall [43] using the entrainment coefficient for line plumes measured by Lee and Emmons [25]. In an attempt to develop a more theoretically based BSP method than that of Law, Thomas expressed the virtual origin elevation as a function of approach flow mass flow rate and depth rather than fire compartment height. Thomas also modeled BSP end entrainment by assuming that one half of an axisymmetric plume was located at either end of the BSP, which led to a non-linear relationship between BSP mass flow rate and elevation.

Analysis of the experimental data used to develop the first generation of BSP mass flow rate estimation methods [42, 43] indicated that BSP mass flow rates may be affected by the particular size of the atrium. For example, the BRE method was unable to accurately predict BSP mass flow rates measured in a 1.4 m wide by 4.2 m long by 1.5 m high atrium [43] unless the atrium smoke layer elevations were artificially reduced by a factor related to the atrium height [40]. Law [22] criticized this 'effective layer depth correction' as unsuitable for application to a wide range of atrium sizes since it was based on data from experiments conducted in a single atrium [43]. Law's and Thomas' methods did not require such a correction to match the experimental data in [43] since both methods were based on correlations to this data and therefore implicitly accounted for the effect of one particular atrium size on BSP mass flow rate. To investigate the impact of atrium size on BSP mass flow rate as well as other issues related to the accuracy of the BRE method, a number of experimental programs were conducted to measure BSP mass flow rates in different atrium geometries [18, 33, 32]. Hansell et al.'s experiments in a 3.06 m high atrium with an area of 3.3 m^2 found that the temperatures below the atrium smoke layer tended to be non-uniform in larger atria, affecting the degree of entrainment into the BSP and therefore its mass flow rate [18]. Experiments conducted by Marshall and Harrison [32] in 2.5 m high atria with areas of 1.0 and 2.0 m^2 showed that recirculation at the atrium walls caused a local deepening of the atrium smoke layer at the atrium walls and increased effective BSP entrainment. Poreh et al. [45] called for a comprehensive parametric study of the variation of BSP mass flow rate with atrium geometry in order to improve the robustness of existing BSP methods. In the absence of data from such a study, the effect of atrium size on

BSP behaviour remains a contentious issue with no clear guidance for designers of atrium smoke management systems. Although measurements of BSP mass flow rate in open conditions would potentially remove the effect of atrium size from the results, such experiments have not been conducted due to the difficulty in measuring BSP velocities and temperatures directly and using them to determine the BSP mass flow rates.

In 1998, data from the experimental program by Marshall and Harrison [32] was used to develop two new methods for estimating BSP mass flow rate. Poreh et al. [45] and Thomas et al. [54] developed independent methods based on Lee and Emmons' [25] line plume model. Values for the entrainment coefficient in the BSP line plume region were calculated from the experimental data of Marshall and Harrison [32] but differed slightly between the two methods due to their respective use of different expressions for determining the elevation of the virtual origin. Poreh et al. followed Thomas's [51] treatment by expressing the virtual origin elevation in terms of approach flow mass flow rate and depth, while Thomas et al. [54] simplified this expression for the virtual origin elevation by relating approach flow mass flow rate and depth via a theoretical expression developed by Morgan [38]. This simplification resulted in a slightly more complicated relationship between BSP mass flow rate and the independent variables of fire size and compartment opening width in Thomas et al.'s method compared to the other BSP methods. Since the experimental program of Marshall and Harrison [32] did not allow entrainment into the BSP ends, neither Poreh et al.'s nor Thomas et al.'s method implicitly considered this effect. A theoretical expression for BSP end entrainment was proposed as an addition to Thomas et al.'s method but was not verified using experimental data. In 2004, Harrison [19] used data from an experimental program in a 2.5 m high atrium with an area of 2.0 m^2 to develop updated versions of Poreh et al.'s and Thomas et al.'s methods. The entrainment coefficients proposed by Harrison were 25% higher than those determined by Poreh et al. and Thomas et al., an increase attributed to entrainment into the BSP ends in the more recent experiments.

1.1.3 Comparison of Existing BSP Methods

The expressions for BSP mass flow in the existing BSP methods differ significantly from each other, partly due to the variety of experimental data used in their derivation and partly due to the different assumptions made about the elevation of the virtual origin and the entrainment rate for the BSP line plume region. Table 1 below lists the BSP mass flow rate expressions from each of the existing BSP methods and their variants in the functional form $m_{BSP} = C\ (z - z_{balc}) + m_0$ where C (kg/s-m) is a proportionality constant, z (m) is the elevation above the atrium floor, z_{balc} (m) is the balcony elevation and m_0 (kg/s) is the BSP mass flow rate at the balcony elevation (i.e. $z = z_{balc}$) which is proportional to the virtual origin elevation, z_0. The BRE method is omitted from Table 1 since its multistep nature makes it

difficult to isolate a single expression for m_{BSP} in terms of the independent variables. The last column of Table 2.1 indicates whether each method accounts for the effect of BSP end entrainment via correlation to suitable experimental data. The asterisks (*) indicate that Thomas's and Thomas et al's method account for BSP end entrainment using a purely theoretical approach. The portion of Thomas' expression for m_{BSP} which varies non-linearly with elevation is omitted from Table 2.1 to allow for a more direct comparison to the other m_{BSP} expressions.

Method	Year	C (kg/s-m)	m_0 (kg/s)	BSP end entrainment
BRE [40]	1979	Not included	Not included	Yes
Law [22]	1986	$0.38\ (QW^2)^{1/3}$	$C\ (0.15\ h_{comp})$	Yes
Thomas [51]	1987	$0.21\ (QW^2)^{1/3}$	$C\ d_{balc} + m_{balc}$	Yes*
Law [24]	1995	$0.35\ (QW^2)^{1/3}$	$C\ (0.25\ h_{comp})$	Yes
CIBSE [7] after Law [24]	1995	$0.36\ (QW^2)^{1/3}$	$C\ (0.25\ h_{comp})$	Yes
Poreh et al. [45]	1998	$0.16\ (QW^2)^{1/3}$	$C\ d_{balc} + m_{balc}$	No
Thomas et al. [54]	1998	$0.159\ (QW^2)^{1/3} + 0.09\ (Q/W)^{1/3}$	$0.0027\ Q + 1.2\ m_{balc}$	Yes*
Harrison [19] after Poreh et al. [45]	2004	$0.20\ (QW^2)^{1/3}$	$C\ d_{balc} + m_{balc}$	Yes
Harrison [19] after Thomas et al. [54]	2004	$0.20\ (QW^2)^{1/3}$	$0.0017\ Q + 1.5\ m_{balc}$	Yes
NFPA [14] after Law [24]	2005	$0.41\ (QW^2)^{1/3}$	$C\ (0.25\ h_{comp})$	Yes

Table 1.1 Functional comparison of BSP mass flow rate expressions ($m_{BSP} = C\ (z - z_{balc}) + m_0$).

Examination of Table 1 shows that all of the existing methods relate BSP mass flow rate to the independent parameters of elevation (z), fire size (Q) and compartment opening width (W) via the functional form $m_{BSP} = f(z, Q^{1/3}, W^{2/3})$. This is consistent with Lee and Emmons' line plume theory, including the linear variation of BSP mass flow rate with elevation. Thomas et al.'s method contains an additional term due to its simplifying assumption relating approach flow mass flow rate and depth. The BSP mass flow rate at the balcony elevation, m_0, is expressed in three main functional forms: $m_0 = f(h_{comp})$, $m_0 = f(d_{balc}, m_{balc})$ and $m_0 = f(Q, m_{balc})$. The first expression is related to Law's proposed correlation of virtual origin elevation, z_0, to fire compartment height, an assumption which was criticized by Thomas [52] and Morgan [39] as not being sufficiently general. The second expression, originally proposed by Thomas [51], is a more acceptable generalization but redundantly expresses m_0 in terms of both the approach flow depth and mass flow rate. The third expression, originally proposed by Thomas et

al. [54], expresses the approach flow's depth in terms of its mass flow rate and the fire size. Since the BSP mass flow rate at the balcony elevation does not vary with elevation, uncertainties in its value will have a small impact on the accuracy of BSP mass flow rate estimates at higher elevations. The main difference between the various expressions in Table 1 is the value of the constant factor in the proportionality constant, C, representing the increase in BSP mass flow rate with elevation. The average value of the factors listed in Table 1.1 is 0.27 kg/s-kW$^{-1/3}$m$^{-5/3}$ with a range of between −41% and +52% about this average. Such a large variance means that estimates of BSP mass flow rate at any given elevation may vary by a factor of up to two depending on which method is used for the calculation. These large uncertainties in estimates of BSP mass flow rate make the design of optimized atrium smoke management systems more difficult. Furthermore, extension of the existing BSP methods to higher elevations is hindered by the fact that such uncertainties in estimated BSP mass flow rate increase with elevation.

Figure 4 illustrates the variance in the BSP mass flow rates predicted by the five main BSP methods when applied to the same scenario of a 5 MW fire occurring in a 5 m high compartment with a 10 m wide opening. Profiles of $m_{BSP} = f(z)$ estimated using each method are plotted. Two $m_{BSP} = f(z)$ profiles are plotted based on the BRE method [40], each assuming a different atrium ceiling elevation. The other four BSP methods do not take the atrium ceiling elevation into consideration and are therefore plotted only once. This comparison is similar to that presented by Morgan et al. [40]. All six of the BSP mass flow rate profiles plotted in Figure 4 exhibit a linear increase in BSP mass flow rate with elevation. The slope of each profile represents the increase in BSP mass flow rate per unit change in its elevation, or the value C in each method's expression for BSP mass flow rate (Table 1.1). The slopes of the profiles from the Poreh et al. [45] and Thomas et al. [54] methods are similar since both methods were developed based on correlations to the same experimental data [32]. Likewise, the slopes of the profiles from the BRE [40], Law [22, 24], and Thomas [51] methods are similar since they are based on the same experimental data [32, 33]. The slopes of the profiles using the latter three methods are approximately double those of the former two methods, indicating a larger increase in m_{BSP} for a given change in elevation. When extrapolated, all of the profiles predict a very small BSP mass flow rate at the balcony elevation, m_{balc}; however, the difference in slope between the six profiles in Figure 4 leads to significant variance in their estimates of BSP mass flow rate at higher elevations. For example, the BSP mass flow at 10 m estimated using Law's method [22, 24] is almost double that obtained using Poreh et al.'s method [45]. Such variances make it difficult to determine an optimal design capacity for any atrium smoke management system. The variances are especially large for higher BSP elevations, indicating that none of the existing methods may be appropriate for estimation of BSP mass flow rates at high elevations.

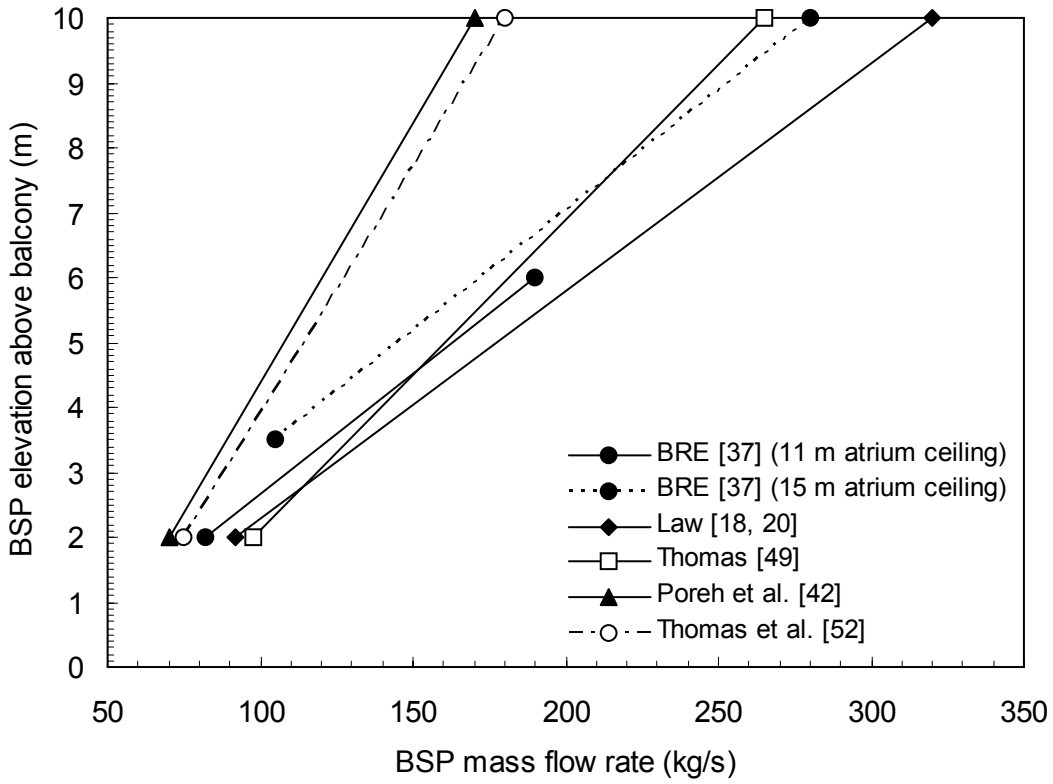

Figure 4. Comparison of BSP mass flow rate expressions [40, 22, 24, 51, 45, 54].

1.1.4 Numerical Modeling of BSPs

A number of researchers have applied computational fluid dynamics (CFD) techniques to the study of BSP behaviour. Miles, Kumar and Cox [36] replicated the experiments conducted by Marshall and Harrison [32] using the CFD software JASMINE. BSP mass flow rates inferred from the exhaust system flow rates compared well with both the experimental data and estimates using Poreh et al.'s and Thomas et al.'s methods. A series of numerical modeling studies by Chow et al. [4, 3] modeled the same experimental facility [32] using the CFD software CC-EXACT. Predicted values of BSP mass flow rate agreed with those estimated using Poreh et al's method. Chow et al. [5] later developed a simple zone model to predict atrium smoke layer filling rates based on expressions for BSP mass flow rate developed by Poreh et al. [45], Thomas et al. [54] and Law [14]. This model was less computationally expensive than a CFD model but its predictions of atrium smoke layer elevation depended entirely on the accuracy of the underlying expressions for BSP mass flow rate. Harrison [19] conducted CFD simulations in parallel with his experimental program using the software Fire Dynamics Simulator (FDS) with a focus

on the approach flow rather than the BSP above the balcony. This study demonstrated that FDS was able to predict approach flow temperatures and depths to a high degree of accuracy compared to the experimental data. This would suggest the utility of FDS in predicting approach flow properties which could then be used with those methods whose expressions for BSP mass flow rate require estimates of the approach flow mass flow rate [51, 45, 54] (See Table 1.1). The existing numerical modeling studies of BSP behaviour have focused exclusively on replicating the data from the low-elevation, one-tenth scale experiments from which the existing BSP methods are derived. To date, no numerical modeling study of BSPs at full-scale, at elevations greater than 9 m above the atrium floor or in open conditions has been published, despite the flexibility of CFD for conducting such modeling.

1.2 Present Research

The existing body of research into BSP behaviour suffers from a number of limitations which hinder development of a method to estimate BSP mass flow rates at high elevations. The accuracy of Thomas et al.'s [53] scaling laws applied to the scale-model BSP experimental data has never been verified due to a lack of full-scale BSP experimental data. The large degree of variance in mass flow rate estimates using the existing methods, even at relatively low elevations, suggests that a new method for estimation of BSP mass flow rates at high elevations should be developed rather than extending the existing methods. This could be done very effectively based on new BSP mass flow rate data obtained at high elevations. To date, none of the BSP experimental programs have produced BSP mass flow rate data for elevations above 9 m, presumably due to the prohibitively high costs of building a high-elevation atrium facility, even at model scale. CFD modeling offers a cost-effective alternative to physical experiments provided the numerical model can be verified appropriately using experimental data. Experimental measurements of BSP mass flow rate may also suffer form inaccuracies due to the effects of the atrium walls on BSP entrainment. Measurements of BSP mass flow rate for a plume in open conditions (i.e. with no surrounding atrium) would remove atrium size effects and would therefore serve as a more solid basis for developing BSP methods. Although such data is prohibitively difficult to obtain experimentally, mass flow rates of BSPs in open conditions are easily obtained in CFD simulations. No such study has been published to date, presumably due to the lack of experimental data with which to evaluate the numerical model.

The present research focuses on developing a model of BSP behaviour at high elevations based on BSP mass flow rates predicted by CFD simulations. The objectives of this research effort are:

1. to develop a CFD model of BSPs in atria and evaluate the model using full-scale experimental data,

2. to produce additional numerical modeling data for BSP mass flow rates at high elevations with the effects of atrium size removed, and
3. to derive a new method to estimate BSP mass flow rates at high elevations.

Data from a full-scale experimental program (Chapter 2) is used to assess the ability of two preliminary CFD models to predict compartment temperatures and BSP mass flow rates at low elevations (Chapter 3). These models are then extended to develop a CFD model of BSP behaviour up to 50 m in elevation (Chapter 4). This model removes the atrium walls in order to model BSP behaviour in open conditions, a unique approach among published numerical studies. Once developed, this new high-elevation BSP model is used to conduct a parametric study of BSP mass flow rate as a function of elevation, fire size and fire compartment geometry (Chapter 4). Finally, the simulated mass flow rate data is used to develop a new method to estimate BSP mass flow rates at elevations up to 50 m.

Chapter 2 Full-Scale Experimental Program

As discussed in Chapter 1, the lack of a comprehensive set of full-scale experimental data on BSP mass flow rates makes development and evaluation of BSP prediction methods difficult. To address this issue, the National Research Council Canada (NRC) and the American Society of Heating, Refrigerating and Air-Conditioning Engineers (ASHRAE) initiated a full-scale experimental program in 2003 to measure BSP mass flow rates in an experimental facility representing a full-scale atrium. The objective of this experimental program is to provide full-scale experimental data on the variation of BSP mass flow rate with elevation and fire compartment geometry that is appropriate for use in evaluation of existing, or development of new, BSP methods. This data is used in the present thesis to compare to simulation results from the CFD model of the full-scale experimental facility described in Chapter 3. Once evaluated using the experimental data, the CFD model of the full-scale experimental facility is extended to higher elevations (Chapter 4) to allow the development of a method to estimate BSP mass flow rates at high elevations. Because of the importance of the full-scale experimental data to this work, the full-scale experimental program is summarized in this chapter with a focus on those details which pertain to the use of the experimental data to evaluate the CFD models. A full description of NRC's full-scale experimental program, as well as the associated data set, are pending publication.

2.1 Experimental Objective and Design

The main objective of the full-scale experimental program is to measure BSP mass flow rates produced by steady fires in a compartment with an attached balcony. The design for the full-scale experiments is similar to that used in the scale experimental programs of Morgan and Marshall [42, 43] and adopted in the majority of subsequent BSP experimental programs [18, 33, 32, 19]. A fire compartment is constructed at floor level within a four-storey atrium with a mechanical exhaust system at the ceiling. Elements of the fire compartment geometry (i.e. opening width, fascia depth and draft curtain depth) are varied between experiments over a range of values typically found in North American atria. Once the atrium smoke layer has reached an equilibrium elevation, the BSP mass flow rate into the bottom of the atrium smoke layer (m_{BSP}) is inferred from the more easily measured exhaust system mass flow rate (m_{exh}). The steady-state atrium smoke layer elevation, z_l, is calculated for each BSP mass flow rate using temperature data from a vertical array of thermocouples. A variable exhaust system located at the atrium ceiling is used to achieve various atrium smoke layer elevations, producing a single profile of BSP mass flow rate as a function of elevation for each combination of fire size and compartment geometry. The

complete set of $m_{BSP} = f(z)$ profiles allows development of a BSP method which estimates BSP mass flow rate as a function of elevation, fire size and compartment geometry.

2.2 Experimental Parameters

Existing methods for estimating BSP mass flow rate typically require two main independent parameters to be specified: fire size (Q) and compartment opening width (W). Two secondary parameters which impact BSP behaviour to lesser degrees are the depth of the fascia at the top of the compartment opening (h_{fasc}), and the depth of the draft curtains located under the balcony and extending perpendicular to the compartment opening (h_{draft}) (Figure 5). Therefore, the variation of BSP mass flow rate as a function of these four parameters are studied in the full-scale experimental program and the CFD modeling study used to develop a new method to estimate BSP mass flow rate at high elevations (Chapter 4). Wide ranges of these parameters were used so that the data, CFD simulation results and resulting BSP methods would be applicable to atrium smoke management system design scenarios typical of those in real atria. At the same time, the ranges were chosen to match those used by Morgan and Marshall [42, 43] and subsequent researchers [18, 33, 32, 19] to allow direct comparison of the present data to data from previous model-scale experimental programs. The ranges of the independent parameters are considered valid for both the low-elevation experimental program and the high-elevation modeling study since it is assumed that atria with different elevations do not have substantially different fire compartment geometries or design fire sizes. The values of the experimental parameters for each experiment are listed in Appendix A and are briefly summarized as follows:

1. *Fire Size (Q)* – Design fire sizes of 0.5 to 1 MW have been suggested to represent fire scenarios in sprinklered office buildings [27, 31], while a fire size of 2.5 MW has been suggested for fire scenarios in retail malls [30]. Atrium smoke management system design guides such as NFPA 92B [15] suggest design fires with convective heat release rates of 5.0 MW for sprinklered retail applications. Therefore, fires with heat release rates of Q = 0.5, 1.0, 2.5 and 5.0 MW were included in the experimental program to cover the range of typical atrium fire scenarios. None of the above guidance on atrium design fires suggests that their heat release rates be changed when designing smoke management systems for higher elevation atria.

2. *Compartment Opening Width (W)* – Compartment opening widths of 5.0, 7.5, 10 and 12 m were used in the experimental program. The width of the atrium that could be accommodated in the experimental facility limited the maximum compartment opening width to a value approximately 85% of the full-scale width of the double-width compartment in Morgan and Marshall's

experimental program [42, 43]. Compartment openings up to 12 m wide are still applicable to a large number of typical atrium fire scenarios.

3. *Compartment Opening Fascia Depth (h_{fasc})*– Removable panels were used to set the fascia depth to values of 0.0 and 1.6 m, providing a range of values typical of those found real atria.

4. *Draft Curtain Depth (h_{draft})*– Removable panels allowed draft curtain to be placed in line with the edges of the compartment opening with depths of 0.0 and 2.9 m.

The literature review conducted as part of the current research (Chapter 1) indicates that there are additional parameters which affect BSP mass flow rate to a lesser extent than the four main parameters identified above. These secondary parameters include: fire compartment size, fire location, compartment heat transfer, balcony depth and compartment height. These parameters were maintained constant throughout the full-scale experimental program in order to reduce the number of experiments required, decrease costs and simplify the overall data analysis. The importance of these parameters and their final values in the experimental program are:

1. *Fire Compartment Size* – The size of the fire compartment affects the entrainment into the compartment fire plume which in turn affects estimates of the approach flow mass flow rate, m_{balc}. Of the existing BSP methods, only the BRE method [40] takes fire compartment size into account. The fire compartment size used in the full-scale experimental program is 13.8 m wide by 5.4 m deep by 5.0 m high as given in Section 2.3.2.

2. *Fire Location* – The fire source was located at the centre of the fire compartment for all experiments in order to reduce the effect of the compartment wall(s) on the compartment fire plume. A fire located near the compartment wall(s) will tend to adhere to the wall, reducing the amount of air entrained into its plume and therefore reducing its mass flow rate. A fire in the middle of a compartment with no attachment will have the highest mass flow rate for a given fire size therefore this scenario was chosen as the most conservative. The fire source was located along the centerline of the fire compartment to maintain approach flow symmetry, a key assumption in most existing BSP methods.

3. *Compartment Heat Transfer* – Conductive heat losses through the fire compartment boundaries reduce the temperature and velocity of and entrainment into the approach flow exiting the compartment opening. The fire compartment in the full-scale experimental program was lined with non-combustible ceramic fibre insulation to protect its structure. This material has low thermal conductivity, minimizing heat losses through the compartment boundaries and maximizing the temperature and velocity of and entrainment into the approach flow. This will

tend to increase the approach flow mass flow rate, leading to conservative estimates of BSP mass flow rate for a given fire size.

4. *Balcony Depth* – A constant balcony depth of 4.2 m was used in the full-scale experimental program. This value matches that in the scale experimental programs conducted by Morgan and Marshall [42, 43] and is consistent with values occurring in real atria.

5. *Compartment Height* – A constant compartment height of 5.0 m was used in the full-scale experimental program. This height is typical of the maximum floor-to-floor height found in many commercial and retail buildings. Since higher compartment heights allow more entrainment into the fire plume (i.e. region 1 in Figure 3) and increase values for the approach flow mass flow rate, a compartment height at the upper end of the range of typical values yields conservative BSP mass flow rates.

The values of these secondary independent parameters were chosen to match those used by Morgan and Marshall [42, 43]. Where possible, the parameter values were also chosen to yield conservatively large BSP mass flow rates which will lead to increased factors of safety in the design of atrium smoke management systems and minimize risks to the life safety of building occupants.

Due to the high cost of undertaking each full-scale experiment, the atrium exhaust system mass flow rate (m_{exh}) was varied during each experiment to allow m_{BSP} to be measured for multiple values of the atrium smoke layer elevation, z_l, and a single combination of fire size and compartment geometry. Note that the high cost of conducting full-scale BSP experiments supports the development of accurate CFD models to predict BSP behaviour for wider ranges of the independent parameters at a much lower cost.

2.3 Full-Scale Experimental Facility

The experimental facility used to conduct the full-scale experimental program is located at NRC's laboratory near Almonte, ON. This facility simulates a four-storey atrium with a variable capacity mechanical exhaust system located at its ceiling. The following sections briefly describe aspects of this facility which are pertinent to development of the CFD model described in Chapter 3.

2.3.1 Atrium

Figure 5 shows top and elevation views of the full-scale experimental facility. An isometric view of the fire compartment is also included in Figure 5 to clarify the relative arrangement of the balcony, compartment opening fascia and draft curtains. The outer boundary of the facility defines a four-storey atrium 16.8 m wide by 30.5 m deep by 12.2 m high. The atrium size was kept constant in all full-scale experiments and in all CFD simulations of the facility. The atrium was constructed by sectioning off one

end of a larger four-storey laboratory building using a fixed panel wall and an adjustable curtain. The east, south and west walls of the atrium are the walls of the larger laboratory building which consist of corrugated steel sheeting. The atrium ceiling is the suspended ceiling of the larger laboratory building consisting of a grid of ceramic fibre panels. The east part of the north atrium wall is a fixed wall made of fibreglass panels. The west part of the north atrium wall is a canvas curtain with a fixed height but adjustable elevation to allow for a variable depth vertical opening at the atrium ceiling. Both the fixed panel wall and the adjustable curtain in its highest position extend from the atrium ceiling to approximately the balcony elevation to allow makeup air to enter the facility under the north atrium wall. No makeup air was allowed to enter the facility through the other three walls. The opening under the north atrium wall was specified in the CFD model as an open boundary condition. Leakage through small gaps in the atrium walls and ceiling was visually determined to be small and therefore was neglected in the analysis of the experimental data and in the specification of the atrium boundaries in the CFD model.

The vertical opening at the top of the adjustable curtains acts as a gravity vent to allow smoke to escape from the atrium smoke layer into the larger laboratory building. Figure 5 illustrates a typical value for the curtain opening depth of 0.6 m. Louvers located at an elevation of 10 m along the east, south and west atrium walls were also opened in selected experiments to allow smoke to escape from the atrium smoke layer. In experiments where an opening was present at the top of the adjustable curtain, similar louvers were opened in the laboratory building surrounding the experimental facility to prevent smoke from accumulating in this building. Controlled leakage through the louvers and curtain opening was used in an attempt to supplement the mechanical atrium exhaust system for experiments where the exhaust system capacity was insufficient to maintain the atrium smoke layer elevation above the balcony elevation. The vertical opening above the adjustable curtain and the louvers were both modeled in the CFD model as open boundary conditions.

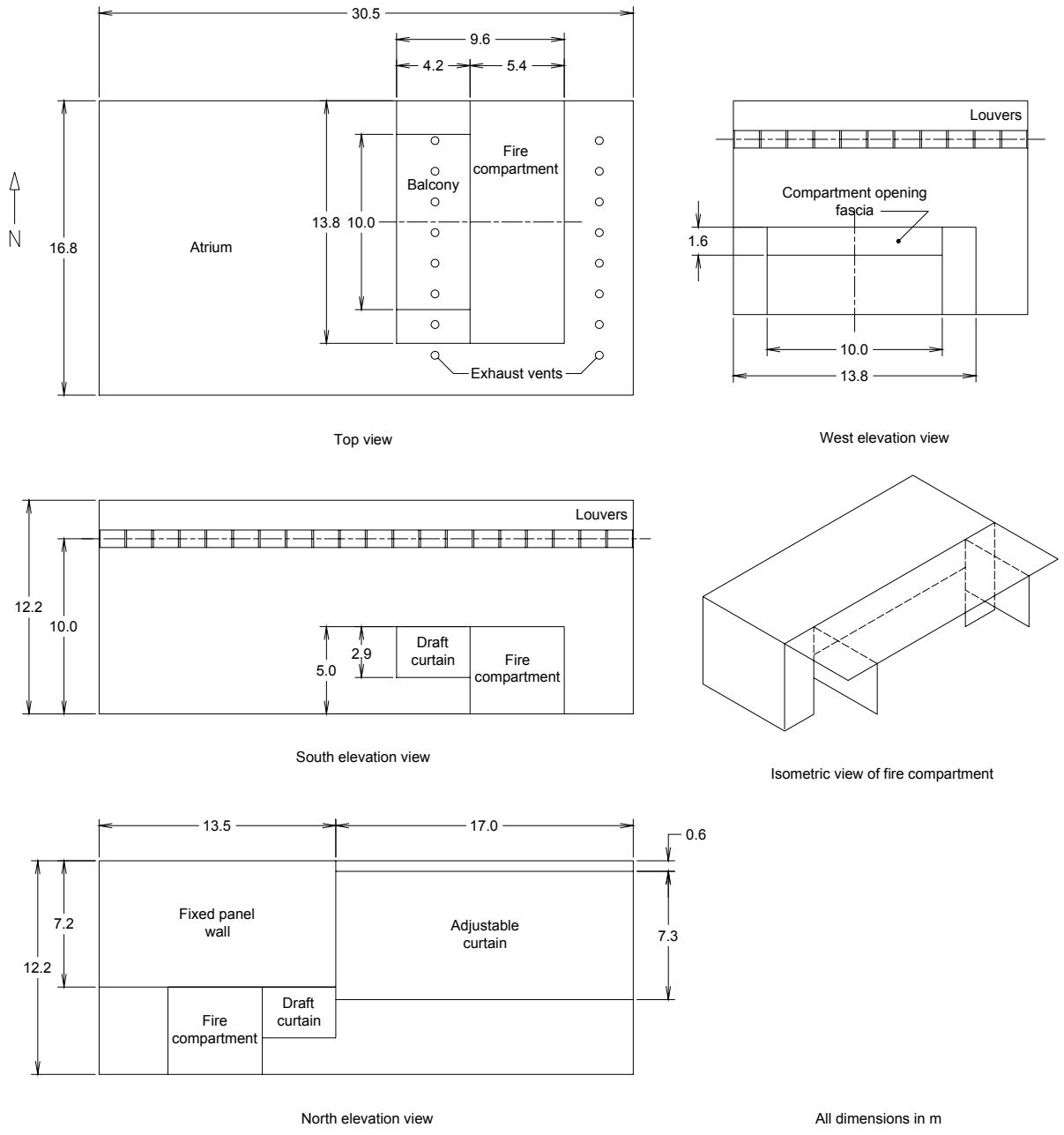

Figure 5. Geometry of full-scale experimental facility.

2.3.2 Fire Compartment

The fire compartment in the full-scale experimental facility is 13.8 m wide by 5.4 m deep by 5.0 m high. Figure 5 above shows the position of the fire compartment near the east end of the experimental facility. This position allows the BSP to project into the atrium as far away as possible from the atrium walls and thereby minimizes their impact on the atrium smoke layer (Section 1.1.2). The atrium and fire compartment centerlines do not coincide because the presence of an unrelated experimental facility to the north limited the atrium width. This asymmetry was assumed not to affect the BSP flow dynamics for the smaller compartment opening widths of W = 5.0, 7.5 and 10.0 m but may have affected the BSP for the widest compartment opening width of W = 12.0 m. The rear (east) and side (north and south) walls and ceiling of the fire compartment are constructed of corrugated steel and non-combustible ceramic fibre insulation to protect against repeated fire exposure. This insulation has low thermal conductivity, thus minimizing conductive heat losses through the compartment boundaries and maximizing the approach flow temperature, velocity and entrainment as it exits the compartment (Section 2.2). The compartment floor is concrete and does not require protection with insulation. The concrete is assumed to have a thermal conductivity comparable to that of the ceramic fibre insulation. Although the compartment opening width, opening fascia depth and draft curtain depth were varied during the experimental program, representative values of W = 10.0 m, h_{fasc} = 1.6 m and h_{draft} = 2.9 m are shown in Figure 5 for illustrative purposes.

Figure 6 illustrates the modular construction of the fire compartment to allow different values for the compartment opening width, compartment opening fascia depth and draft curtain depth. As with Figure 5, representative values of W = 10.0 m, h_{fasc} = 1.6 m and h_{draft} = 2.9 m are shown in Figure 6 for illustrative purposes. The front (west) wall of the fire compartment consists of a set of removable panels constructed of corrugated steel with no ceramic fibre insulation. Compartment opening widths of W = 5.0, 7.5, 10.0 and 12.0 were defined by panels extending from the compartment ceiling to the floor with all openings centered on the compartment centerline. A compartment opening fascia was defined for selected experiments by 1.6 m deep panels installed at the top of the compartment opening. Draft curtains were defined for selected experiments by panels installed under the full depth of the balcony normal to the front wall of the fire compartment and in line with the compartment opening edges. These draft curtains were originally 2.0 m in depth for early experiments but were extended to 2.9 m because the approach flow was observed to leak under them. Draft curtains were not installed for the experiments with the widest compartment opening width of W = 12 m since the atrium walls were assumed to channel the BSP in a similar manner. Figure 6 also shows the 4.2 m deep balcony installed over the entire width of the fire compartment. The balcony was constructed of corrugated steel with negligible thickness compared to the dimensions of the fire compartment.

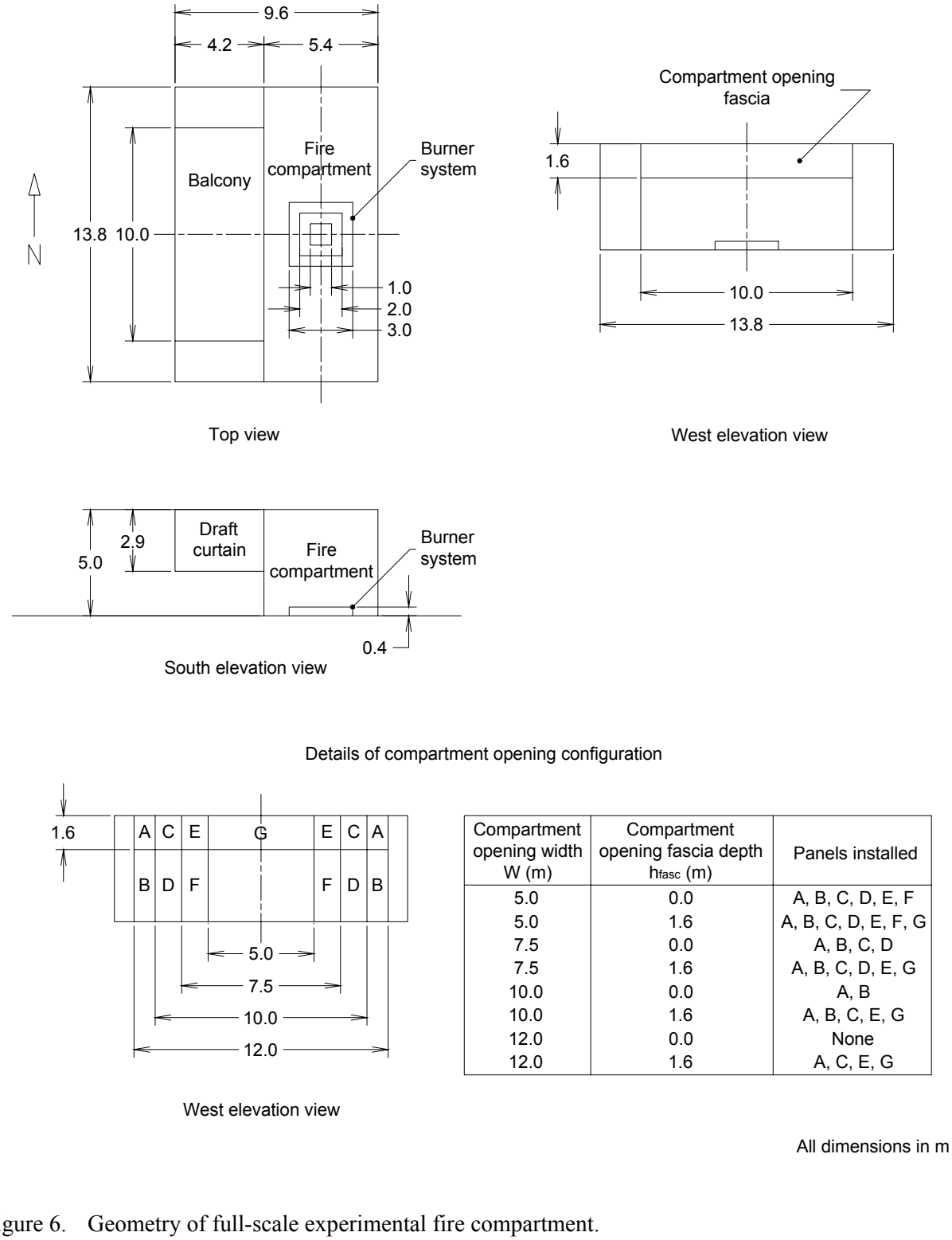

Compartment opening width W (m)	Compartment opening fascia depth h_{fasc} (m)	Panels installed
5.0	0.0	A, B, C, D, E, F
5.0	1.6	A, B, C, D, E, F, G
7.5	0.0	A, B, C, D
7.5	1.6	A, B, C, D, E, G
10.0	0.0	A, B
10.0	1.6	A, B, C, E, G
12.0	0.0	None
12.0	1.6	A, C, E, G

Figure 6. Geometry of full-scale experimental fire compartment.

2.3.3 Fire Source

The fire source is a square modular burner fuelled by propane. Previous research on atrium smoke management systems at NRC [28, 29, 30] have demonstrated that modular propane burners are well-suited to conducting parametric studies of plume mass flow rates since steady, measurable fire sizes can be maintained for extended durations of each experiment. For these experiments, the burner system is located in the center of the fire compartment at an elevation of 0.41 m. The position and dimensions of the burner system are shown in Figure 6; Figure 7 is a photograph of the burner system to illustrate its construction. A border of corrugated steel panels is placed around the sides of the burner system to reduce airflow underneath the fire in order to better simulate the flow into a fire on the fire compartment floor.

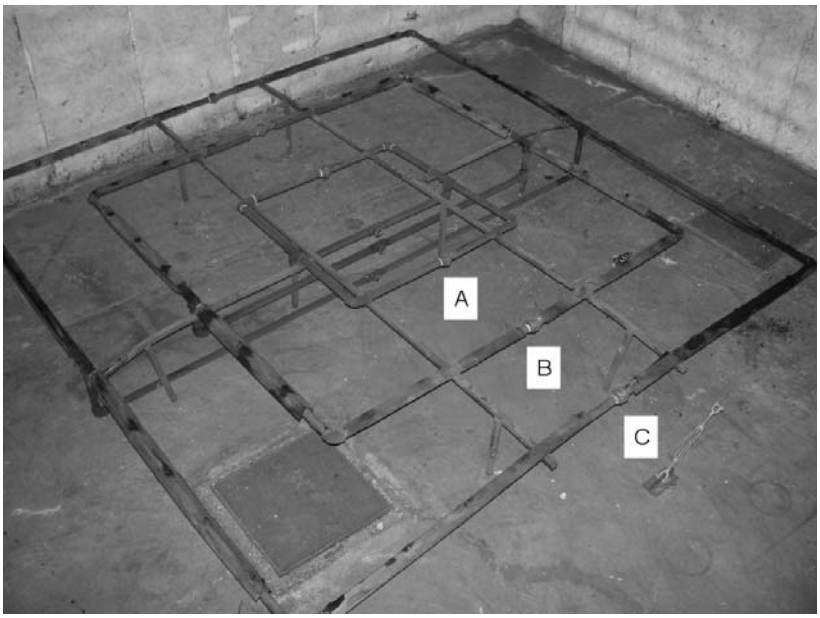

Figure 7. Burner system in experimental facility (A: 1 m by 1 m burner; B: 2 m by 2 m burner; C: 3 m by 3 m burner).

Propane was selected as the fuel for the full-scale experimental program since it is more convenient to use than liquid fuels such as heptane and measurement of the propane flow rate is relatively straightforward. Propane is supplied to the burner system through a set of pressure regulators and rotameters to allow measurement of the volumetric flow rate and the resulting heat release rate of the fire, Q. Further details of the propane measurement system are given in Section 2.3.5 as part of the description of the instrumentation in the experimental facility.

The propane exits from numerous small holes in pipes forming three concentric squares with side lengths of 1, 2 and 3 m. A system of valves allows propane to flow through any combination of the three square burners, producing fires with approximate base sizes of A_{burner} = 1, 4 and 9 m^2. Current guidance for atrium smoke management system design [20, 40] suggests that fire densities, Q/A_{burner}, between 0.25 and 0.75 MW/m^2 are acceptable approximations to typical commercial and retail fire loads in atria. Outside of this range, the plume produced by the fire will have different dynamics and mass flow rates than a typical atria fire and will therefore inaccurately represent the approach flow and BSP mass flow rate. During the full-scale experimental program, fire sizes in the range of Q = 0.5 to 5.0 MW were used; the appropriate combination of burners were operated in each experiment to achieve fire densities between 0.25 and 0.75 MW/m^2.

2.3.4 Exhaust System

Various atrium smoke layer elevations were achieved in the full-scale experimental program using a mechanical smoke exhaust system located at the atrium ceiling. This system has a variable capacity of V_{exh} = 0 to 25 m^3/s and exhausts from the atrium through 16 horizontal circular vents located approximately 0.5 m below the atrium ceiling with a combined open area of 2.63 m^2. The range of exhaust system mass flow rates measured during the full-scale experimental program is between m_{exh} = 1 and 30 kg/s (Appendix A). Figure 5 illustrates the position of the circular exhaust system vents in relation to the fire compartment. The fact that these vents are not evenly distributed along the atrium ceiling or near its center is assumed to have no impact on the BSP flow dynamics. The CFD model of the experimental facility models the exhaust system using a single rectangular vent at roughly the same position as the circular vents but with a larger area. Specification of the atrium exhaust system in the CFD model of the experimental facility is described in Chapter 3. Smoke from the atrium smoke layer is exhausted to the exterior of the facility via a 1.22 m diameter duct. Details of the exhaust system instrumentation are contained in Section 2.3.5.

In addition to the primary airflow induced by the exhaust system, some secondary airflow occurred in the full-scale experimental facility. As described in Section 2.3.1, makeup air entered the atrium from underneath the north atrium wall in all experiments. The vertical opening above the adjustable curtain and louvers in the atrium east, south and west walls were used as gravity vents in selected experiments. In experiments where an opening was present at the top of the adjustable curtain, louvers were opened in the laboratory building surrounding the experimental facility to prevent smoke from accumulating in this building. Details of the louver and curtain opening configuration for each experiment are given in Appendix A.

2.3.5 Instrumentation

The full-scale facility was instrumented to allow measurement of the two primary dependent parameters identified in Section 2.1: BSP mass flow rate (m_{BSP}) and atrium smoke layer elevation (z_l). Additional instrumentation was used to either verify values of the heat release of the fire, Q, as the only non-geometric independent parameter identified in Section 2.2 or to provide more detailed data related to the characterization of BSP mass flow rates, such as vertical approach flow temperature profiles at the compartment opening. Data measured during the full-scale experiments was used in the CFD modeling effort either to define boundary conditions (for example, exhaust system mass flow rate) or for direct comparison to, and evaluation of, the simulation results.

Figure 8 shows top and elevation views of the experimental facility indicating the atrium instrumentation locations. Two vertical arrays of thermocouples are installed in the atrium to determine the atrium smoke layer elevation, one located on the compartment centerline at a distance of 21.0 m from the east atrium wall and a second 4.2 m north of the first array. In the discussion and figures which follow, these two thermocouple arrays are referred to as "atrium CL" and "atrium N", respectively. Each array consists of twenty thermocouples installed at equal spacings of 0.4 m, and extending from an elevation of 4.4 m to 12.0 m above the floor with the top thermocouple located 0.2 m below the atrium ceiling. Temperature data from these two thermocouple arrays were used to calculate the atrium smoke layer elevation, z_l, as described in Section 2.5. Two thermocouple arrays were installed in the atrium in order to assess the uniformity of the atrium smoke layer elevation, as discussed in Section 2.5.

Figure 9 shows top and elevation views of the fire compartment indicating the instrumentation locations. Three vertical thermocouple arrays are installed in the fire compartment: one at the compartment center above the burner system, a second one-quarter of the fire compartment width north of the first and a third one-quarter of the fire compartment width south of the first. The three fire compartment thermocouple arrays are referred to as "fire compartment CL", "fire compartment N" and "fire compartment S", respectively. The fire compartment arrays consist of six thermocouples each at elevations of 1.50, 2.50, 3.50, 4.00, 4.50 and 5.00 m. The three fire compartment arrays are intended for use in calculating the compartment smoke layer elevation; for the current research effort, they are used to evaluate the CFD predictions of conditions in the fire compartment. Three vertical thermocouple arrays were installed at the fire compartment opening, one at the centerline, a second one-quarter of the opening width north of the first and a third one-quarter of the opening width south of the first. The three compartment opening thermocouple arrays are referred to as "compartment opening CL", "compartment opening N" and "compartment opening S", respectively. Although Figure 9 shows the thermocouple array locations for an illustrative opening width of W = 10.0 m, these arrays were moved to maintain distances of W/4 north and south of the compartment opening center array as changes in W were made

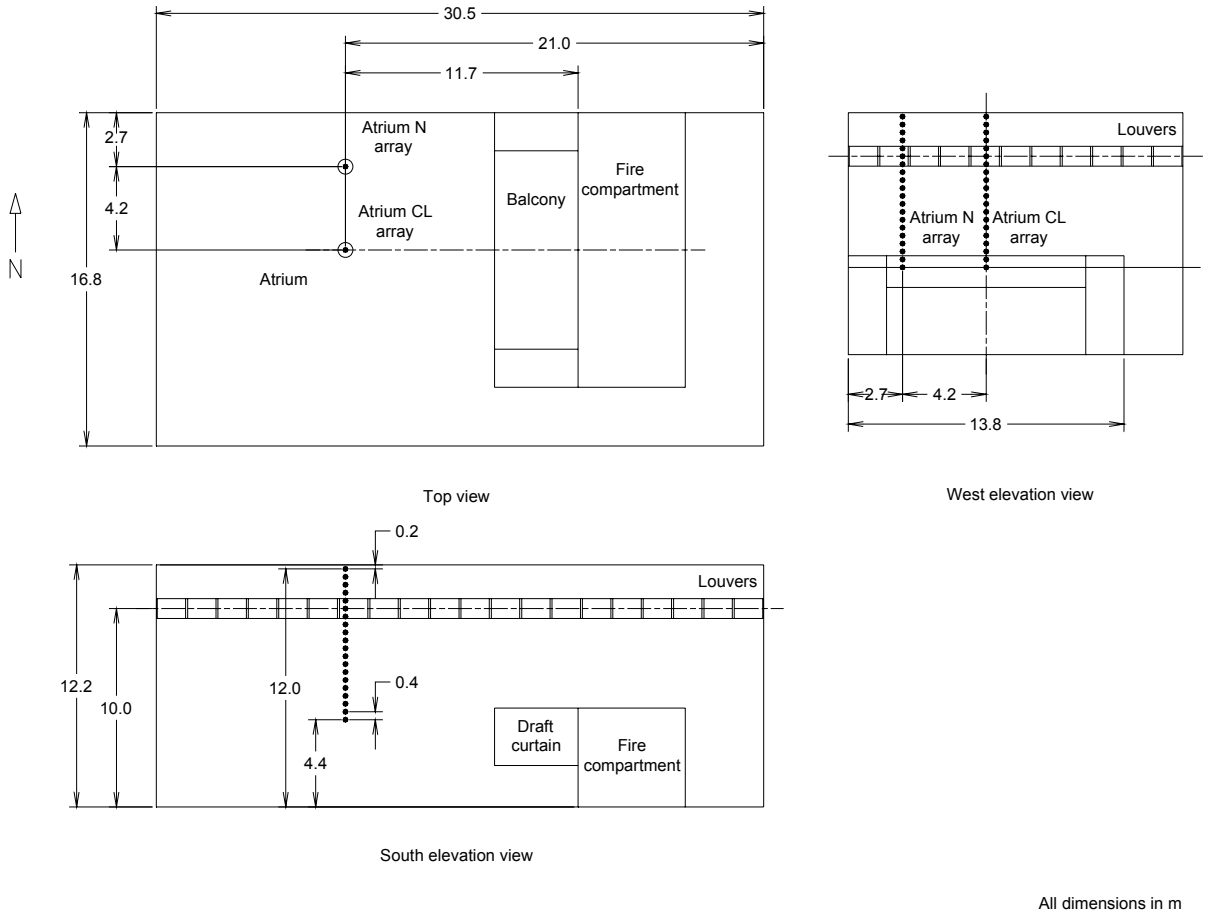

Figure 8. Instrumentation locations in full-scale experimental facility atrium.

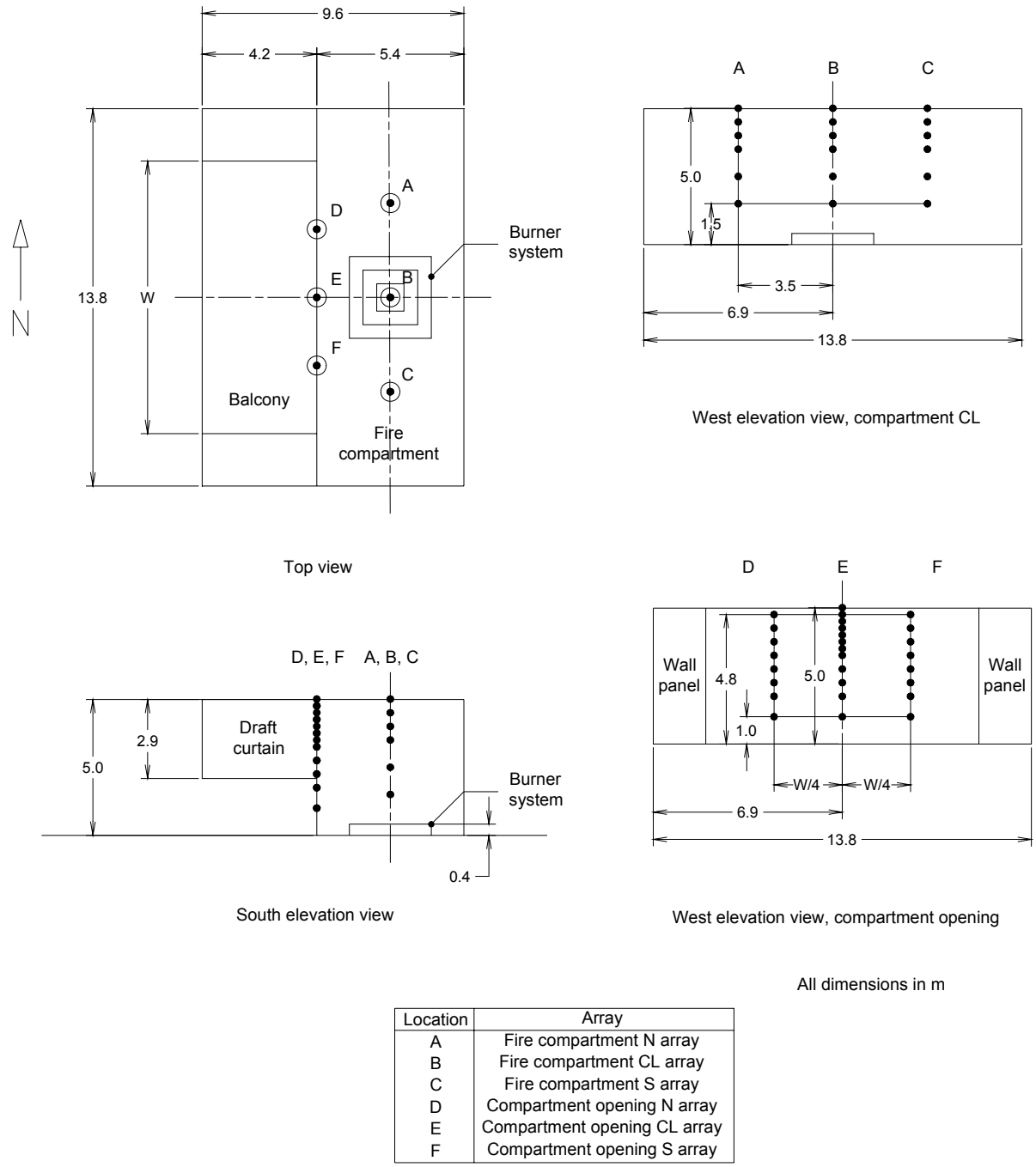

Location	Array
A	Fire compartment N array
B	Fire compartment CL array
C	Fire compartment S array
D	Compartment opening N array
E	Compartment opening CL array
F	Compartment opening S array

Figure 9. Instrumentation locations in full-scale experimental facility fire compartment.

during the experimental program. The compartment opening center array consists of twelve thermocouples located at elevations of 1.00, 1.75, 2.25, 2.75, 3.25, 3.50, 3.75, 4.00, 4.25, 4.50, 4.75 and 5.00 m. The north and south compartment opening arrays each consist of eight thermocouples at elevations of 1.00, 1.75, 2.25, 2.75, 3.25, 3.75, 4.25 and 4.75 m. The elevations of the thermocouples on all three compartment opening arrays are reduced by 1.6 m when the compartment opening fascia is present, causing the lowest thermocouple on each array to give invalid data. The three compartment opening arrays are intended for use in calculating the approach flow depth, d_{balc}, at the compartment opening. In the current research, they are used to evaluate the CFD predictions of temperatures at the fire compartment opening.

All thermocouples used in the full-scale experimental facility are Type K beaded 24 ga without shielding or other radiation compensation. The inherent precision of these thermocouples is assumed to be ± 2˚C [44]. The effect of thermocouple time lag on the temperature data is removed by temporally averaging the data over a steady-state period (Section 2.5). The impact of radiation on the temperatures measured in the fire compartment is discussed in Section 2.6.

The atrium exhaust system mass flow rate, m_{exh}, is measured using a pitot tube, micromanometer and two thermocouples installed in the exhaust duct. The combined measurement error gives a typical error range for m_{exh} of approximately ± 5% over the range of m_{exh} = 0 to 30 m^3/s. Oxygen, carbon dioxide and carbon monoxide concentrations in the exhaust duct are measured in an attempt to measure the heat release rate, Q, of the propane burner fire using the oxygen depletion calorimetry technique [1]. The resulting estimates of Q are clearly inaccurate and are therefore omitted from further analysis or discussion.

The propane flow rate through the burner system is measured using rotameters. This data is used to calculate the heat release rate of the fire, Q, assuming complete combustion of the propane. Combined uncertainties in the propane physical properties and measurement errors associated with the rotameters yield a typical error in the heat release rate estimates, Q, of approximately ± 10%. Due to the infeasibility of the oxygen depletion calorimetry technique [1] described above, values for Q are obtained solely from the propane flow measurements.

Most of the data from the full-scale experiments, including all of the temperature data, is recorded simultaneously at 2 s intervals using a computer-based data acquisition system. The propane pressure and flow rate are visually determined and were monitored every few minutes to ensure that the propane flow rate was steady. The times at which the exhaust system flow rates were changed were manually recorded for later use in defining time intervals over which to average the data (Section 2.5). Limited video and still camera footage was taken during selected experiments.

2.4 Experimental Procedure

Eighty-five experiments were conducted in NRC's full-scale experimental facility using various combinations of fire size and compartment geometry. Appendix A gives a complete list of the experiments including the values of the independent parameters identified in Section 2.2. In general, each experiment was conducted using a single fire size, constant compartment geometry and six different exhaust system mass flow rates in order to achieve five steady-state atrium smoke layer elevations, z_l. Nominal exhaust system mass flow rates of m_{exh} = 1, 5, 10, 15, 20 and 25 kg/s were used in all experiments, although slight variations occurred due to changes in the ambient temperature. During each experiment, the exhaust system flow rate was changed every 500 s since preliminary experiments showed that the atrium smoke layer elevation required this amount of time to achieve a steady-state value. A steady-state atrium smoke layer elevation was assumed to occur after the time at which a plot of temperature data from the atrium thermocouple arrays vs. time appeared visually flat, ignoring turbulent variations. A more rigorous check of steady-state conditions was performed during the analysis of the experimental data (Section 2.5).

Before each experiment, the compartment geometry was modified including the opening width, fascia depth and draft curtain depth. The opening at the top of the adjustable curtain and the louvers in the atrium and surrounding laboratory building were adjusted as required. Instruments were checked and calibrated if they indicated measurements which differed from normal ambient conditions. The exhaust system was set to its lowest mass flow rate of 1 kg/s. Data was collected approximately 60 s prior to ignition of the burner system to record one minute of ambient background data. The burner system was ignited manually at a low level and increased to the steady-state fire size, Q, over a period of two to three minutes. The exhaust system flow rate was then maintained for approximately 500 s to allow a steady-state atrium smoke layer to form, then was increased to the next highest setting. Smoke bombs were placed under the burner during selected experiments to allow visualization and photography of the BSP flow. After all exhaust flow rate settings had been achieved, the propane burner system was extinguished and data collection was terminated.

2.5 Results

The following quantities measured during the full-scale experimental program were compared to results from the CFD models of the experimental facility: vertical profiles of temperatures in the fire compartment and at its opening, vertical profiles of atrium temperatures and atrium smoke layer elevations determined from the atrium temperatures. This section presents typical examples of each of these quantities taken from the experimental data and discusses their features. Parameters for all of the experiments are listed in Appendix A. Individual experiments as referred to by number (for example, B4138-063).

Figure 10 and Figure 12 plot the temperature data from the fire compartment center thermocouple array and the compartment opening center thermocouple array for one representative experiment (B4138-063). The other four thermocouple arrays located in the fire compartment and at its opening demonstrate similar trends and are not plotted here. As illustrated most clearly in Figure 12, after an initial transient period where the temperatures in the fire compartment are stabilizing, all of the temperatures in the fire compartment, including at its opening, are relatively constant if turbulent fluctuations are ignored. This is not as clear in Figure 10 since the highly turbulent compartment fire plume induces much larger fluctuations in the temperatures measured by the compartment center thermocouple array. Figure 11 and Figure 13 plot the same data as in Figure 10 and Figure 12, respectively, but focused on the period between 3000 and 3500 s in order to illustrate the temperature fluctuations measured at the fire compartment center and compartment opening center. Comparison of Figure 11 and Figure 13 confirm that the magnitudes of the temperature fluctuations measured in the fire compartment are up to thirty times greater than those measured at the compartment opening. The relative stability of temperatures at all locations within the fire compartment indicates that changes in the exhaust system mass flow rate during each experiment do not affect temperatures in the fire compartment. Accordingly, profiles for each of the three thermocouple arrays in the fire compartment and each of the three arrays at the fire compartment opening can be represented by one average profile for each experiment. Figure 14 and Figure 15 illustrate such average compartment temperature profiles for the same experiment as Figure 10 and Figure 12, but including the other four thermocouple arrays omitted from these earlier figures (refer to Figure 9 for instrumentation locations). Temperature data from each thermocouple is averaged between 1000 s after the start to the end of the experiment to yield a single temperature value for each experiment.

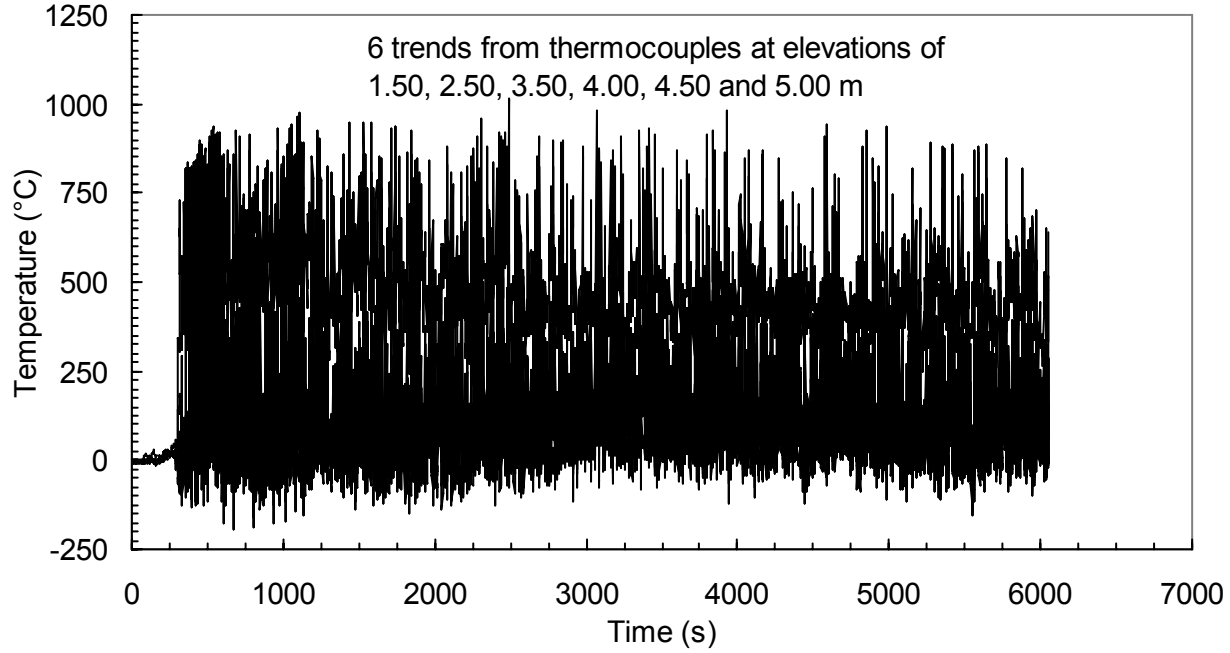

Figure 10. Typical temperature data from the fire compartment center array (B4138-063).

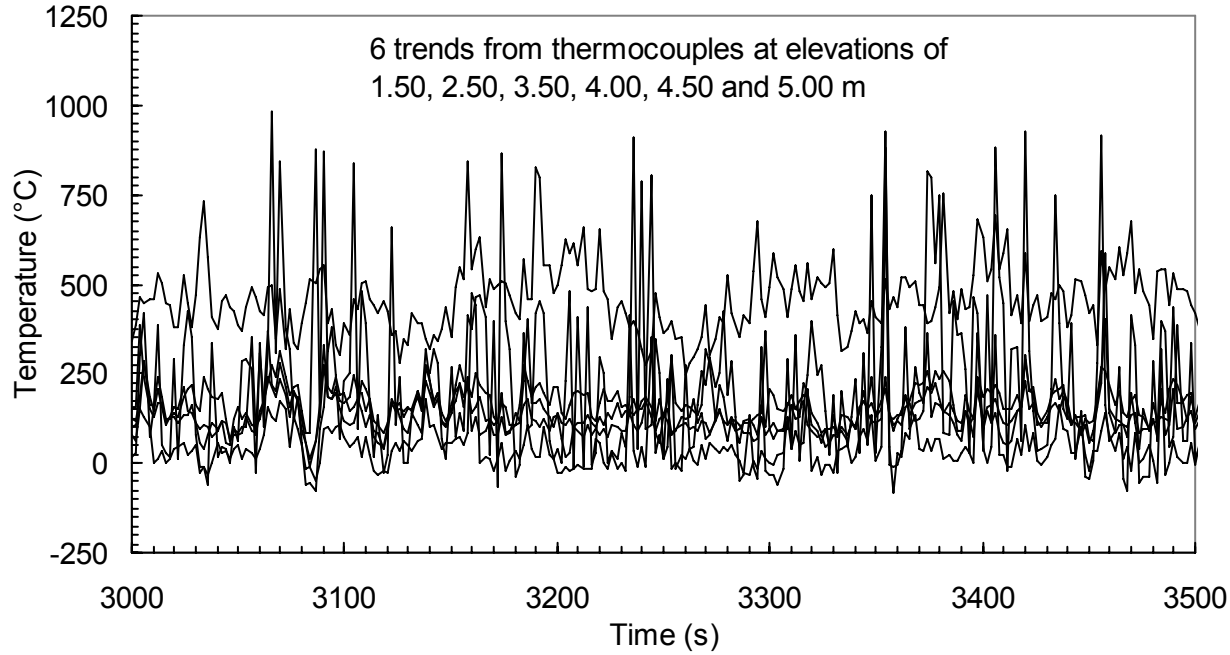

Figure 11. Typical temperature data from the fire compartment center array with expanded timescale (B4138-063).

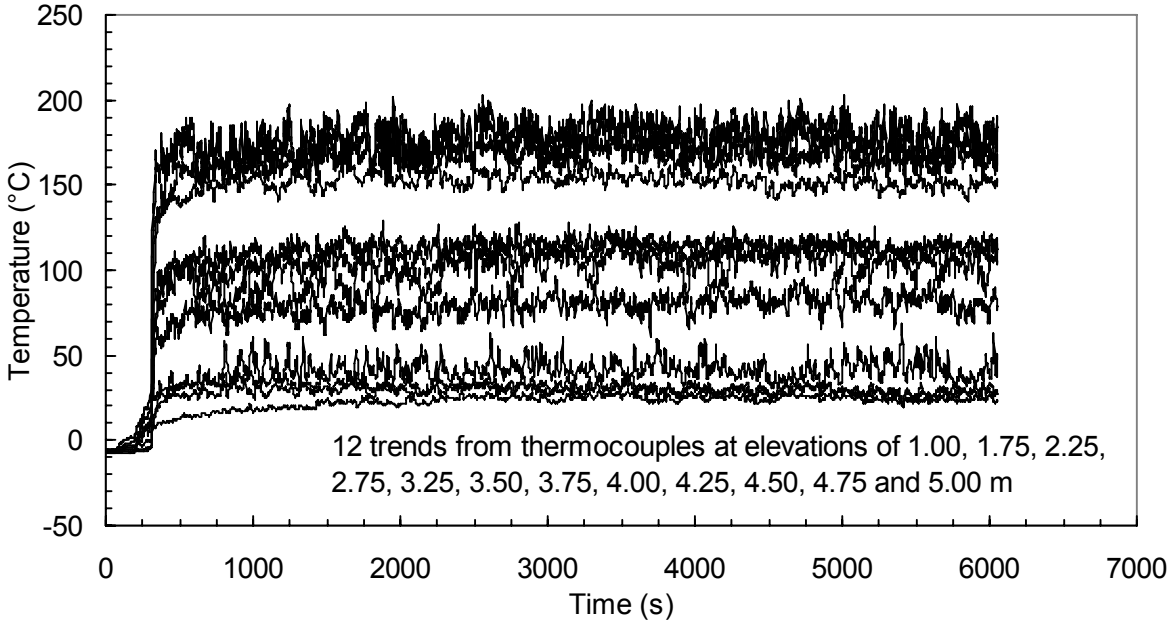

Figure 12. Typical temperature data from the compartment opening center array (B4138-063).

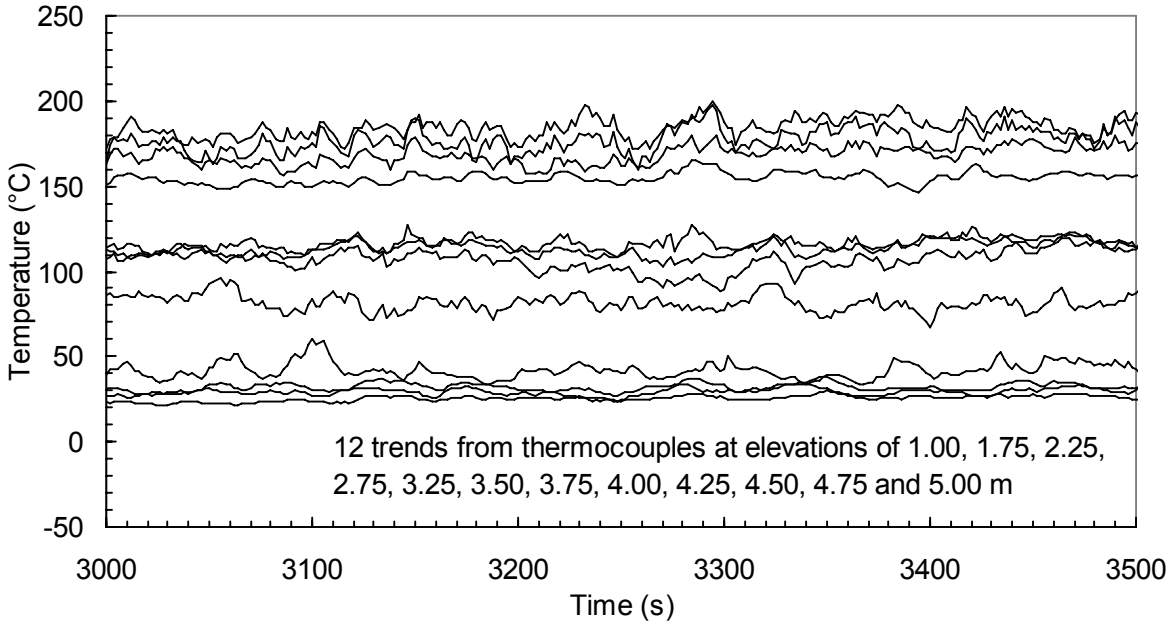

Figure 13. Typical temperature data from the compartment opening center array with expanded timescale (B4138-063).

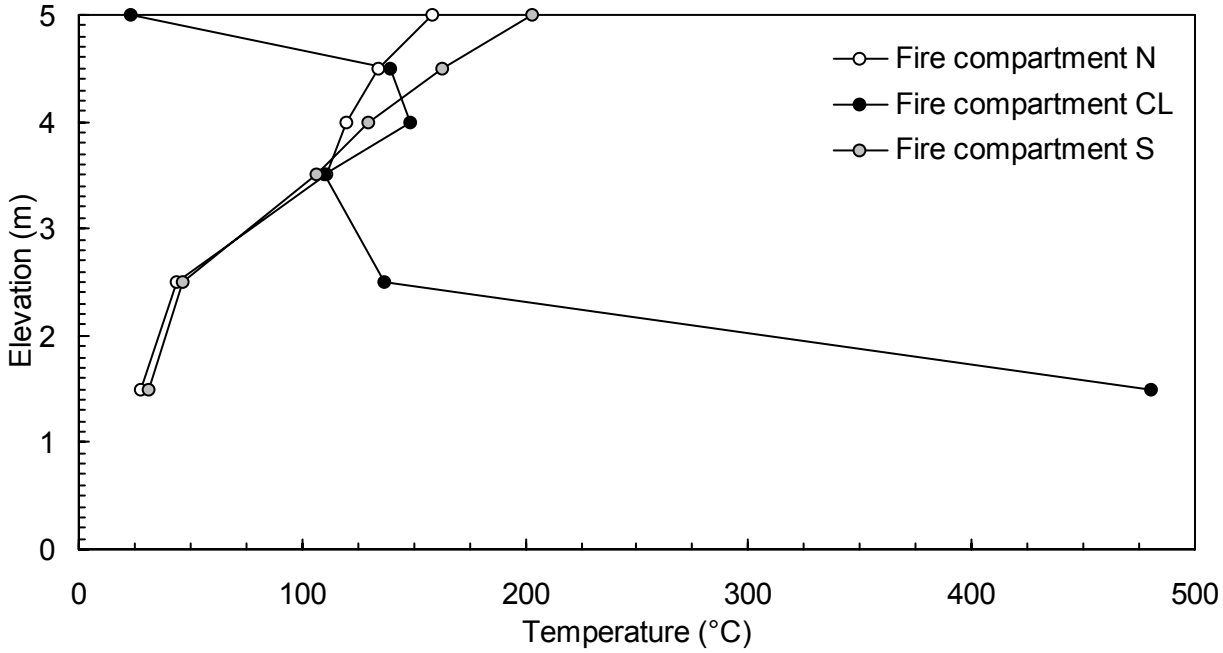

Figure 14. Typical average temperature profiles in the fire compartment (B4138-063; Ref: Figure 9).

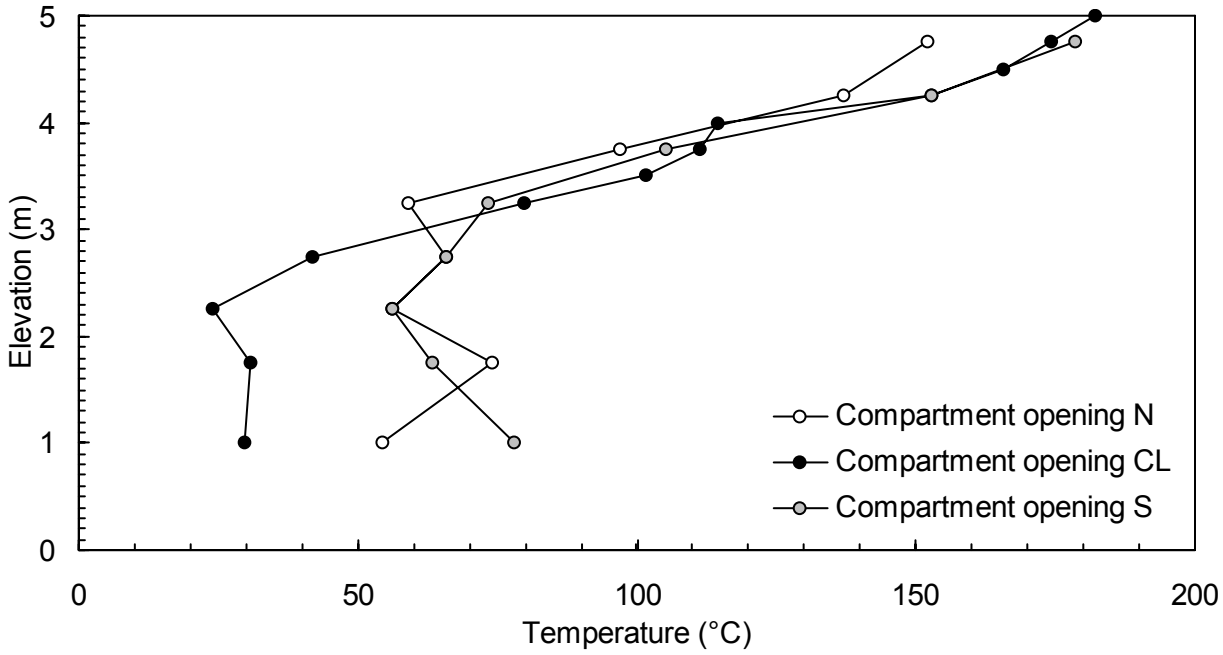

Figure 15. Typical average temperature profiles at the compartment opening (B4138-063; Ref: Figure 9).

In general, both the fire compartment and compartment opening temperature profiles exhibit a cold layer at lower elevations indicating the temperature of the makeup air entering the fire compartment and a hot layer at higher elevations with nearly linear temperature increases indicating the temperature of the hot gases from the fire. The exception to this behaviour is for the center fire compartment array which exhibits the opposite behaviour i.e. higher temperatures at lower elevations. These thermocouples are immersed in the fire and its plume and therefore indicate temperatures much higher than in the rest of the compartment. For the remaining five temperature profiles, the relative depth of the hot and cold layers and the maximum hot layer temperature will vary with both fire size, Q, and compartment opening width, W. Figure 16 and Figure 17 show the vertical temperature profiles for the three fire compartment arrays and the three compartment opening arrays for two experiments. Experiment B4138-058 was conducted with Q = 1.0 MW and W = 10.0 m, yielding relatively low temperatures across all six arrays. Experiment B4138-042 was conducted with Q = 5.0 MW and W = 5.0 m, yielding much higher temperatures for all six arrays compared to experiment B4138-058. The values for fire size, Q, and compartment opening width, W, in experiments B4138-058 and B4138-042 are at the extreme ends of their respective ranges, therefore the fire compartment and compartment opening temperature profiles for all other experiments are expected to range between those shown in Figure 16 and Figure 17.

Temperature data from the two vertical arrays of thermocouples installed in the facility atrium are used to determine the atrium smoke layer elevation, z_l, for each specific combination of fire size, compartment geometry and exhaust system mass flow rate, m_{exh}. Figure 18 shows a typical plot of temperatures from the atrium center array during the course of an experiment (B4138-063). In general, the highest temperature values are recorded by the thermocouples at the highest elevations. The temperature data from each thermocouple exhibits considerable fluctuations over time due to variations in the flow caused by changing the exhaust system flow rate, mixing between the hot BSP and ambient environment and turbulent flow within the atrium. The variation in the temperature data at higher elevations is greater than that at lower elevations, indicating that the degree of mixing and turbulence in the atrium smoke layer is greater than that in the atrium cold layer. Although difficult to see, Figure 18 indicates that each atrium thermocouple follows a decreasing stepped profile caused by the stepped increases in atrium exhaust system mass flow rate during each experiment at times indicated by the vertical lines. The close groupings of individual temperature trends in Figure 18 at high and low elevations delineate the atrium hot gas/smoke layer and cold layer, respectively, where vertical temperature gradients (dT/dz) are relatively low. The larger variations between individual temperatures at intermediate elevations indicate the transition region between atrium smoke and cold layers where the vertical temperature gradient (dT/dz) is relatively high. The temperature data in Figure 18 indicates that the atrium smoke layer elevation increases in steps and the average atrium smoke and cold layer temperatures decrease in steps as

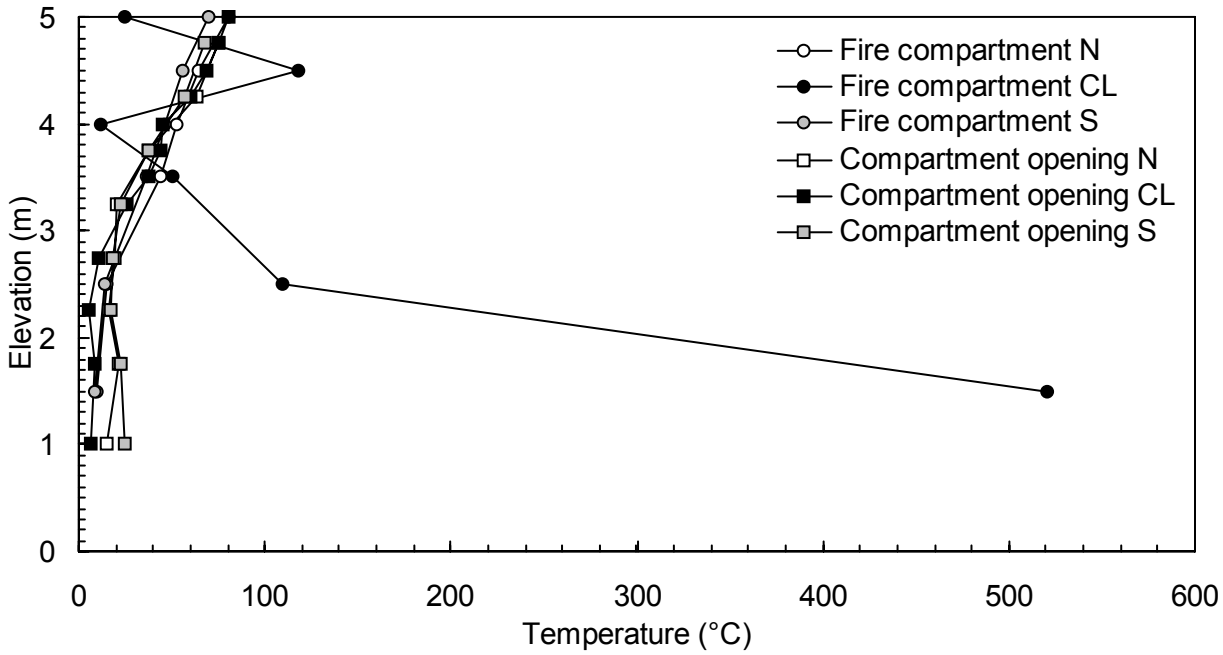

Figure 16. Temperature profiles in the fire compartment (B4138-058: Q = 1.0 MW, W = 10.0 m).

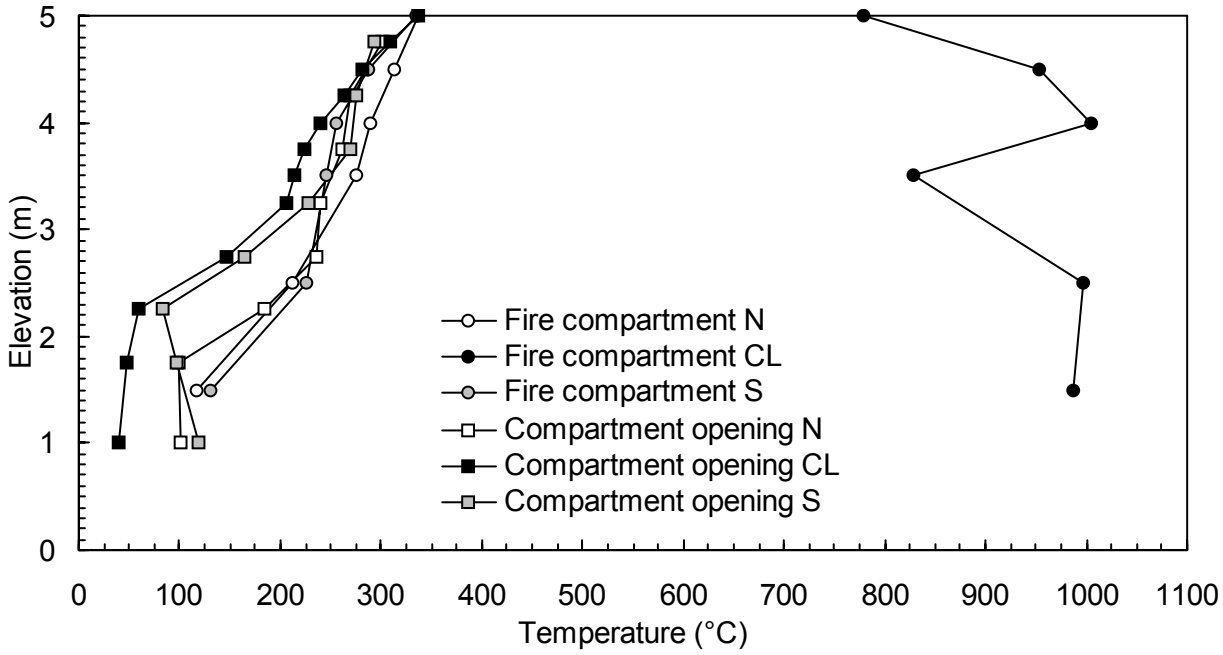

Figure 17. Temperature profiles in the fire compartment (B4138-042: Q = 5.0 MW, W = 5.0 m).

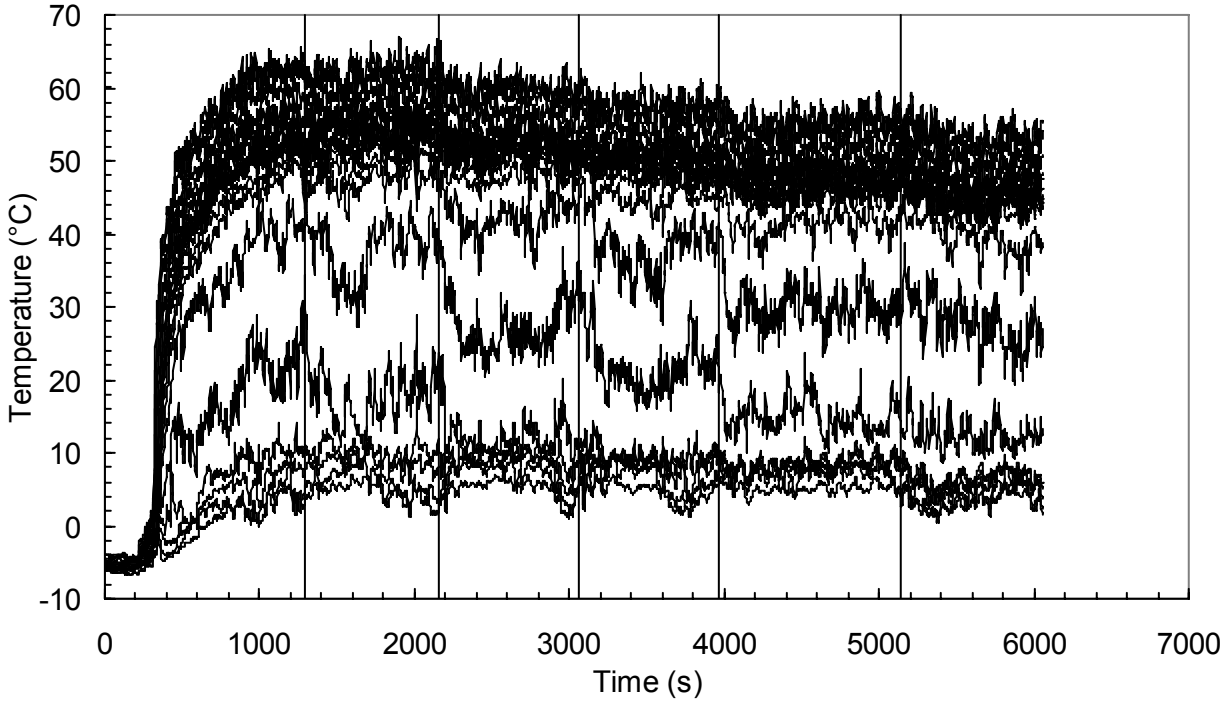

Figure 18. Typical temperature data from atrium CL thermocouple array (B4138-063).

the exhaust flow rate is increased in each experiment. These trends are more clearly illustrated after the raw atrium temperature data has been processed, as described below.

Instead of calculating z_l as a transient quantity throughout each experiment, a single steady-state value is determined for each exhaust system mass flow rate from an average vertical profile of atrium temperatures. During each experiment the exhaust system flow rate, m_{exh}, was varied approximately every 500 s to achieve a series of steady-state atrium smoke layers. A vertical temperature profile is obtained for each m_{exh} setting by averaging the temperature data from each atrium CL thermocouple over a 30 s period beginning 90 s before the end of each m_{exh} setting. To ensure that the temperature data is sufficiently steady-state during this period, a linear regression is applied to the data over the last 12 s of each averaging period for all thermocouples on the atrium CL array in all experiments. Figure 19 illustrates this procedure graphically for a single atrium thermocouple in experiment B4138-065. The temperature recorded by a thermocouple on the atrium CL array at an elevation of 12.04 m is shown as a grey continuous line in all three plots. The temperature trend in Figure 19 a) exhibits a downward spike at approximately 4200 s which is larger in magnitude than the majority of fluctuations in the temperature data. Such spikes in the atrium temperature data are attributed to instrumentation error caused by the impact of electrical noise on the thermocouples. These errors occur rarely (<0.5% of total temperature

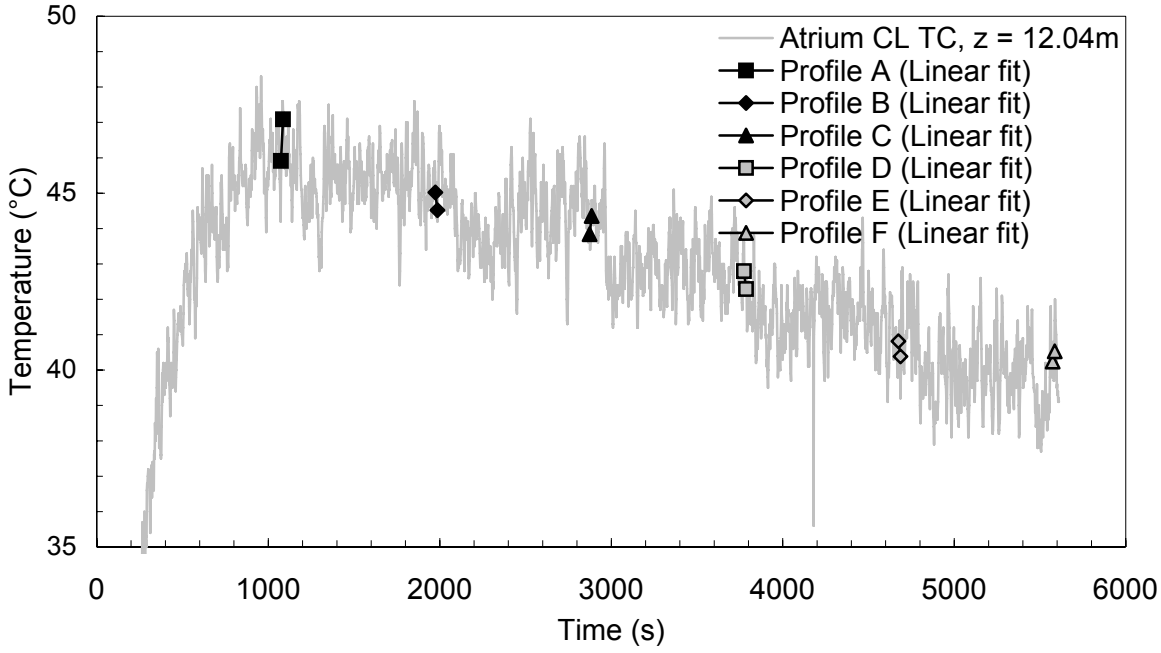

a) temperature data over entire experiment (B4138-065)

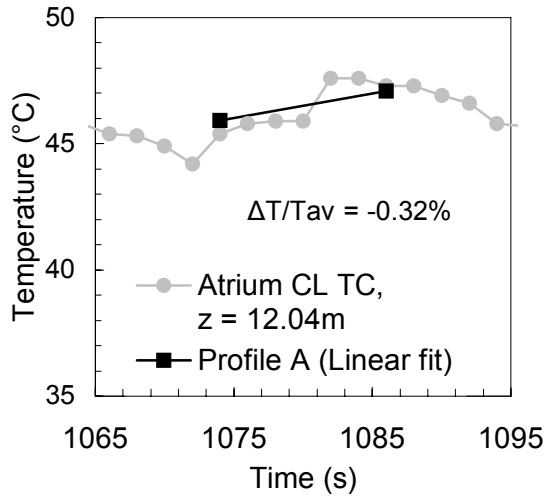

b) closeup of a) for end of exhaust mass flow rate setting A

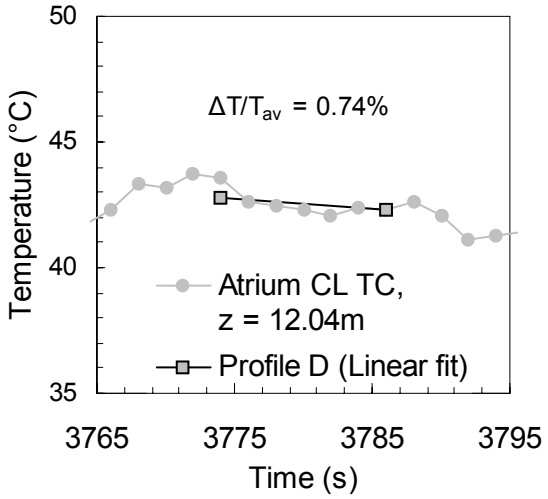

c) closeup of a) for end of exhaust mass flow rate setting D

Figure 19. Example of steady-state determination of atrium temperature data for thermocouple at z = 12.0 m using linear regression over the last 12 s for each exhaust mass flow rate setting (B4138-065).

measurements) and are therefore assumed to have a negligible effect on the atrium temperature trends. Line segments determined via linear regression to the temperature data in each 12 s averaging period are labelled A through F in Figure 19 a). The bottom two plots (b), c)) show a subset of the data from the upper plot focused on the 12 s averaging periods at the end of the first (A) and fourth (D) m_{exh} settings. The variation of the temperature during this 12 s period (ΔT), as determined by the slope of the line segment, is divided by the average temperature during the same period (T_{av}) to give an indication of how steady-state the temperature is during this period. The temperature data is considered steady-state if the ratio $\Delta T/T_{av}$ is below an arbitrary limit of 5%. Applying this method to all of the full-scale experimental data indicates that the vast majority of atrium temperature data was steady-state over a 30 s period beginning 90 s before the end of each m_{exh} setting.

Figure 20 and Figure 21 show the average atrium CL temperature profiles from experiment B4138-039 (Q = 0.5 MW, W = 5.0 m) and experiment B4138-082 (Q = 5.0 MW, W = 12.0 m), respectively, for each exhaust system mass flow rate. The BSP in experiment B4138-039 produced some of the shallowest atrium smoke layers in the experimental program; a visual estimate of atrium smoke elevation from Figure 20 yields $z_l \approx 7.5$ to 9.0 m above the floor, or 2.5 to 4.0 m above the balcony elevation. Conversely, the smoke layers for experiment B4138-082 are among the deepest obtained during the experimental program with $z_l \approx 5.5$ to 6.0 m above the floor. These two experiments are chosen to show the range of atrium smoke layer elevations obtained during the full-scale experimental program. Both figures demonstrate the increase in z_l and decrease in average temperature for the atrium smoke and cold layers as m_{exh} is increased. The transition regions between the smoke and cold layers are much deeper for the profiles shown in Figure 20 than those in Figure 21, making it difficult to visually determine values of the atrium smoke layer elevation, z_l. This is attributed to the greater buoyancy and stronger stratification produced by the larger fire size in experiment B4138-082 (5.0 MW) compared to experiment B4138-039 (0.5 MW). The temperature profiles in Figure 21 have shallow transitions regions from which z_l may be easily estimated, but it is difficult to determine the variation of z_l with m_{exh} due to the close clustering of the profiles. To calculate a single value for z_l for each of the average atrium temperature profiles produced in the full-scale experimental program, three established algorithms to estimate z_l from a vertical profile of temperature data exist: percentage [8], maximum slope [13, 7] and integral [46]. Application of these algorithms to the average atrium temperature profiles proved inconclusive in determining a single value of z_l, therefore the vertical profiles of averaged experimental temperature data were used in subsequent comparisons to results from the CFD simulations (Section 3.3.2).

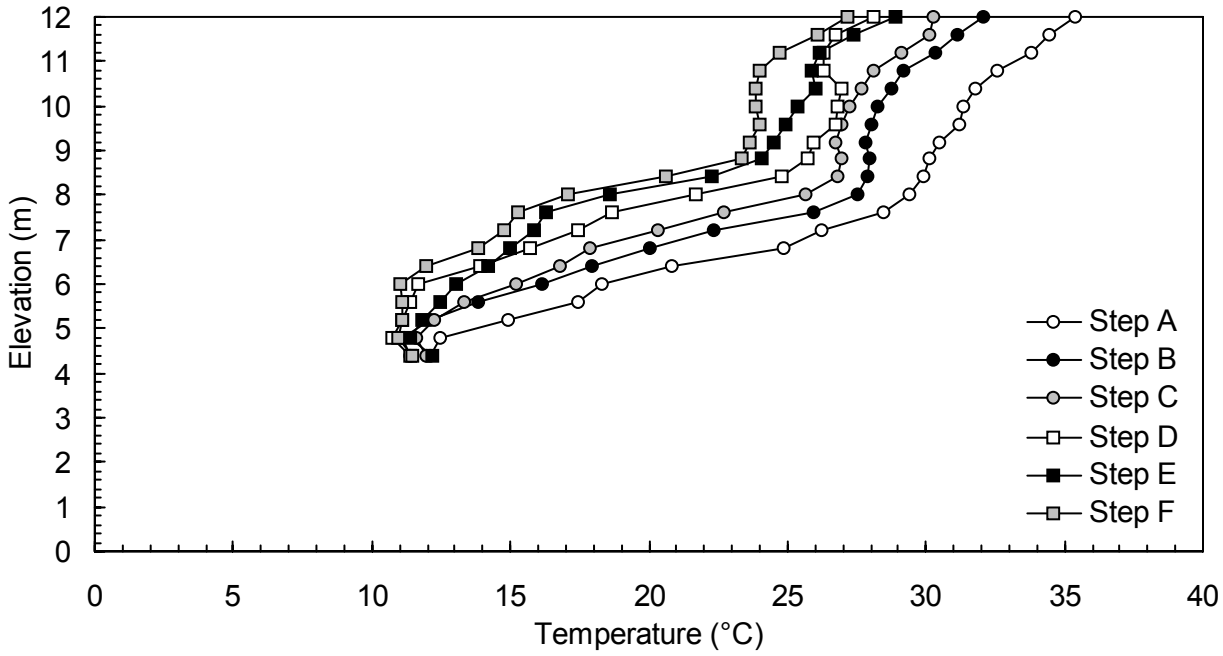

Figure 20. Typical average atrium temperature profiles for a shallow atrium smoke layer (B4138-039).

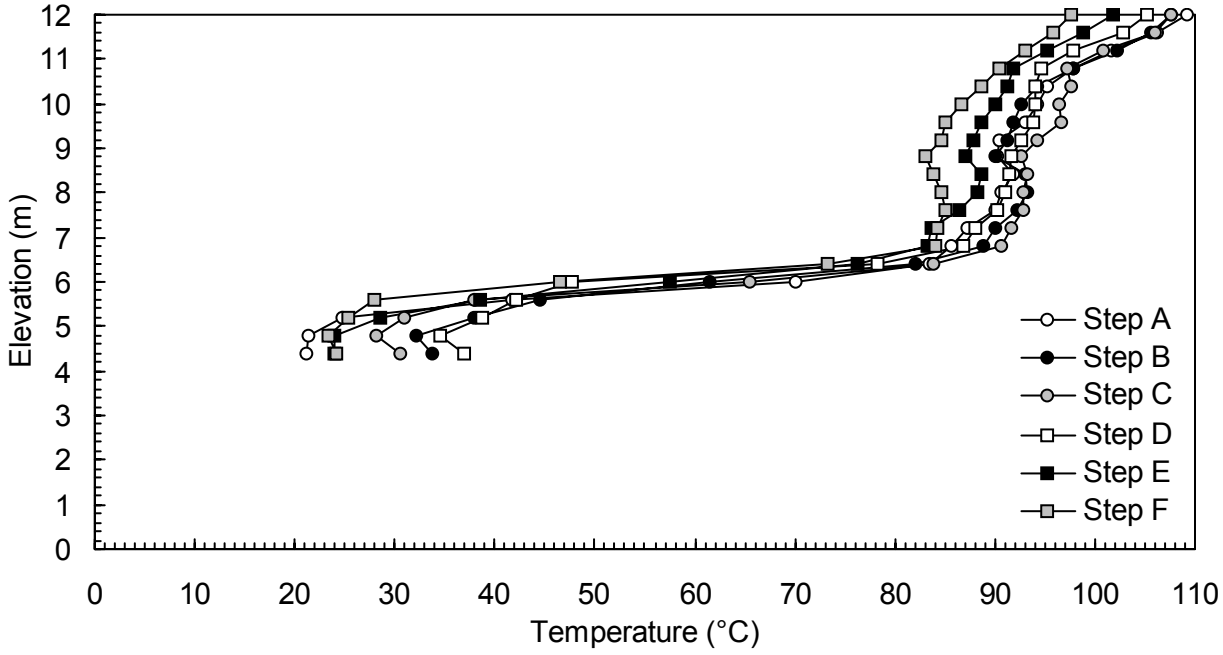

Figure 21. Typical average temperature profiles for a deep atrium smoke layer (B4138-082).

The two atrium thermocouple arrays from the full-scale experimental program are used to assess the uniformity of the atrium smoke layer elevation. Experimental data from Marshall and Harrison [32] and CFD modeling data from Miles et al. [36] show that non-uniform atrium smoke layers can affect the accuracy of the measured $m_{BSP} = f(z_l)$ profiles. The north atrium array is also used to indicate experiments where the atrium smoke layer elevation was low enough to be affected by the opening under the north atrium wall. Specifically, if smoke from the atrium smoke layer exited through this opening, the temperatures in the north atrium would be colder and the atrium smoke layer elevation would be lower than that at the atrium centerline if the latter position is assumed to be far enough away from the north atrium wall opening to avoid being affected by smoke leakage under the north atrium wall. Figure 22 illustrates the differences between the atrium north and centerline temperature profiles for experiment B4138-024 (Q = 2.0 MW, W = 5.0) during the portion of the experiment where the exhaust system flow rate was 24.7 kg/s. Experiment B4138-024 exhibits some of the largest total differences between the atrium centerline and north temperature profiles. The lower temperatures for the atrium north profile shown in Figure 22 compared to the atrium center profile indicate that smoke is exiting the atrium under the north atrium wall. The data from such cases were excluded from comparisons with the CFD simulation results due to possible inaccuracies introduced by smoke leakage. Further, due to inconsistencies in the atrium north temperature profiles, only the atrium center temperature profiles are compared with results from the CFD simulations (Section 3.3.2).

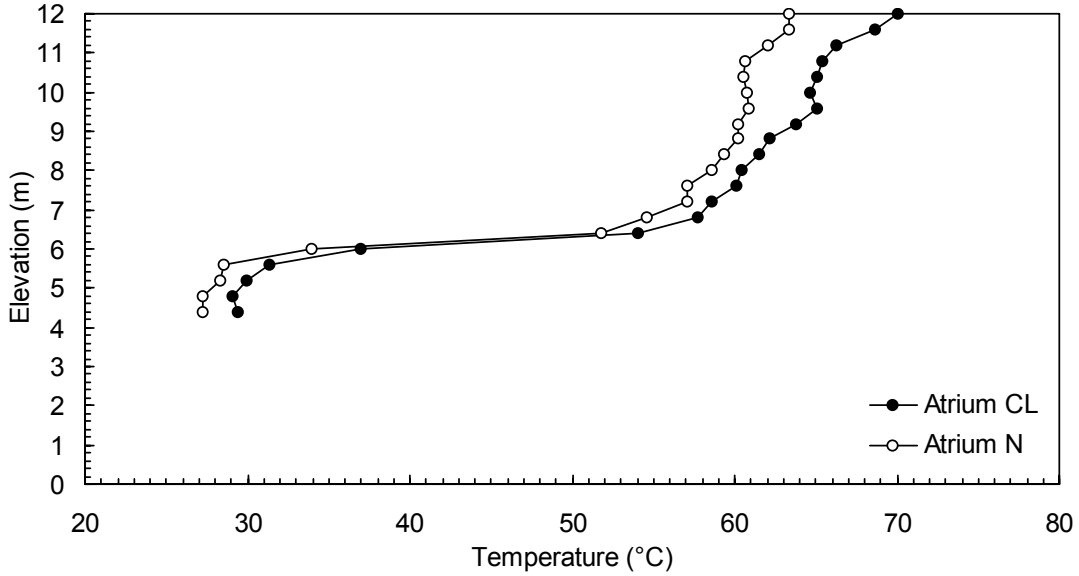

Figure 22. Example of difference in atrium CL and N temperature profiles due to smoke leakage under north atrium wall (B4138-024, m_{exh} = 24.7 kg/s).

2.6 Assumptions and Limitations

A number of assumptions and limitations may impact the use of data from the full-scale experiments in evaluating the CFD model of the experimental facility. These issues are briefly discussed here.

In selected experiments where the BSP mass flow rate exceeded the capacity of the exhaust system, smoke was allowed to exit the atrium through the curtain opening and/or atrium louvers to effectively increase m_{exh}. These experiments are identified in Appendix A. The mass flow rate of smoke through the curtain opening and louvers was not measured; these values are estimated based on expressions for the flow of buoyant smoke from a rectangular opening [49]. As required, these estimates are added to the measured exhaust flow rates, m_{exh}, from the experiments to infer the BSP mass flow rates, m_{BSP}. These curtain openings and louvers are modeled as openings in the CFD model of the experimental facility, therefore, the mass flow rate of smoke through them should be accounted for automatically, and as accurately, as any other calculations of mass flow rate in the model.

The thermocouples used in the full-scale experimental program were not shielded, aspirated or otherwise compensated for the impact of radiation on measured temperature. The atrium thermocouples are assumed to be sufficiently removed from the fire and any heated fire compartment surfaces ($\geq$ 21.0 m) such that error in measured temperature due to the effects of radiation is neglected. Temperature data in the fire compartment and at the compartment opening will certainly be affected by radiation but are not directly used to determine atrium smoke layer elevation. Comparisons of the compartment temperatures from the full-scale experimental program to results from the CFD model should, however, take this radiation error into account.

The full-scale experimental program represents the first effort to measure BSP mass flow rates at full-scale, addressing one of the limitations of the current body of BSP research discussed in Chapter 1. This experimental data is used in development and evaluation of the CFD model of the experimental facility described in Chapter 3. However, the maximum BSP elevation measured in the full-scale experimental program was still quite low, approximately 9 m above the atrium floor and 4 m above the balcony (Figure 20). This is not sufficient to fully address the lack of high-elevation BSP mass flow rate data, but does prove useful in development of the CFD model of BSP behaviour at high elevations described in Chapter 4.

2.7 Summary

The full-scale BSP experimental program conducted at NRC generated data which defines a set of $m_{BSP} = f(z)$ profiles for a range of typical fire sizes, compartment geometries and exhaust flow rates. This data will be used to evaluate existing, and develop new methods, to estimate BSP mass flow rate as a function of fire size, compartment width, compartment opening fascia depth, draft curtain depth and elevation. In the context of the present research, data from this experimental program is used to evaluate the CFD model of the experimental facility described in Chapter 3.

Chapter 3 CFD Models of the Experimental Facility

Two of the major limitations of the existing body of BSP research identified in Chapter 1 are the lack of full-scale data for BSP mass flow rates and the lack of data for BSP mass flow rates in high-elevation atria i.e. $h_{atr} \geq 10$ m. Both limitations put the accuracy of existing methods for estimation of BSP mass flow rates into question. The full-scale experimental program described in Chapter 2 addresses the first limitation, but, as discussed in Section 2.6, does not provide BSP mass flow rate data for elevations greater than 4 m above the balcony elevation. A numerical modeling study of BSP mass flow rates at high elevations (Chapter 4) was therefore conducted in order to address the second limitation of the existing body of BSP research. As a necessary first step in the development of the high-elevation BSP model, two CFD models of the full-scale experimental facility, the first of the fire compartment and the second of the entire experimental facility, are developed and evaluated. This chapter first discusses the CFD software used to model the combustion and buoyancy-driven flows in the current research. The development and evaluation of the two CFD models of the experimental facility is then described. Vertical profiles of temperatures in the fire compartment and at its opening, vertical profiles of atrium temperatures and average temperatures in the atrium smoke and cold layers are compared to the CFD results to evaluate the CFD software and modeling methodologies used, as well as to identify limitations of the models and the CFD software with which they are implemented.

3.1 Fire Dynamics Simulator (FDS)

The CFD software chosen to model the BSP experimental facility is Fire Dynamics Simulator (FDS), available from the National Institute of Standards and Technology (NIST) [34, 35]. FDS was chosen primarily because it allows development of a large eddy simulation (LES) model of the full-scale experimental facility and includes many sub-models which are tailored specifically for use in simulating full-scale building fires. FDS is widely used in the fire research and engineering communities due to its accessibility, apparent simplicity and open source nature which allows modifications and improvements to be made relatively easily. An informal survey of FDS users conducted by NIST in 2005 found over 45 applications of FDS to the analysis of smoke movement due to fires within buildings, 20 of which focused on the design and evaluation of atrium smoke management systems [10]. FDS is specifically designed to model unconfined, reacting fluid flows and includes mechanisms for modeling combustion chemistry, radiation, smoke production and transport, and fuel pyrolysis. Low Mach number combustion equations [47] optimized for low-speed, buoyancy-driven flows are used to reduce computational

requirements. An explicit predictor-corrector scheme with second order temporal and spatial accuracy is used. Spatial derivatives are approximated by second order central differences.

FDS models turbulence using a Smagorinsky form LES turbulence model [50]. The application of LES turbulence models to buoyant fire plumes is intended to increase the temporal and spatial accuracy of predicted flow properties compared to those from Reynolds-averaged Navier-Stokes (RANS) turbulence models, albeit with increased computational requirements [11]. Such improvements have been neither proven nor refuted by a direct comparison of buoyant fire plume properties predicted by LES and RANS models. A limited comparison by Chow and Yin showed only that the two turbulence models predicted comparable mass flow rates in the axisymmetric plume produced by a 470 kW fire [6]. LES treatments model turbulence by directly calculating the flow properties due to eddies larger than the control volume size (i.e. grid-scale eddies). Eddies smaller than the control volume size (i.e. subgrid eddies) represent the turbulent part of the flow and are modeled approximately. Modeling of the subgrid eddies is typically assumed not to significantly affect the accuracy of the flow properties calculated at the grid scale. Since LES does not perform temporal or spatial averaging of the fluid dynamics conservation equations, the accuracy of the predicted flow properties increases steadily as control volume sizes are reduced. In contrast, RANS turbulence models (for example, k-ε) are fundamentally limited in their application to the modeling of buoyant fire plumes since their temporal averaging of the fluid dynamics conservation equations leads to an artificial smoothing of the predicted flow properties. This smoothing does not disappear completely as control volume sizes are decreased since the smallest resolvable length scales are determined by the product of the local velocity and the averaging time rather than the control volume size. Application of RANS turbulence models to buoyant fire plumes does not accurately model their characteristic large eddy structure, which in turn will inaccurately predict entrainment into the plume. Of the CFD modeling studies of BSP behaviour reviewed in Section 1.1.4, all use RANS-based k-ε turbulence models except for the study by Harrison [19] which makes use of the Smagorinsky form LES turbulence model incorporated in FDS.

FDS approximates the conservation equations on a rectilinear grid, which is well-suited to the geometry of the experimental facility (Figure 5, Figure 6). FDS v.4.00 allows the use of multiple grids and/or transformed grids with varying control volume sizes to selectively refine the grid(s) in critical regions of the flow. Grid transformations are limited to two co-ordinates in any single three-dimensional grid. The grid designs for the CFD models of the experimental facility make use of both multiple and transformed rectilinear grids, as described in Sections 3.2.1 and 3.3.1. The grids designed for CFD models of the fire compartment and experimental facility typically increase the control volume resolution above the burner to more accurately model the combustion in the fire compartment. The grids are not refined near the fire compartment or atrium boundaries to resolve the boundary layers nor at the BSP boundaries to resolve the

motion of entrained air into the BSP. The grids used in the CFD models developed as part of this thesis are described in more detail in Sections 3.2.1, 3.3.1 and 4.2.

Standard boundary conditions can be implemented in FDS including open vents, symmetry planes and thin and thick wall conduction. Solid surfaces are assigned thermal boundary conditions and parameters describing the ignition and burning characteristics of the material (for example, ignition temperature, heat release rate and density). Tabulated materials property data are typically used to define these parameters. For LES simulations, heat and mass transfer to and from solid surfaces are calculated using empirical correlations. Specific boundary condition combinations used in the CFD models of the experimental facility are described in more detail in Sections 3.2.1 and 3.3.1.

Control volume sizes in LES simulations of fires in buildings are generally not small enough to accurately resolve the diffusion of fuel and oxygen using a global one-step, finite-rate chemical reaction algorithm. Accordingly, FDS uses a mixture fraction model [2] to model combustion chemistry. Mixture fraction is a conserved scalar quantity defined as the fraction of gaseous fuel at a given point in the flow field. Fires are modeled as injected masses of fuel which react with oxygen in the flow domain. Mass fractions of the major reactants and products are calculated from the mixture fraction via state relations which are in turn derived from a combination of simplified analyses and experimental data. These state relationships are used to determine where sufficient fuel and oxygen are available to support combustion. Where combustion can occur, mixing-controlled combustion and infinitely fast fuel oxidation are both assumed and heat generation is calculated based on the heat of combustion of the fuel. The mixture fraction model can also account for conditions that would inhibit combustion, including oxygen depletion and temperatures below the ignition temperature for a specific fuel-air mixture. The mixture fraction model is assumed to be sufficiently accurate for the propane fires simulated in all of the CFD models developed as part of this thesis. Due to the effects of numerical diffusion, the mixture fraction combustion model will inaccurately estimate heat release rates if the combustion zone is inadequately resolved [35].

FDS models radiative heat transfer by solving the radiation transport equation for a non-scattering grey gas; an optional wide band radiation model is also available. The radiation equation is solved by applying a finite volume method, similar to that used for convective transport, over approximately 100 discrete angles. Solution of the radiation equation requires approximately 15% of the total computational time for a simulation [34]. FDS assumes a constant radiative fraction for a given fuel, which is one of the major approximations in the radiation model since actual radiative fractions vary with flame temperature and combustion product concentrations. FDS' default value of $\chi = 0.35$ is used in the majority of the CFD simulations conducted as part of this thesis. For a CFD model of BSP flow dynamics, the accuracy of

radiation estimates from the fire will primarily affect the compartment temperatures and the mass flow rate of the approach flow exiting the compartment. Radiation effects should not directly impact the accuracy of BSP mass flow rate estimates since the majority of the BSP mass flow is contributed by air entrained into the plume in the atrium.

CFD simulations involving combustion and buoyancy-driven flows in buildings typically require grids with large numbers of control volumes due to the wide range of length scales which characterize the underlying chemical and physical processes. Since combustion processes occur at length scales smaller than 10^{-3} m and building geometries typically range on the order of 10^{2} m, the dynamic range (i.e. ratio of largest to smallest eddy length scales) required for accurate modeling of all relevant combustion and fluid flow processes is approximately 10^{5}. Current workstations can conduct CFD simulations in reasonable amounts of time (i.e. on the order of days rather than weeks) for grids with the number of control volumes in the range 10^{6}. Converting from a control volume (m^3) to an eddy length scale (m) yields a practical dynamic range on the order of approximately 10^{2}, or three orders of magnitude less than that required for accurate modeling of all combustion and fluid flow processes. In general, the use of larger control volumes in LES simulations leads to lower predicted temperatures and velocities throughout the flow domain, which in turn affect the accuracy of predicted radiative and convective heat transfer [35]. Most CFD simulations of fires in buildings use grid(s) which produce more accurate estimates of fluid flow in areas of the flow domain beyond the combustion zone. Nonetheless, the resulting lack of accuracy in modeling the combustion zone is deemed acceptable in most cases since accurate modeling of the flame front and detailed modeling of multiple combustion products is not the main objective in most building fire simulations. The grid designs used in the CFD simulations conducted as part of this thesis follow this methodology, and therefore model the fire in the compartment less accurately than the fluid flow in the rest of the atrium. This is justified because the current research is primarily focused on predicting BSP behaviour in the atrium, not the fire dynamics within the compartment.

Table 3.1 lists the default values for selected FDS parameters used in the CFD simulations conducted as part of this thesis. Several of these parameters were varied in specific simulations to evaluate the impact of these parameters on the CFD simulations (Sections 3.2.2, 3.3.2). Unless otherwise noted, the parameter values in Table 3.1 are used.

Parameter	Value
Turbulence model	LES
Smagorinsky coefficient, C_s	0.20
Radiation model	Non-scattering grey gas
Fuel properties	Propane: m_{mol} = 44.00 g/mol, H_{comb} = 47 251 kJ/kg, χ = 0.35
Combustion model	Mixture fraction
Ambient air temperature	20 °C
Thermal and ignition properties of surfaces (Table 3.2)	Inert

Table 3.1. Default values for FDS parameters used in the experimental facility and high-elevation BSP CFD models.

Numerical data is generated by FDS either at discrete points in the flow field (for example, temperature, velocity) or over specific areas or volumes (for example, mass flow rate, heat release rate). Specific details of the data recorded for each of the CFD simulations conducted as part of this thesis are given in Sections 3.2.1, 3.3.1 and 4.2. FDS allows temperature data in the flow domain to be represented as either the predicted gas temperatures or as the temperatures that would be recorded by a theoretical spherical thermocouple in an equivalent gaseous environment [34]. These two temperatures are related via an expression for heat transfer to a sphere from a surrounding gas at elevated temperature [56] which in effect compensates for an estimated radiation error in thermocouple measurements of temperature. Particularly in the fire compartment, the radiation correction algorithm should allow the full-scale experimental data, which consists of temperatures recorded with radiation error, to be more directly compared to data from the CFD simulations; an illustration of this algorithm's accuracy is given in Section 3.2.2. The Smokeview [12] program distributed with FDS displays simulation results graphically, allowing visualization of flow dynamics.

FDS is capable of modeling all of the key physical processes which determine BSP flow dynamics: buoyancy, turbulent entrainment, combustion, and heat transfer via radiation and convection. Although FDS requires physical boundaries to be defined using a rectilinear grid, this limitation does not impact its ability to simulate BSP behaviour in atria with simple geometries, such as that in the full-scale experimental facility (Figure 5). The modeling capabilities of FDS are therefore well-suited to

development of CFD models of BSP behaviour in simple atria, which justifies the use of this software in the current research effort. Since FDS is also gaining popularity with designers of atrium smoke management systems [10], identification of its potential strengths and limitations in modeling buoyant plume flows typically encountered during atrium fire scenarios is an important secondary justification for its use in the current research effort. The numerical modeling studies described in Section 3.2, Section 3.3 and Chapter 4 assess the use of FDS in modeling BSP flow dynamics, or more generally, buoyant plumes in atria.

3.2 Fire Compartment Modeling Study

This section describes a modeling study of the full-scale experimental fire compartment conducted using FDS. The CFD model of the fire compartment is described as well as its evaluation using data from the full-scale experimental program. Results from CFD simulations of the fire compartment are used to determine the optimal grid design and resolution for accurate modeling of fire dynamics in the compartment. Accurate modeling of the compartment fire dynamics affects the accuracy of predicted temperatures and airflows in the fire compartment and is a necessary precursor to accurate modeling of the BSP in the CFD model of the full-scale experimental facility. A limited number of CFD simulations of the fire compartment are conducted to aid in preliminary grid design for the CFD model of the full-scale experimental facility (Section 3.3). It also serves to build expertise in the use of FDS and in the interpretation of the simulation results. Finally, the fire compartment modeling study demonstrates the sensitivity of the FDS predictions to different modeling methodologies such as specification of the burner surface and thermal properties of the fire compartment boundaries.

3.2.1 CFD Model of the Fire Compartment

The geometry used for the CFD model of the fire compartment is shown in Figure 23. Dimensions were specified to a precision of 0.001 m to allow exact placement of measurement positions within the model. The compartment is 13.844 m wide by 5.385 m deep by 4.985 m high to match the dimensions of the full-scale experimental fire compartment (Section 2.3.2). The compartment opening width, W, is either 13.844 or 12.000 m, depending on the actual experimental configuration being modeled, and is specified as an open boundary condition. No balcony is modeled since the flow domain is constrained to the fire compartment interior. The compartment boundaries are modeled as solid surfaces with zero thickness and thermal and ignition properties of either an ideal inert material or a typical concrete whose thermal properties are provided with FDS v.4.00 (Table 3.2). These properties are assumed to accurately approximate those of the real compartment boundaries since three of the compartment walls consist of steel insulated with ceramic fibre (i.e. inert) and the floor consists of concrete (Section 2.3.2). The fourth

wall, which defines the compartment opening, consists of uninsulated steel but is approximated as an inert material to match the other walls with the assumption that its small area relative to the other boundaries (6.8%) will limit any potential errors in predicted heat transfer and their effect on simulation results.

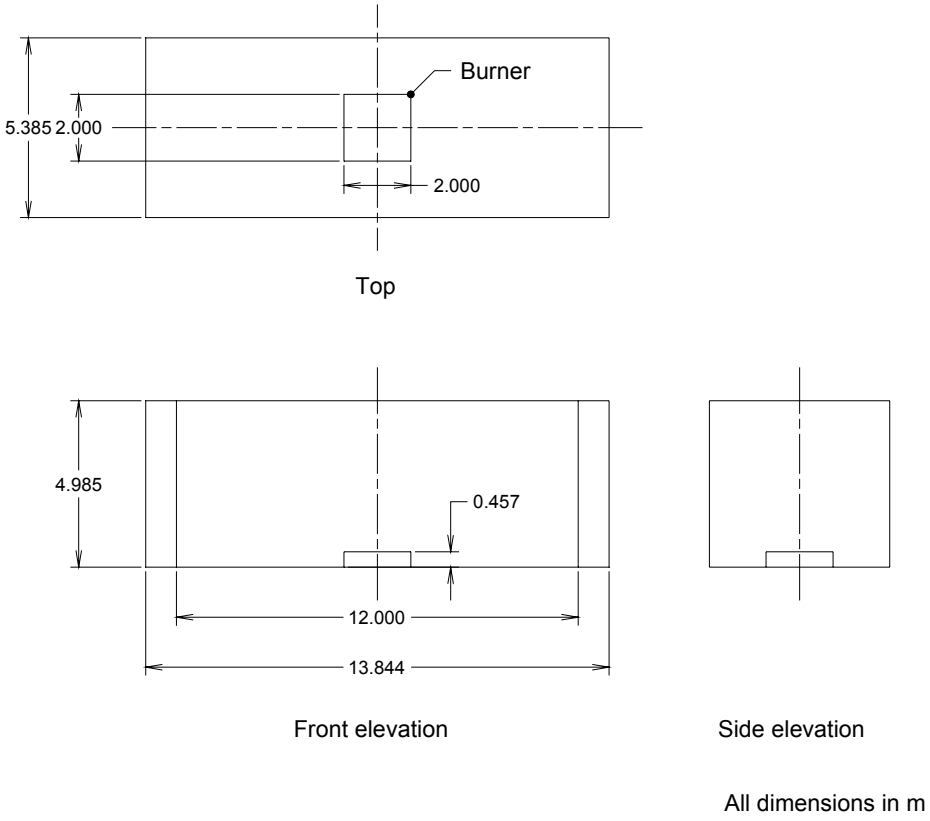

Figure 23. Geometry of the CFD model of the fire compartment.

The burner system is modeled as a fuel injection boundary condition over a 2 m by 2 m horizontal plane located at the center of the fire compartment at an elevation of 0.457 m. As shown in Figure 23, in certain simulations this elevated plane is extended to the compartment floor ($z = 0.000$ m) to form a rectangular volume whose top surface is specified as a fuel injection boundary condition. These two methodologies for modeling the fuel injection boundary condition are used to determine the impact of an elevated fuel injection boundary condition on the predicted fire compartment temperatures. A fire size of $Q = 2.0$ MW was modeled in all simulations by specifying a heat release rate per unit area of 500 kW/m^2 over the fuel injection boundary condition area of 4 m^2. Based on the specified heat release rate per unit area, FDS calculates the required mass flow rate of propane (kg/s) through the fuel injection boundary condition by assuming a constant heat of combustion for propane (kJ/kg) (Table 3.1).

Several grid designs for the CFD model of the fire compartment are evaluated to determine which yields the most accurate results with the least number of control volumes. The latter criterion directly affects the total computation time required for each simulation. The grid designs evaluated in the fire compartment modeling study differ through successively increased grid resolution in the combustion zone (i.e. above the fuel injection boundary condition) which is specified to increase the accuracy of the temperature, velocity and radiation heat transfer estimates in the developing fire plume. Figure 24 illustrates the four grid designs used in the fire compartment simulations: a) single, b) single transformed, c) double embedded and d) triple overlapping. Each grid design makes use of one, two or three main grids, each grid consisting of control volumes whose dimensions (Δx, Δy and Δz) may vary from those of other grids in the same design. The single grid design applies one grid over the entire flow domain with constant control volume dimensions. The single transformed grid design also makes use of one grid to define the flow domain but transforms this grid in the x and y directions to decrease the control volume dimensions near the burner. This grid transformation divides the compartment into nine sub-grids with varying control volume dimensions. The double embedded grid design defines one grid consisting of larger control volumes over the entire flow domain and a second grid embedded within the first over a plan area of 2.4 m by 2.4 m centered on the burner surface and consisting of smaller control volumes. The triple overlapping grid design defines three grids which slightly overlap, the first consisting of smaller control volumes centered on the burner surface and the second and third consisting of larger control volumes on either side of the first to define the remainder of the flow domain. The control volume dimensions in any single grid are constant except for the case of the single transformed grid where the nine sub-grids each have different control volume dimensions. Each grid design is used in a number of simulations with different control volume dimensions as indicated in Appendix B; the particular control volume dimensions shown in Figure 24 are for illustrative purposes only. In general, simulations were run with control volume dimensions varying between $\Delta = 0.05$ and 0.5 m.

Appendix B lists the parameters used in each of the CFD simulations of the fire compartment. Default values for the propane combustion properties, radiation model and ambient conditions listed in Table 3.1 are used for all simulations. Simulation times of 600 and 300 s were specified in simulations B4138-C01 and B4138-C02 respectively. Since temperature data from these simulations at selected points in the compartment appeared visually steady for $t \geq 120$ s when turbulent variations were ignored, simulation times of 120 s were chosen in subsequent simulations as representative of steady-state conditions. Temperatures are predicted at locations which closely match those of the instrumentation for the full-scale experimental fire compartment (Section 2.3.5, Figure 9) to allow evaluation using the experimental data. Velocities predicted at these locations are not used in the evaluation effort due to the lack of velocity data from the experimental program.

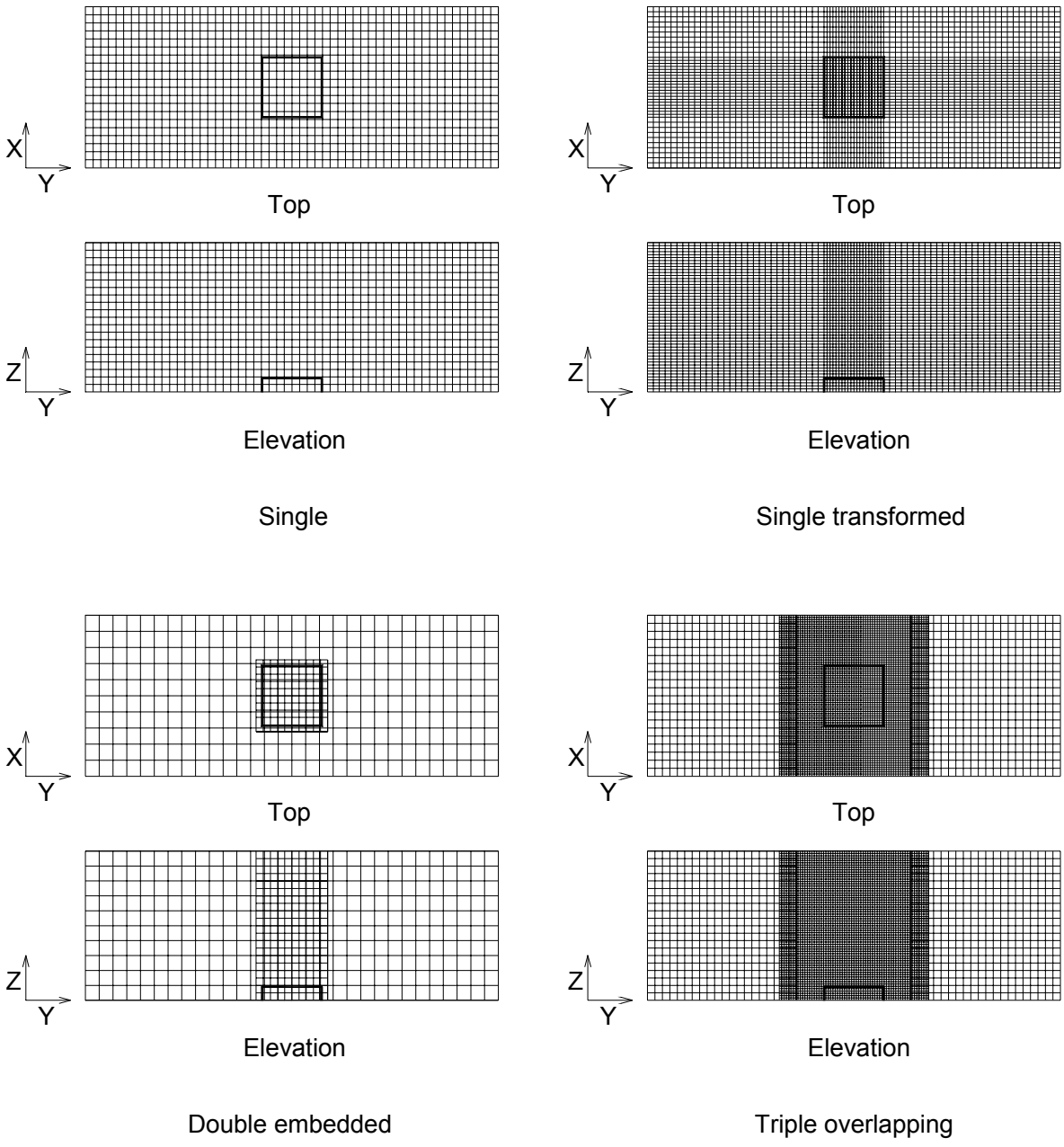

Figure 24. Grid designs for the CFD model of the full-scale experimental fire compartment.

3.2.2 Results

The ability of the CFD model to accurately predict fire compartment temperatures is evaluated using four sets of data from full-scale experiment B4138-003 (Q = 2.0 MW, W = 12.0 m): the average fire compartment CL and N temperature profiles and the average compartment opening CL and N temperature profiles. These profiles are generated by averaging each point temperature measurement in each simulation over the steady-state portion of the simulation, typically between t = 90 and 120 s. This procedure is similar to that applied to the full-scale experimental data to obtain average temperature profiles (Section 2.5). The fire compartment S and compartment opening S profiles are assumed to be very similar to the N profiles due to the symmetry of the CFD model and are excluded from further analysis and discussion. Appendix B contains plots of the fire compartment CL and N and compartment opening CL and N profiles for each of the CFD simulations of the fire compartment as well as for experiment B4138-003. Selected data from Appendix B is presented and discussed here to illustrate typical trends in the simulation results. CFD simulations of the fire compartment are referred to by number (for example, B4138-C07).

Comparisons between the fire compartment temperatures predicted in the simulations and those measured in the full-scale experiments would be facilitated if the effects of radiation on the predicted temperatures could be accurately estimated. Results from selected simulations are used to evaluate the accuracy of FDS' radiation correction algorithm [56] (Section 3.1) in estimating these effects. Figure 25 compares the fire compartment CL temperature profiles from two typical simulations (B4138-C08 and C09) to the profiles from experiment B4138-003. These two simulations differ only in the size of the control volumes used; $\Delta \approx 0.25$ m for simulation B4138-C08 and $\Delta \approx 0.10$ m for simulation B4138-C09 (Appendix B). The predicted fire compartment temperatures differ by as much as −750 °C compared to the experimental data. A second profile is shown for each CFD simulation that represents the temperatures obtained by applying the FDS radiation correction algorithm. This figure shows that applying the radiation correction algorithm to the predicted fire compartment CL temperatures does not appreciably improve the agreement between the CFD simulation results and the experimental data. In Figure 26, the compartment opening CL temperature profiles with and without radiation correction are compared to data from experiment B4138-003. In this case, applying the FDS radiation correction algorithm to predicted compartment opening CL temperatures slightly improves their agreement with the experimental data, but discrepancies of up to −50 °C remain between the simulation results and the experimental data. However, both simulations accurately predict the depth of the hot smoke layer exiting the compartment based on the opening CL temperature profiles (d_{balc} = 1.0 m, extending from z = 4.0 to 5.0 m). Figure 25 and Figure 26 both indicate that at certain elevations, the FDS temperature predictions, after radiation correction, are lower than the predicted temperatures of the surrounding gas, an apparently

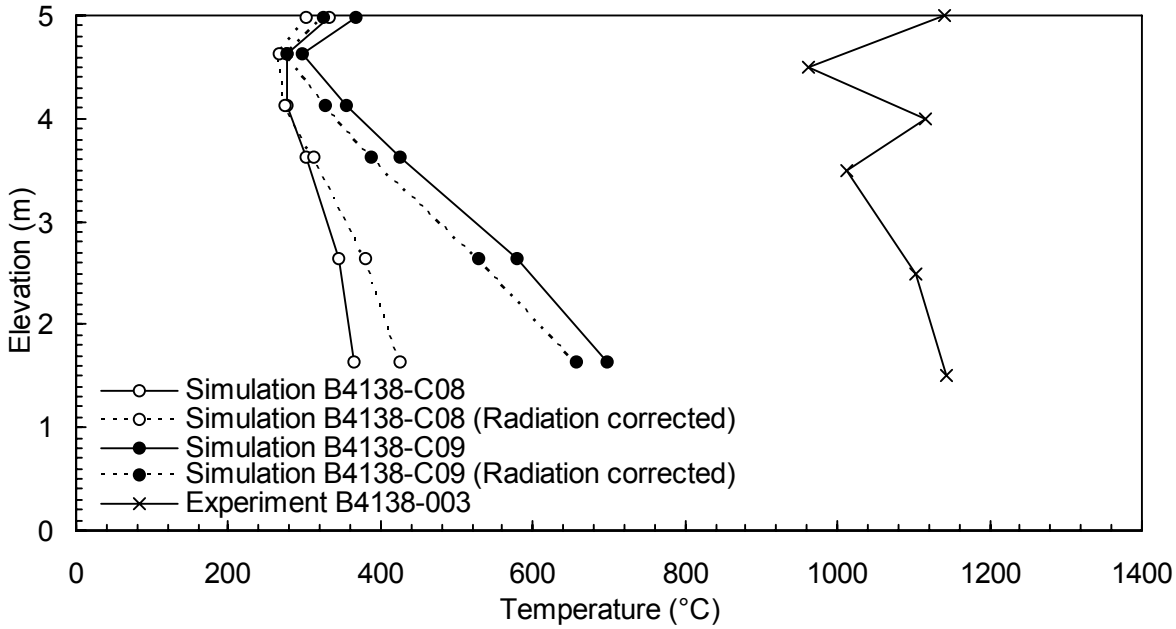

Figure 25. Comparison of fire compartment CL temperature profiles from CFD simulations and experiment B4138-003 with and without radiation correction.

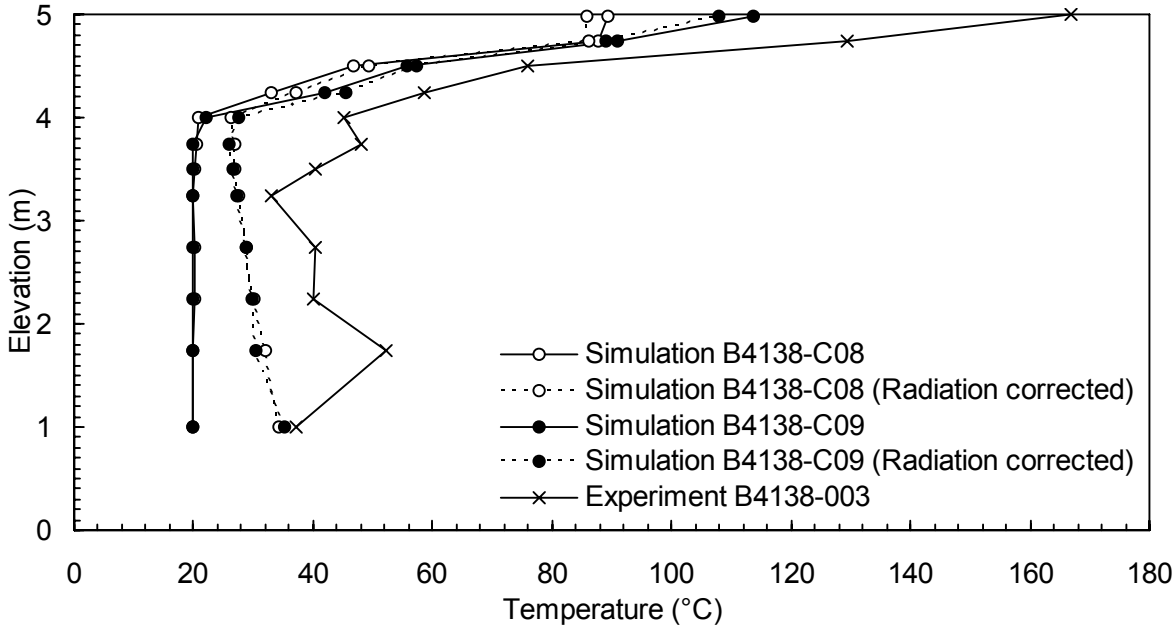

Figure 26. Comparison of compartment opening CL temperature profiles from CFD simulations and experiment B4138-003 with and without radiation correction.

physically unreasonable result. Figure 27 and Figure 28 plot the differences between the predicted thermocouple and gas temperatures for the fire compartment and compartment opening CL profiles for all simulations. Although most of the estimated thermocouple temperatures are higher than the gas temperatures, as would be expected with radiation feedback heating the thermocouple bead, the opposite trend occurs frequently, especially for the fire compartment CL profiles and at higher elevations for the compartment opening CL profiles. Negative differences between the thermocouple and gas temperatures even occur in simulations where the smallest control volume sizes are used for the combustion zone i.e. where predictions of radiative heat transfer from the fire to each thermocouple are expected to be most accurate. These discrepancies suggest that the radiation correction algorithm overpredicts the radiative heat loss from the thermocouple beads, possibly because compartment and atrium surface temperatures are underpredicted in the simulations compared to the experiments, leading to higher radiative heat loss from the thermocouple beads to these surfaces. Such apparently low estimates of thermocouple temperatures predicted by the CFD simulations may be due to inconsistencies in the radiation correction algorithm, violation of the assumptions under which it was developed for the particular CFD model presented here or additional unknown reasons. Regardless, the lack of an accurate method to account for radiation error in the CFD simulations makes any evaluation using the full-scale experimental data more difficult so that none of the CFD simulations of the fire compartment can be considered fully validated using the data from experiment B4138-003. The remainder of the evaluation effort for the CFD model of the fire compartment instead focuses on characterizing the effects of different modeling methodologies on the predicted results.

The size of the control volumes used in any CFD simulation affects both the numerical inaccuracies inherent in the predicted temperatures and velocities as well as the amount of computation time required to solve the simulation. To determine the optimal control volume size for modeling of the fire compartment, four simulations are conducted to evaluate the impact of control volume size on the predicted fire compartment temperatures. Simulations B4138-C07 through C09 and C13 each use the simplest grid design (single) with nominal control volume sizes of Δ = 0.5, 0.25, 0.1 and 0.075 m respectively. Figure 29 and Figure 30 show the predicted fire compartment CL and compartment opening CL temperature profiles for all four simulations. Figure 29 shows that decreasing the control volume size results in increased values of the fire compartment CL temperatures over the entire compartment elevation. This is attributed to more accurate modeling of the combustion in the fire compartment as control volume sizes decrease. The difference in the temperature profiles between simulation B4138-C09 ($\Delta(x,y,z) \approx 0.1$ m) and B4138-C13 ($\Delta(x,y,z) \approx 0.075$ m) is much less than the difference in the profiles between simulations B4138-C07 ($\Delta(x,y,z) \approx 0.5$ m) and B4138-C09 ($\Delta(x,y,z) \approx 0.1$ m). The similarity of the temperature profiles between simulations B4138-C07 and C09 indicates that decreasing control

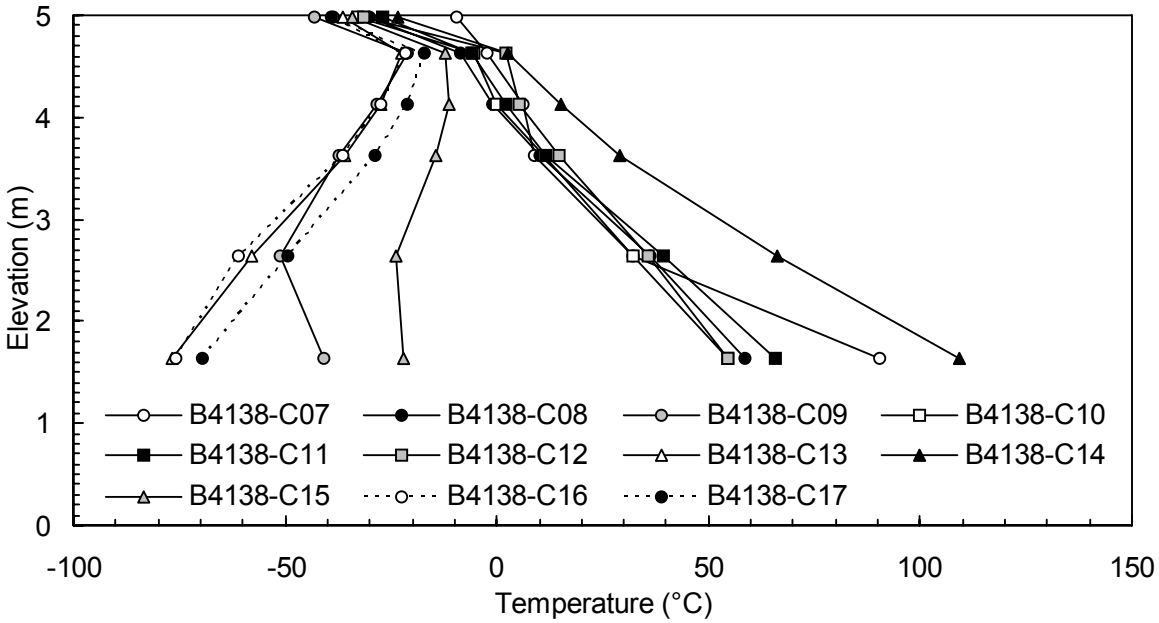

Figure 27. Differences between estimated thermocouple and predicted gas temperatures for fire compartment CL profiles.

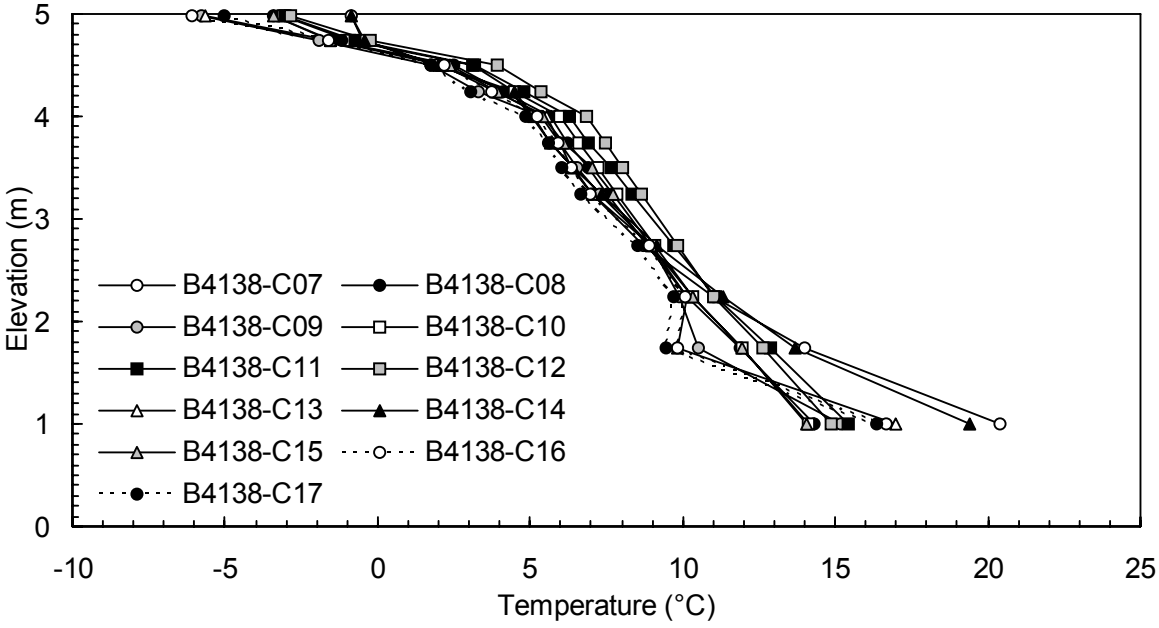

Figure 28. Differences between estimated thermocouple and predicted gas temperatures for compartment opening CL profiles.

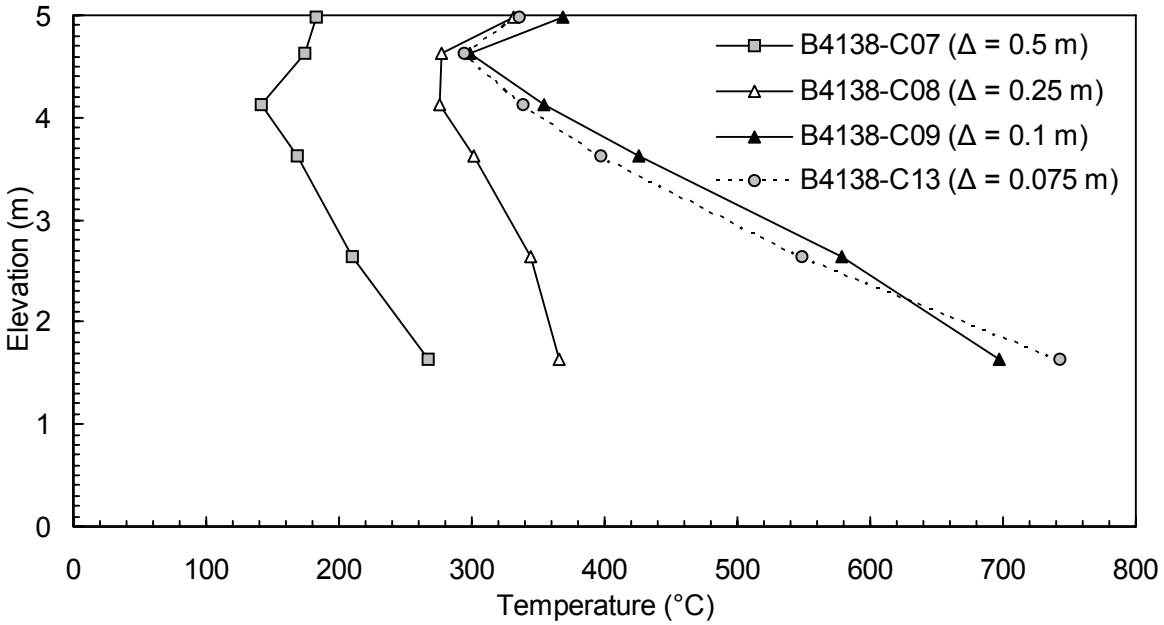

Figure 29. Fire compartment CL temperature profiles from selected CFD simulations illustrating the effect of decreasing control volume size.

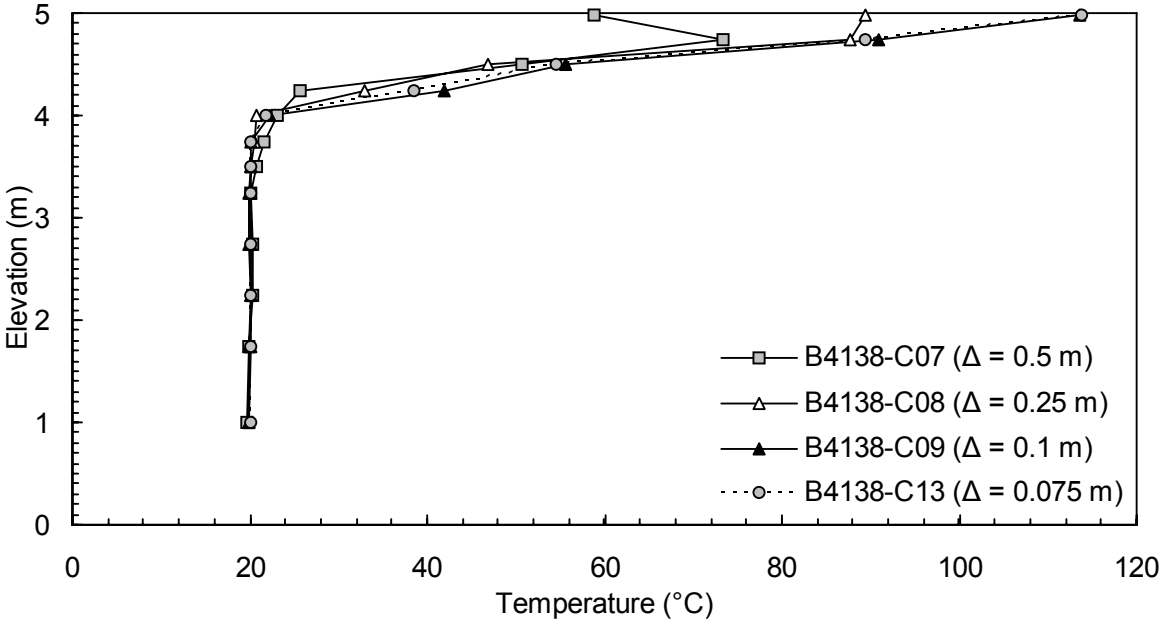

Figure 30. Compartment opening CL temperature profiles from selected CFD simulations illustrating the effect of decreasing control volume size.

volume sizes to less than 0.1 m may result in no further changes to the predicted temperatures and velocities in the fire compartment. Figure 30 shows a similar increase in compartment opening CL temperatures with decreasing control volume size but differences between the predictions have much lower magnitudes than those found for the compartment CL temperatures. Figure 30 also clearly shows the increase in temperature at the compartment ceiling as control volume size decreases. This is attributed to more accurate modeling of the ceiling boundary layer as the control volume sizes decrease. Analysis of the temperature profiles from simulations B4138-C07 through C09 and C13 indicates that control volume sizes of $\Delta = 0.1$ m produce grid-insensitive predictions of fire compartment temperatures. Grid-insensitivity is a necessary but not sufficient requirement for accurate predictions from CFD simulations. Therefore, refinement on the control volume size to 0.1 m in the fire compartment is used as a starting point in developing the CFD model of the full-scale experimental facility (Section 3.3).

Since the implementation of the single transformed and multiple grid capabilities in FDS v.4.00 are not fully documented in its accompanying reference documentation [34, 35], the validity of using transformed or multiple grid designs is uncertain. The fire compartment modeling study therefore examines the effect of various grid designs on the predicted results. Of the four grid designs evaluated for the fire compartment simulations (single, single transformed, double embedded and triple overlapping), the latter three are intended to maintain the accuracy of the CFD results while reducing computation times by specifying small control volumes over the combustion zone and larger control volumes over the rest of the fire compartment. Figure 31 through Figure 33 compare predicted fire compartment CL and compartment opening CL temperature profiles from simulations using each type of transformed and multiple grid design with those from simulations using a single grid design with comparable control volume sizes. Similar plots of the compartment opening CL temperature profiles are contained in Appendix B. In general, simulations using the single transformed and double embedded grid designs did not predict the same temperatures as simulations using the single grid designs. For example, Figure 31 shows that the fire compartment CL temperature profile for simulation B4138-C06 (single transformed) agrees more poorly with the experimental data than the profile from simulation B4138-C09 (single), even though the former has the same control volume size as the latter throughout the fire compartment and half the control volume size over the combustion zone. Figure 32 shows that simulation B4138-C15 (double embedded) does not compare as well with the experimental data as simulation B4138-C09 (single) even though both simulations use the same control volumes size over the combustion zone. One exception to this behaviour is simulations B4138-C05 (single transformed) and C09 (single) which use the same control volumes size over the combustion zone and predict similar temperature profiles, although the former simulation uses less control volumes in total. Simulations using the triple overlapping grid design

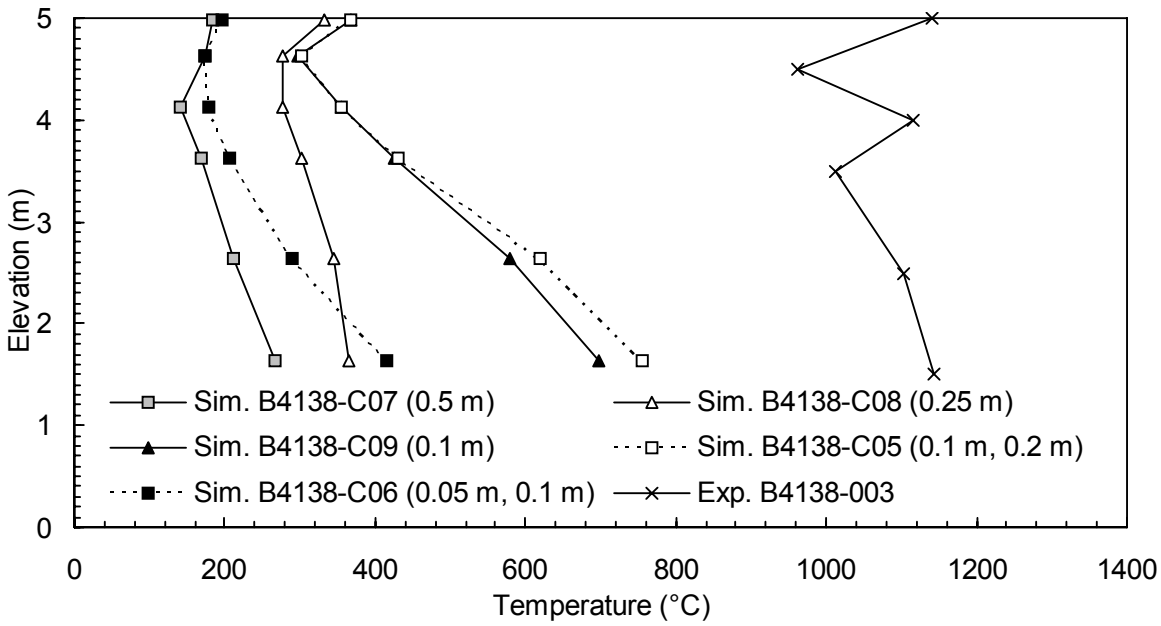

Figure 31. Fire compartment CL temperature profiles from CFD simulations with single and single transformed grid designs.

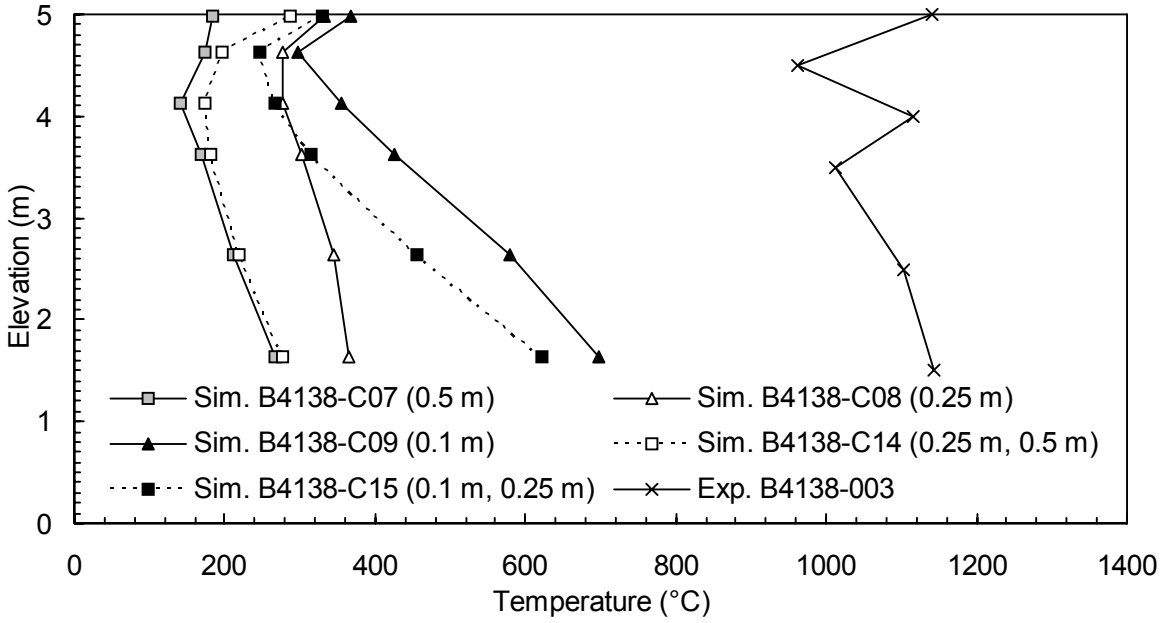

Figure 32. Fire compartment CL temperature profiles from CFD simulations with single and double embedded grid designs.

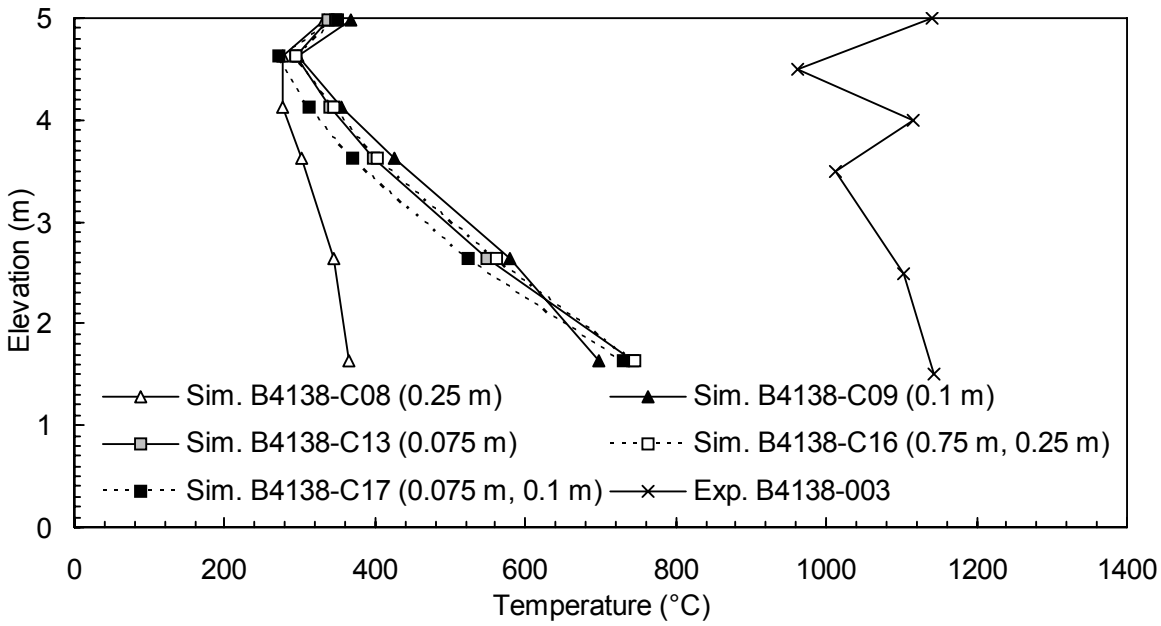

Figure 33. Fire compartment CL temperature profiles from CFD simulations with single and triple overlapping grid designs.

seem to maintain the accuracy of their results. Figure 33 shows that simulation B4138-C17 (triple overlapping) predicts comparable temperatures to B4138-C13 (single). The former simulation uses 564 912 controls volumes, the latter 884 736, representing a reduction in the number of control volumes of 36%. Based on the results of the evaluation of the CFD model of the fire compartment, only single and triple overlapping grid designs are recommended for use in FDS. The effect of grid design on predicted temperatures outside of the fire compartment is examined in Section 3.3.2 as part of the modeling study of the entire experimental facility.

Simulations B4138-C08 and C10 through C12 are conducted to show the effect of two modeling assumptions on the predicted results: 1) the thermal and ignition properties of the fire compartment boundaries and 2) the geometry of the fuel injection boundary condition. Specifically, the thermal and ignition properties of the fire compartment boundaries are specified as either an inert material (B4138-C08 and C10) or a typical concrete (B4138-C11 and C12) (Table 3.2) and the fuel injection boundary condition is specified either as a horizontal plane at z = 0.457 m (B4138-C08 and C11) or as the top plane of a rectangular volume extending from z = 0.000 to 0.457 m (B4138-C10 and C12). All four simulations are conducted using a single grid design with the same control volume size. The variances in temperatures between the four simulations for the fire compartment N, compartment opening CL and compartment opening N profiles are less than 5 °C and therefore are considered negligible. Figure 34

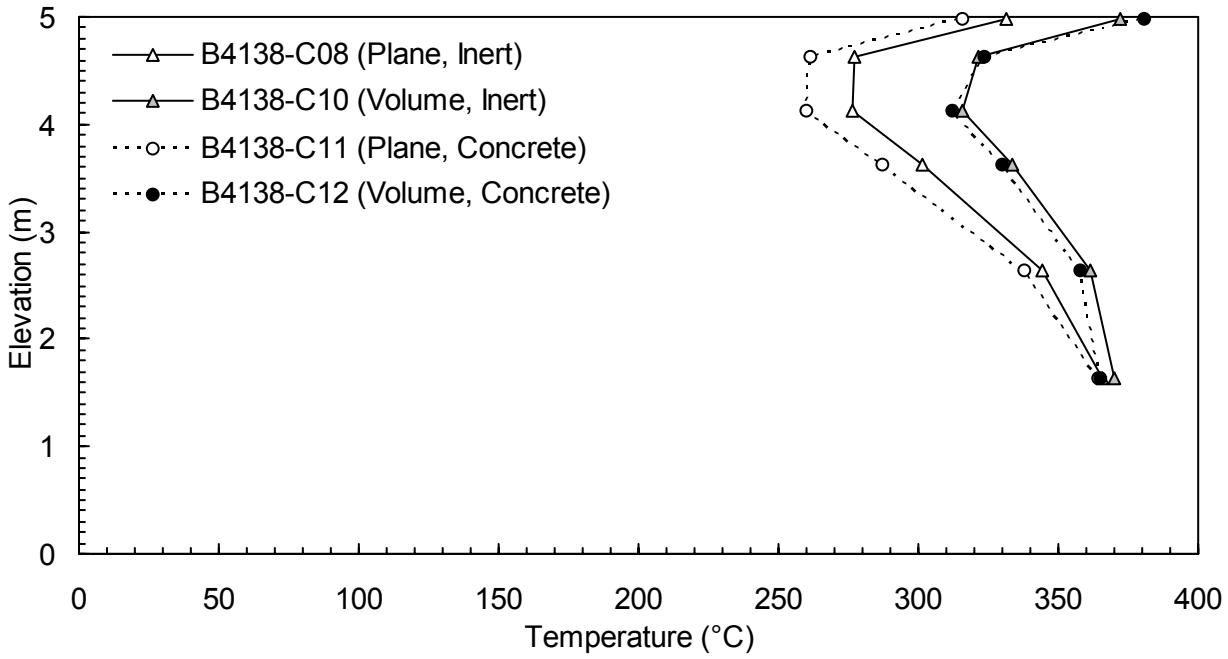

Figure 34. Fire compartment CL temperature profiles for selected CFD simulations illustrating the effect of changing the compartment boundary thermal properties and burner surface specification.

shows the differences in the fire compartment CL temperature profiles from the same simulations where simulation B4138-C08 specifies the burner surface as a horizontal plane at an elevation of z = 0.457 m and simulation B4138-C10 specifies the burner surface as the top face of a rectangular volume extending from z = 0.000 to z = 0.457 m. The temperature profile for simulation B4138-C10 is significantly higher (≤40 °C) over its entire elevation than the profile for B4138-C08, likely due to an inherent loss of heat from the flow domain in simulation B4138-C08. It is unclear from the documentation for FDS [34, 35] how heat transfer through fuel injection boundary conditions is modeled; however, the results compared in Figure 34 clearly show that specifying the burner as either an elevated plane or a volume significantly affects the predicted fire compartment temperatures. The effect of the fuel injection boundary condition specification on predicted temperatures outside of the fire compartment is examined in Section 3.3.2 as part of the modeling study of the entire experimental facility.

The effect of specifying different thermal and ignition properties for the fire compartment boundaries is also shown in Figure 34. Simulation B4138-C08 specifies the fire compartment boundaries as having inert thermal properties; Simulation B4138-C11 specifies these boundaries as having the thermal properties of a typical concrete. Both simulations model the burner as a similar elevated fuel injection boundary condition. The temperature profile for simulation B4138-C11 is lower (≤20 °C) over its entire

elevation than that for simulation B4138-C08, illustrating the effect of heat loss from the flow domain via conduction through the compartment boundaries. Simulation B4138-C12 models the burner as a rectangular volume and specifies the fire compartment boundaries as having the thermal properties of concrete. The resulting temperature profile is similar (≤8 °C) over its entire elevation to that from simulation B4138-C10. The results from simulations B4138-C08 and C10 through C12 indicate that modeling the effects of conductive heat transfer through the fire compartment boundaries has a minor effect on the fire compartment temperatures. Section 2.2 describes how minimizing heat losses from the fire compartment via conduction yields conservative estimates of BSP mass flow rates. Accordingly, most subsequent CFD simulations of the full-scale experimental facility and BSP behaviour at high elevations assume the fire compartment boundaries have inert thermal properties. The effect of surface thermal and ignition properties on predicted temperatures outside of the fire compartment is examined in Section 3.3.2 as part of the modeling study of the entire experimental facility.

3.2.3 Conclusions of the Fire Compartment Modeling Study

The CFD model of the fire compartment underpredicts the temperatures in the fire compartment by as much as −750 °C compared to the full-scale experimental data. This is attributed to radiation error inherent in the full-scale experimental data. The radiation correction algorithm in FDS v.4.00 is unable to resolve the differences between the predicted and measured compartment temperatures caused by radiation and predicts apparently non-physical temperatures in some cases. Although the temperature profiles predicted by FDS are qualitatively similar to those obtained in the full-scale experimental program, the quantitative accuracy of the CFD model of the fire compartment cannot be conclusively validated given the available data. Nonetheless, the ability of the model to predict the depth of the hot smoke layer exiting the compartment appeared sufficiently consistent that a second evaluation effort using the CFD model of the experimental facility was undertaken, as described in Section 3.3.

Results from the fire compartment modeling study allow key conclusions to be made regarding the FDS modeling methodologies which most accurately predict compartment fire dynamics. The fire compartment CFD simulations indicate that grid-insensitive modeling of the compartment fire dynamics requires a maximum control volume size of $\Delta = 0.1$ m. Single and triple overlapping grid designs are recommended over single transformed and double embedded grid designs. Specifying the burner fuel injection boundary condition as either an elevated plane or a rectangular volume affects predicted temperatures in the fire compartment. Specifying the thermal and ignition properties of the fire compartment boundaries as inert gives conservative estimates of BSP mass flow rates. These modeling methodologies were incorporated into the CFD model of the full-scale experimental facility described in the following section.

3.3 Experimental Facility Modeling Study

Following development and verification of the CFD model of the fire compartment, an extended CFD model of the full-scale experimental facility was developed. Forty-four simulations were conducted to evaluate the ability of this model to accurately predict BSP flow dynamics in the facility with a focus on modeling the BSP flow under the balcony and in the atrium area. Accurate modeling of BSP mass flow rates in the four-storey atrium represented by the experimental facility is a necessary precursor to development of a CFD model of BSP behaviour at high elevations (Chapter 4); however, the simulations conducted using the model of the experimental facility also demonstrate various limitations with FDS related to the use of multiple grids and the modeling of heat transfer at fuel injection boundary conditions.

3.3.1 CFD Model of the Experimental Facility

The geometry used for the CFD model of the experimental facility, shown in Figure 35, reflects the geometry of the actual facility as closely as possible (Section 2.3: Figure 5, Figure 6). Differences in the geometry are due to updated measurements of the facility that were obtained after the CFD simulations were complete. The flow domain is defined to include the entire 30.480 m deep by 16.720 m wide by 12.120 m high atrium. A 13.290 m wide by 5.040 m deep by 4.985 m high fire compartment is located at ground level with its northeast corner positioned 4.235 m west of the atrium's northeast corner. The compartment opening width, W, varies between 5.000 and 12.000 m depending on the simulation and is specified as an open boundary condition. A 4.195 m deep balcony is attached to the fire compartment. The fire compartment and atrium boundaries are modeled in most simulations as solid surfaces with zero thickness and thermal and ignition properties of an ideal inert material. In selected simulations, these boundaries are modeled as either steel or concrete in order to further understand the impact of conductive heat losses from the flow domain on the predicted results. Table 3.2 lists the thermal and ignition properties defined by FDS v.4.00 for all materials used in the CFD models. Two open boundary conditions measuring 4.235 m wide by 4.710 m high and 21.205 m wide by 4.710 m high are specified along the north flow domain boundary to model the openings under the panel wall and adjustable curtain. The co-ordinate system origin for the model is located at the compartment opening centerline at ground level with the positive x-axis oriented westward, the positive y-axis oriented northward and the positive z-axis oriented vertically, as shown in Figure 35.

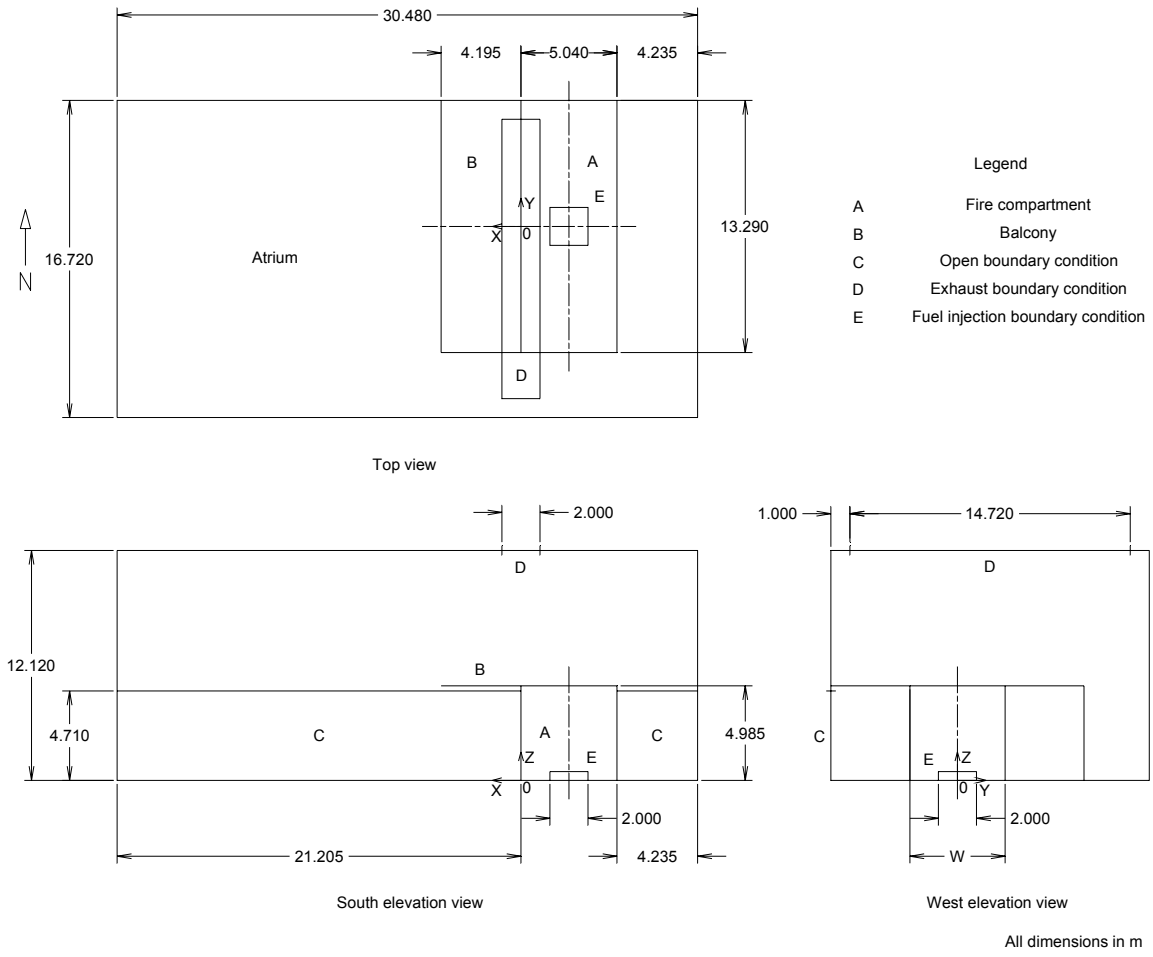

Figure 35. Geometry of the CFD model of the experimental facility.

Material	Thermal model	T_{surf}	Δ (m)	ρ (kg/m^3)	c (kJ/kg-K)	$c\Delta\rho$ (kJ/K-m^2)	k (W/m-K)	T_{ign} (°C)
Inert	N/A	20 °C				$\approx \infty$	$\approx \infty$	$\approx \infty$
Concrete	thermally thick material backing to void	Variable	0.200	450.	3.90		1.0000	5000.0
Steel	thermally thin material backing to void	Variable				20.00		5000.0

Table 3.2. Thermal and ignition properties of selected materials in FDS v.4.00.

The burner system is modeled as a fuel injection boundary condition specified over a 2 m by 2 m horizontal plane located at the center of the fire compartment at an elevation of 0.457 m. Selected simulations extend this elevated plane to the compartment floor ($z = 0.000$ m) to form a rectangular volume whose top surface is a fuel injection boundary condition. These two modeling methodologies for specifying the fuel injection boundary condition are used to determine the impact of an elevated fuel injection boundary condition on the predicted atrium temperatures (Table 3.3). Figure 35 illustrates the latter modeling methodology for the fuel injection boundary condition. Specific fire sizes are modeled by specifying heat release rates per unit area (kW/m^2) from which FDS calculates the required mass flow rate of propane (kg/s) through the fuel injection boundary condition (m^2), assuming a constant heat of combustion (kJ/kg) (Table 3.1). Steady fires are modelled in the experimental facility simulations to correspond to the steady fires used to generate BSPs in the experimental program.

The exhaust system is modeled as a 2.000 m deep by 14.720 m wide rectangular boundary condition located at the atrium ceiling. The long axis of the exhaust boundary condition is positioned above the fire compartment opening plane (Figure 35). The sixteen circular exhaust vents in the experimental program (Figure 5) are consolidated into a single exhaust boundary condition in order to simplify the boundary condition definition in FDS and conform to the software's requirement of rectilinear geometry. The location of the exhaust boundary condition is chosen to approximate the position of the experimental facility exhaust system. The average exhaust system mass flow rate measured during a single exhaust system setting in the full-scale experiments is modelled as an equivalent steady volumetric flow rate through the exhaust boundary condition. This equivalent volumetric flow rate, V_{sim}, is calculated from the measured exhaust system mass flow rate, m_{exh}, by assuming that the exhausted smoke is an ideal gas with a temperature equal to the average atrium smoke layer temperature ($V_{sim} = m_{exh}/(T_\infty/T_{s,ave})\rho_\infty$). The exhaust boundary condition in the simulations is much larger in area (29.44 m^2) than the total area of the sixteen circular vents in the experimental facility (2.63 m^2). Since the exhaust mass flow rates in the simulations and experiments are approximately equal, the difference in exhaust areas may cause gas velocities near the exhaust to be lower in the simulations than in the experiments. These lower velocities presumably change the flow in the atrium smoke layer near the exhaust boundary condition but are assumed to have negligible impact on the bulk BSP flow dynamics, including the atrium smoke layer elevation and the average atrium smoke layer temperature. Where applicable, the louvers and adjustable curtain opening (Section 2.3.1) are modelled as open boundary conditions.

The use of multiple grids is evaluated again in the simulations of BSP behaviour in the experimental facility in order to reduce the number of control volumes and reduce solution times while maintaining the accuracy of predicted results. Two main grid designs are used for the simulations: a single transformed grid design and a quintuple grid design. These two grid designs are selected based on the conclusions of

the fire compartment modeling study (Section 3.2.3). Figure 36 illustrates both grid designs schematically. The single transformed grid design transforms a single grid in the x and y co-ordinates to decrease control volume sizes in the fire compartment relative to control volumes sizes in the atrium; no transformation is made in the z co-ordinate. Six transformations are made in each of the x and y directions to yield thirty-six regions with different control volume sizes. The quintuple grid design uses five adjoining (i.e. non-overlapping) grids to define the flow domain: one for the fire compartment, a second for the atrium volume in front of the compartment, a third for the atrium volume behind the compartment, a fourth for the atrium volume beside the compartment and a fifth for the entire atrium volume above the fire compartment elevation. The first two grids in the quintuple grid design are transformed to exactly place control volume edges at key features of the fire compartment geometry. The fire compartment grid consists of smaller control volumes than the four atrium grids. For the same fire compartment control volume size, the quintuple grid design requires less total control volumes than the single transformed grid design. The control volume sizes in the experimental facility simulations range from 0.100 to 0.250 m. The lower end of this range is chosen to obtain grid-insensitive results in the fire compartment based on the conclusions of the fire compartment modeling study (Section 3.2.3); the upper end is chosen to maintain the total number of control volumes to less than 10^6, a realistic limit for efficient solution on a single workstation. The effect of grid design and control volume size on the accuracy of predicted atrium temperatures is evaluated as part of the experimental facility modeling study (Section 3.3.2).

Simulation times of 300 s are specified for most simulations in order to achieve steady-state conditions for a single exhaust system flow rate setting. Default values for the propane combustion properties, radiation model and ambient conditions listed in Table 3.1 are used for all simulations. A number of combinations of fire size, compartment geometry and exhaust flow rate are simulated corresponding to a subset of the full-scale experiments. Temperatures are predicted at locations which closely match those of the instrumentation for the full-scale experimental facility (Figure 8, Figure 9) to allow evaluation of the model using the experimental data.

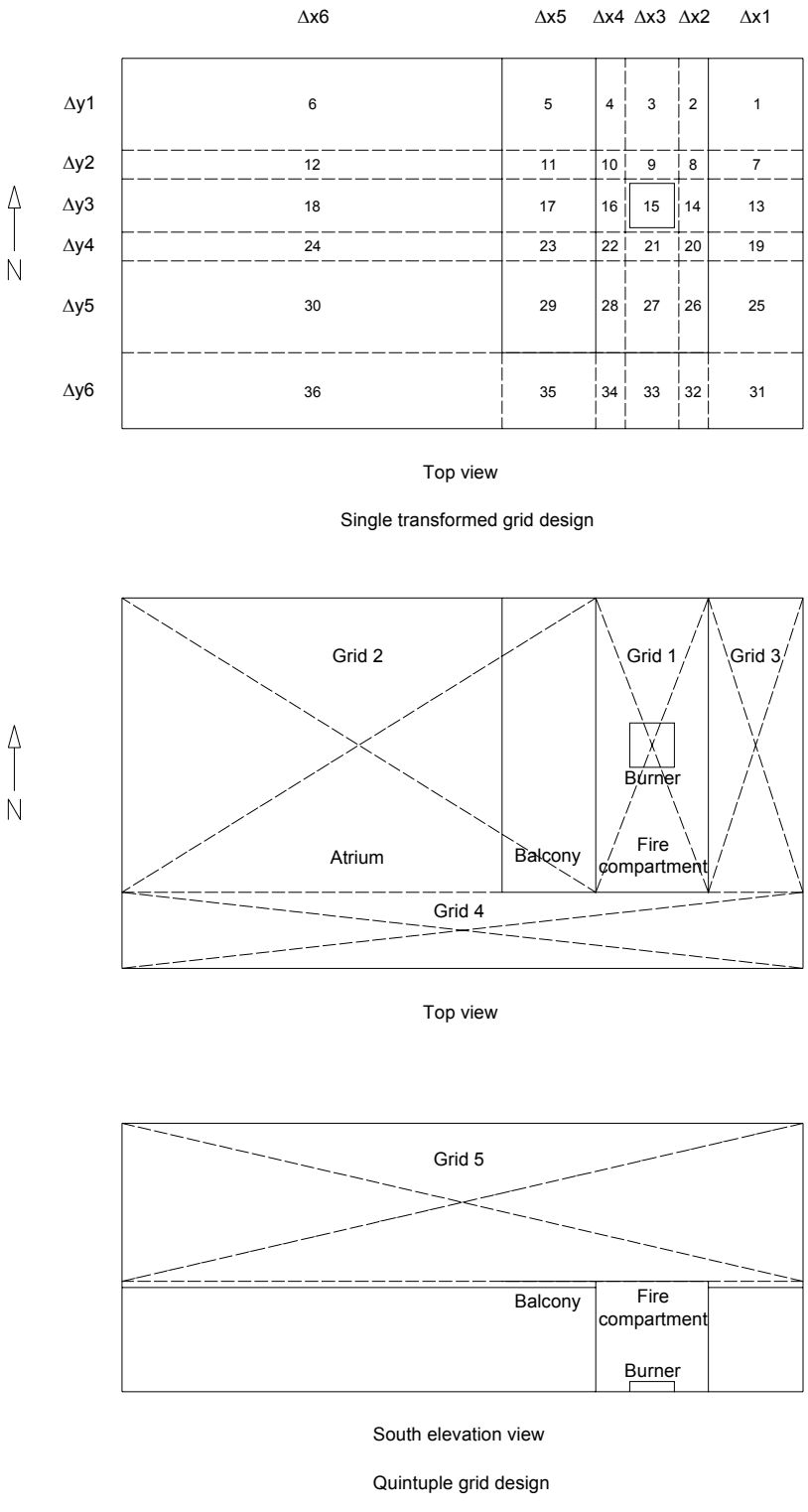

Figure 36. Main grid designs for the CFD model of the experimental facility.

3.3.2 Results

The CFD model of the experimental facility is compared against data from full-scale experiment B4138-024 (Q = 2.0 MW, W = 5.0 m) during the period when exhaust flow rate setting E was active (m_{exh} = 24.73 kg/s). No louvers or adjustable curtain opening were used during this experiment. Two sets of data from this experiment are chosen for evaluation of the CFD model: the atrium CL temperature profiles and the average atrium smoke and cold layer temperatures. Accurate prediction of the atrium temperature profile, characterized mainly by the atrium smoke layer elevation, implies that the CFD model of the experimental facility also accurately predicts BSP mass flow rate since z_l and m_{BSP} are directed related (Table 1.1). This section also illustrates the effect of changing various modeling methodologies on the predicted atrium temperatures and identifies limitations of FDS related to predicting atrium temperatures. The full dataset from the experimental facility modeling study is available electronically from the author upon request.[1]

Two types of BSP visualizations are presented to illustrate the general shape of the BSP predicted by simulations of the experimental facility. Figure 37 shows a typical visualization of the BSP based on the predicted atrium temperatures from simulation B4138-0047a. The instantaneous temperature distribution in the flow domain at t = 300 s is plotted along the x-z plane intersecting the compartment and BSP centerline (y = 0.000 m). The flow domain temperatures at this time range from 20 to ≈ 1 270 °C with the highest temperatures occurring in the fire compartment. The BSP approach flow, turning and buoyant line plume regions, as well as the atrium smoke and cold layers, are evident but not clearly defined in Figure 37. The simulation predicts that the BSP projects a significant horizontal distance (≈ 4 m) from the balcony edge into the atrium before impacting the atrium ceiling. This behaviour agrees qualitatively with visualizations obtained during the full-scale experimental program and laser-induced fluorescence (LIF) measurements of BSPs in a scale experimental facility by Yii [57]. Figure 38 shows a typical three-dimensional visualization of the BSP based on the predicted atrium temperatures from simulation B4138-0047a. An isothermal surface (T_{surf} = 50 °C) plotted at t = 300 s suggests that the BSP perimeter has a complex shape at any instant in time.

[1] The author can be contacted via e-mail at: cameron_mccartney@hotmail.com.

Figure 37. Typical visualization of BSP based on an instantaneous temperature field (B4138-0047a, y = 0.000 m, t = 300 s).

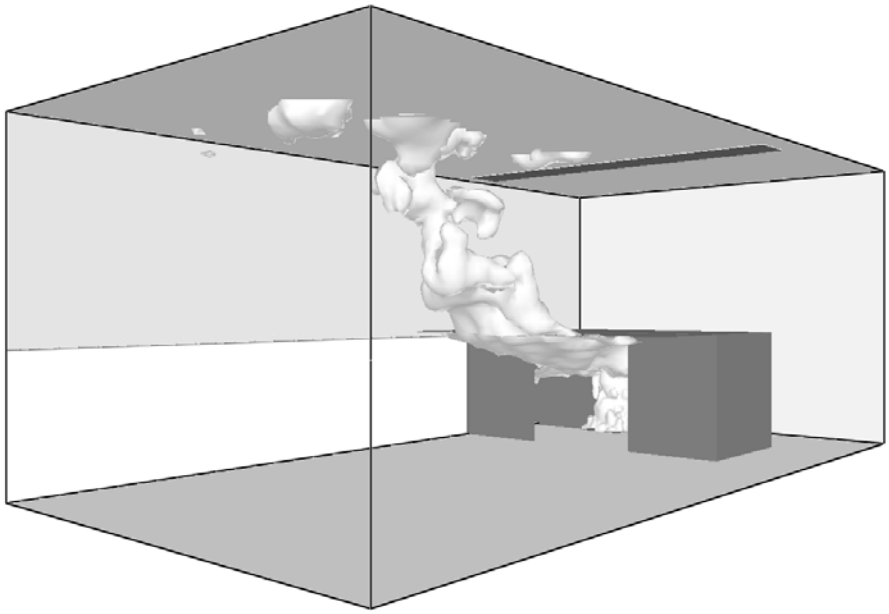

Figure 38. Typical three-dimensional visualization of BSP based on an isothermal surface (B4138-0047a, T_{surf} = 50 °C, t = 300 s).

The main data used to compare the CFD model of the experimental facility to the experimental data are the atrium CL temperature profiles. Figure 39 shows a comparison of the atrium CL temperature profiles from simulation B4138-0047a and experiment B4138-024 during exhaust setting E (designated B4138-024E), both of which use the same fire size and compartment geometry. The exhaust system mass flow rate of 24.73 kg/s from experiment B4138-024E is modeled as a volumetric flow rate of 24 m^3/s in simulation B4138-0047a based on an average atrium smoke layer temperature of $T_{s,ave} \approx 70$ °C (Figure 39). The simulation temperature profile is produced by averaging the temperature data at each elevation over the assumed steady-state period of t = 240 to 300 s. A similar averaging procedure for the experimental data is described in Section 2.5. The ambient temperature in experiment B4138-024 is ≈ 22 °C based on the temperature measured by the lowest atrium CL array thermocouple at t = 0 s. This is similar to the ambient temperature of 20 °C used in simulation B4138-0047a, therefore the atrium CL temperature profiles are plotted as temperatures (T) rather than as temperature rises above ambient ($T - T_\infty$).

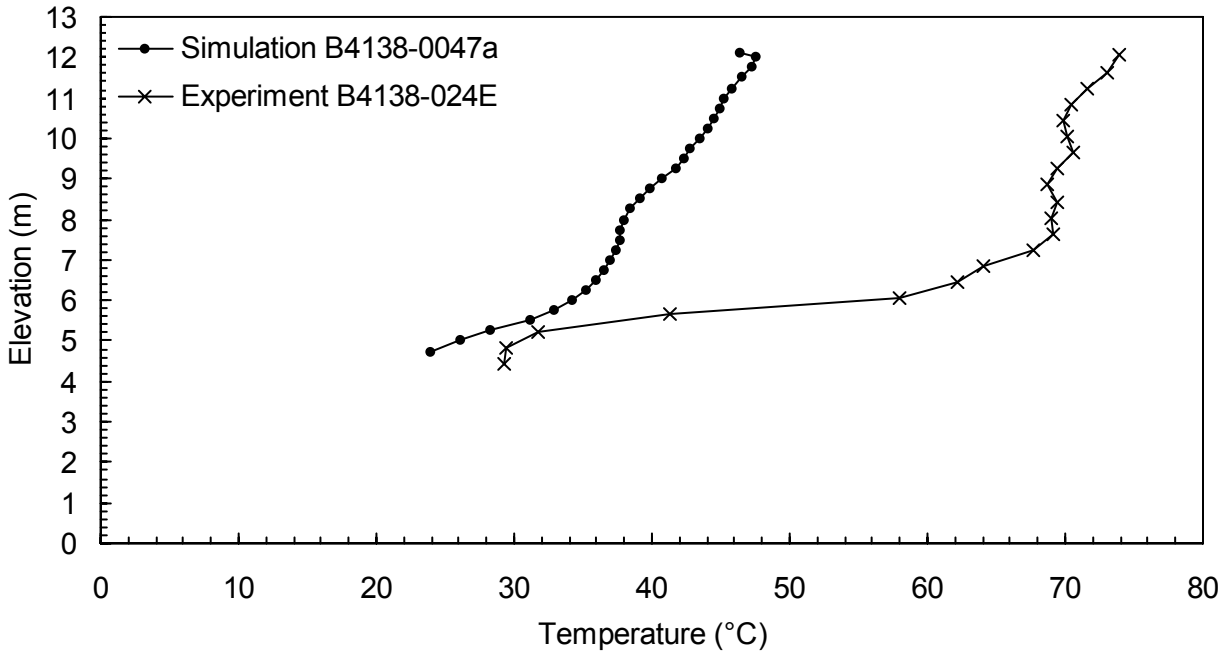

Figure 39. Atrium CL temperature profiles from simulation B4138-0047a and experiment B4138-024E.

Figure 39 compares the atrium CL temperature profile measured in experiment B4138-024 with that predicted by simulation B4138-0047a. The two profiles are similar in shape with an atrium smoke layer that increases nearly linearly in temperature and a transition region with a higher vertical temperature gradient than the smoke layer. The simulation underpredicts the atrium smoke layer temperature by

≈ 30 °C at all elevations which, even accounting for uncertainty in the measured temperatures, represents a significant discrepancy between the predicted results and the experimental data. The atrium cold layer is difficult to visualize in most of the experiments and simulations due to the lack of temperature data at lower elevations. Nonetheless, the atrium cold layer temperatures predicted by the CFD simulations generally appear to be lower than those measured in the experiments. Accurate prediction of atrium smoke layer elevation is important with regards to the use of CFD models to predict BSP mass flow rate since these two quantities are directly related (Table 1.1). Application of existing algorithms [8, 13, 7, 46] to the atrium temperature profiles measured in the experimental program proved inconclusive in determining a single value of z_l (Section 2.5). Given that the measured and predicted atrium temperature profiles are similar in shape, the same problem will arise if these algorithms are applied to the simulation results. Therefore, values of z_l for the CFD simulations were visually determined by selecting elevations located at the center of the transition region based on plots of predicted atrium CL temperatures similar to Figure 39. Predictions of atrium smoke layer elevations, z_l, visually determined from the CFD simulations are typically lower than those measured in the experiments but are still reasonably accurate given the uncertainty in defining z_l somewhere within the transition region (Section 2.5). A reasonable lower bound on the accuracy of measured or predicted values for z_l is assumed to be ± 0.5 m since the minimum depth of the transition layer found in the full-scale experimental program is ≈ 1 m. As a supporting example, the estimates of z_l visually determined from Figure 39 yield $z_l \approx 5.6$ m from simulation B4138-0047a and $z_l \approx 6.0$ m from experiment B4138-024E for a relative error of 0.4 m. Underpredictions of the atrium temperature and smoke layer elevations are systemic throughout all of the CFD simulations of the experimental facility. These discrepancies are suspected to arise from inaccuracies in the modeling of heat losses from the flow domain, leading to lower predicted temperatures throughout the entire flow domain. This issue is investigated further through a series of comparative CFD simulations discussed below.

The experimental facility modeling study examines the effect of two different grid designs and several control volume sizes on the predicted atrium temperatures. Simulation B4138-0047a uses a quintuple grid design with control volume sizes ranging from 0.100 to 0.250 m. Simulation B4138-0046 is conducted using a single transformed grid design with the same range of control volume sizes as simulation B4138-0047a. Simulation B4138-0045 is conducted using a single transformed grid design with control volume sizes ranging from 0.200 to 0.250 m i.e. larger control volumes are used in the fire compartment than in simulations B4138-0047a and 46. Figure 40 compares the atrium CL temperature profiles from simulations B4138-0047a, 46 and 45 as well as that from experiment B4138-024E. All three predicted profiles have generally the same shape as the measured profile and predicted temperatures

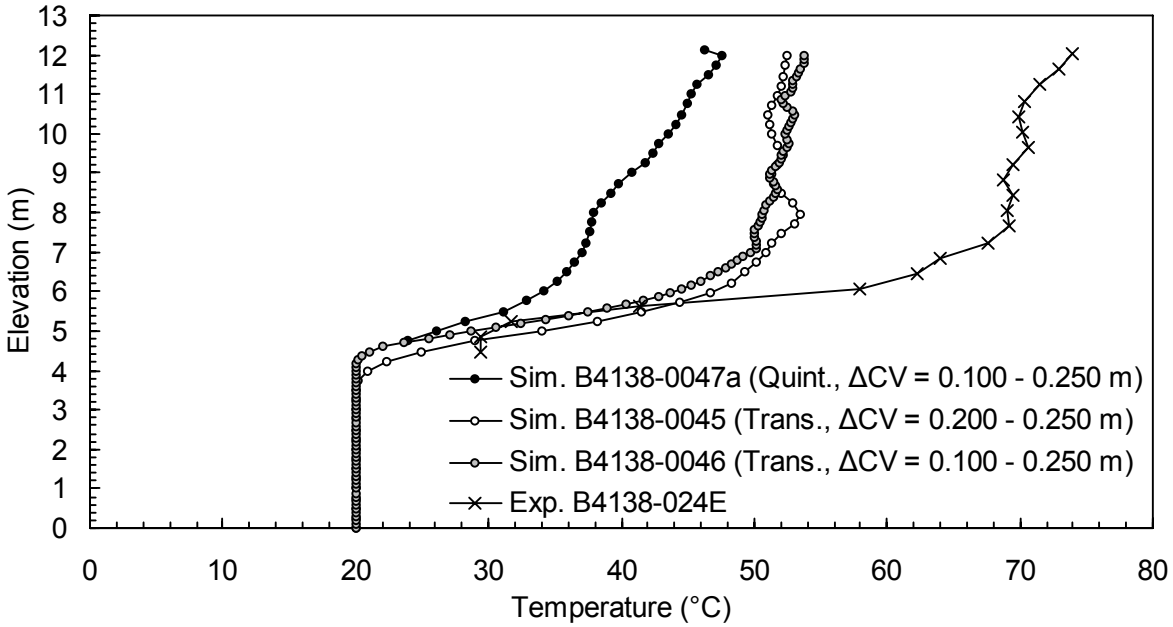

Figure 40. Atrium CL temperature profiles for selected experimental facility simulations showing the impact of grid design and control volume size, Δ.

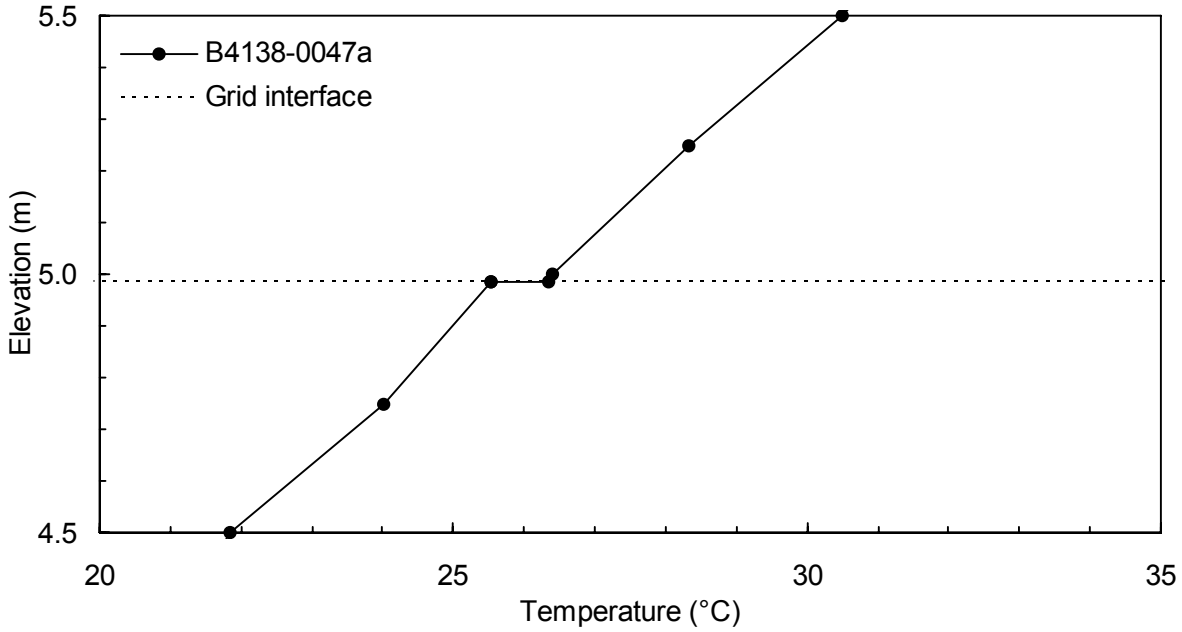

Figure 41. Atrium CL temperature profile from simulation B4138-0047a near grid interface elevation (z = 4.985 m).

are lower than the measured temperatures. However, the two simulations using the single transformed grid design are more similar in shape and predict atrium temperatures closer to the experimental data (≈ 20 °C error) than simulation B4138-0047a using the quintuple grid design (≈ 30 °C error). This may indicate that there are issues with the setup and implementation of multiple grids in FDS. Figure 41 plots the atrium CL temperature profile from simulation B4138-0047a previously presented in Figure 39 but focuses on the section of the profile where two of the five grids adjoin (z = 4.985 m). Temporally averaged temperature data is plotted every 0.250 m between elevations from 4.500 to 5.500 m as well as at elevations of 4.984, 4.985 and 4.986 m to illustrate the temperature profile near the grid interface. The atrium CL temperature profile is discontinuous at the grid interface elevation of 4.985 m, increasing ≈ 1 °C at this elevation. While this may appear a relatively small difference, discontinuous temperature profiles at grid interfaces may indicate that the conservation equations are not appropriately coupled between the grids. The supporting documentation for FDS [34] cautions against specifying grid interfaces in areas of the domain where high spatial or temporal gradients of temperature, velocity, etc. are predicted, given that "the exchange of information across mesh boundaries is not as accurate as cell to cell exchanges within one mesh". Related research by the author on CFD modeling of smoke flows in atria using FDS [16] demonstrates that the use of multiple grids with disparate control volume sizes can generate temperature and velocity discontinuities across grid interfaces. Therefore, the use of multiple grids to decrease solution times of FDS simulations of buoyant fire plumes in atria should be approached with caution, and, if their use is necessary, results should be carefully examined to confirm their validity and consistency, particularly along grid boundaries and interface areas. The fire compartment modeling study described in Section 3.2 concludes that single transformed grid designs predict compartment fire dynamics less accurately than single grid designs (Section 3.2.3). Furthermore, Figure 40 indicates that when the full experimental facility is simulated, predictions from a single transformed grid design correlate significantly better with the experimental data than those which use a multiple grid design. Although the predicted atrium temperatures using a single transformed grid are lower than those measured in the experimental program, the predicted temperature profile matches the shape of the measured profile and, more importantly, gives a reasonably accurate (± 0.5 m) prediction of atrium smoke layer elevation, z_l, based on visual determination. Since z_l is directly affected by BSP mass flow rate (Table 1.1), accurate prediction of z_l implies that m_{BSP} is also predicted to a reasonable degree of accuracy. Therefore, results from the CFD simulations of the experimental facility support the ability of FDS models to accurately predict BSP mass flow rates. For extension of the present model to one of BSP behaviour at high elevations, single or single transformed grid designs are recommended over multiple grid designs.

Comparison of the profiles predicted by simulations B4138-0045 and 46 (Figure 40) with the same grid design (single transformed) and different control volume sizes shows that decreasing the minimum control volume size from $\Delta = 0.200$ to 0.100 m does not significantly affect predictions of the atrium smoke layer temperatures. The main difference between the atrium CL temperature profiles predicted by these simulations is the higher atrium smoke layer elevation predicted in simulation B4138-0046 due to the use of control volumes with a smaller height: $\Delta z = 0.100$ m in simulation B4138-0046, $\Delta z = 0.250$ m in simulation B4138-0045. This supports the conclusion of the fire compartment modeling study that simulations with control volume sizes larger than $\Delta = 0.100$ m are not grid-insensitive with respect to predicted compartment temperatures (Section 3.2.3). However, the lack of results from simulations of the experimental facility with $\Delta < 0.100$ m due to computational limitations does not allow a similar conclusion to be made with regard to the predicted atrium temperatures. Since FDS allows grid transformations only in two co-ordinate directions, the control volume dimension along the third co-ordinate must be small over the entire flow domain to accurately model the fire compartment dynamics. This limits the potential of using transformed grids in FDS to apply small control volumes over the fire compartment while increasing the size and reducing the number of control volumes over the atrium. The impact of this issue on the grid design for the CFD model of BSP behaviour at high elevations is discussed in Section 4.1.

To improve the correlation of the CFD simulation results with the experimental data and investigate possible errors in modeling heat losses from the flow domain, a series of CFD simulations based on simulation B4138-0047a (quintuple grid, $\Delta = [0.1, 0.25]$) are conducted with changes to the modeling methodology. These changes, summarized in Table 3.3, address the modeling issues identified during the fire compartment modeling study (Section 3.2.3) as well as the impact of varying the radiative fraction, χ, on the predicted atrium temperatures. All of these changes impact the accuracy of predicted heat losses from the flow domain and therefore may contribute to the discrepancies between the predicted and measured atrium temperatures demonstrated above.

Results from the fire compartment modeling study indicate that including the effects of conduction through the fire compartment boundaries has a minor impact on the predicted fire compartment temperatures (Section 3.2.2). For the experimental facility simulations, it is expected that including any conductive heat losses from the flow domain through the atrium boundaries will cause predicted atrium temperatures to decrease, worsening the correlation between the predicted and measured atrium temperatures. To verify this behaviour, simulation B4138-048 is conducted based on simulation B4138-0047a but with the fire compartment and atrium boundaries modeled as concrete rather than inert (Table 3.2). Figure 42 compares the atrium CL temperature profiles from both simulations as well as the profile from experiment B4138-024E. All three profiles are similar in shape, exhibiting an atrium smoke

Simulations	Modeling methodology	Change	Purpose
47a, 48	Surface thermal and ignition properties	Change from inert to concrete (Table 3.2)	Determine the impact of conductive heat losses from the flow domain on the predicted atrium temperatures
47a, 59	Burner elevation	Change from 0.457 m as in the experimental program to 0.000 m	Determine whether FDS accurately models heat transfer through fuel injection boundary conditions not located on flow domain boundaries
47a, 60	Fuel injection boundary condition surface temperature, T_{surf}	Change from the default value of T_{surf} = 20 °C to a typical flame temperature of T_{surf} = 1 200 °C (1 473 K)	Determine whether the default value of T_{surf} = 20 °C causes an effective heat loss from the flow domain through the fuel injection boundary condition
47a, 49	Radiative fraction, χ	Change from the default value of χ = 0.35 to χ = 0.25	Determine the sensitivity of the predicted atrium temperatures to the radiative fraction, χ

Table 3.3. Modeling methodology changes made during the experimental facility modeling study.

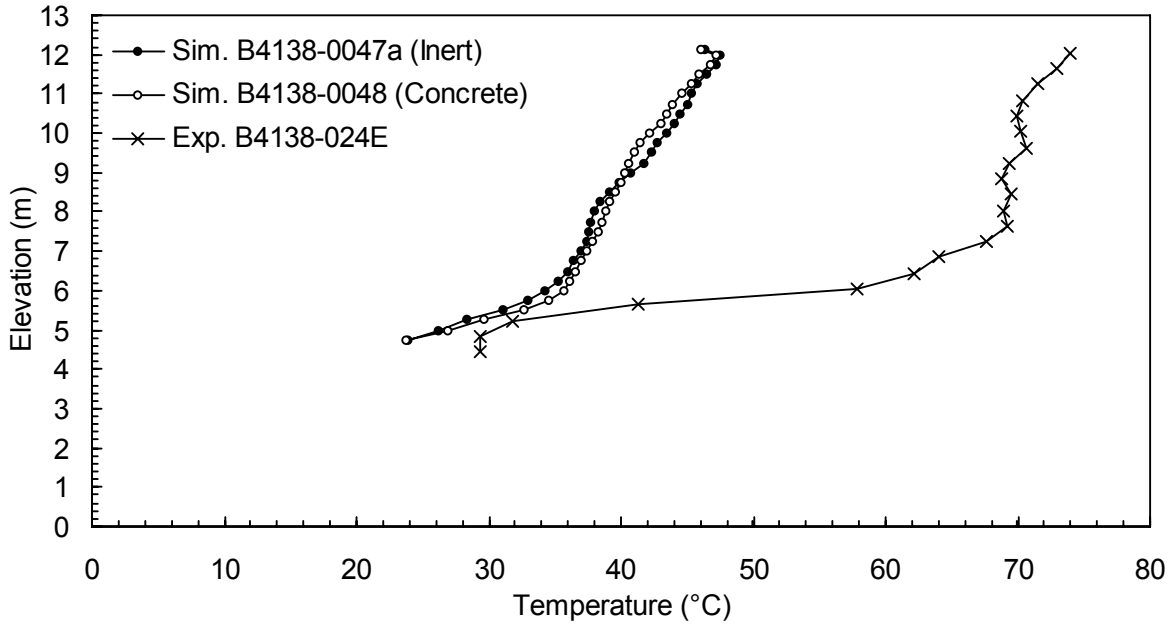

Figure 42. Atrium CL temperature profiles for selected experimental facility simulations showing the effect of different surface thermal and ignition properties.

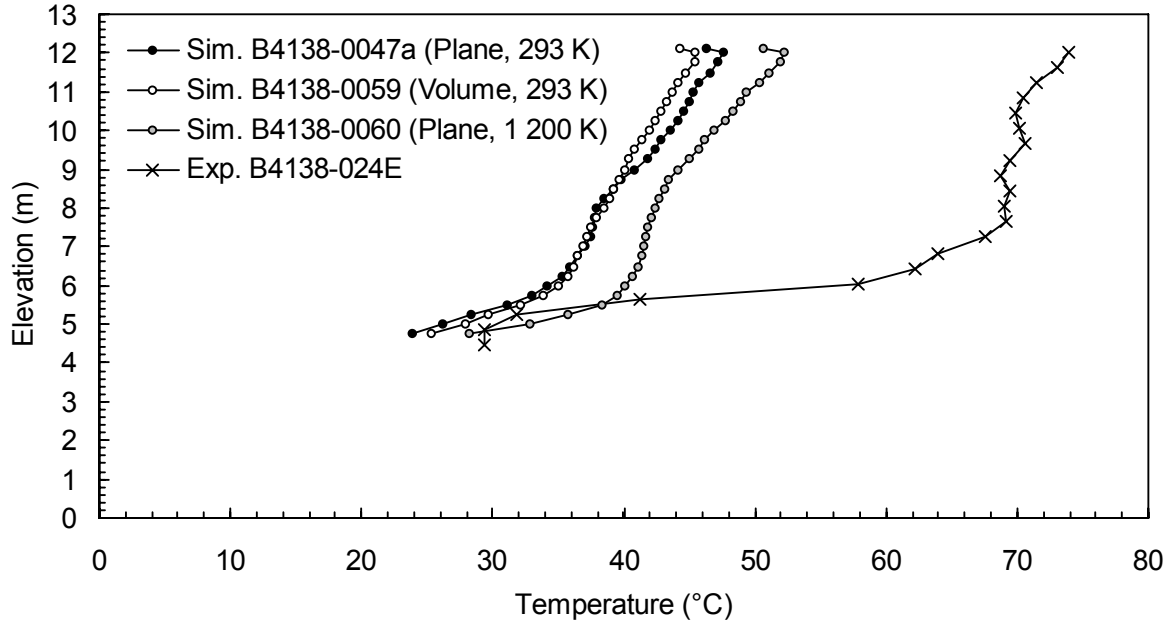

Figure 43. Atrium CL temperature profiles for selected experimental facility simulations showing the effect of different fuel injection surface modeling methodologies.

layer and transition region, although the two simulations underpredict the atrium smoke layer temperatures by ≈ 30 °C compared to the experimental data. Predicted atrium smoke layer elevations are lower than those measured in the experiment but are within the previously stated error limit of ±0.5 m. The predicted atrium temperatures from the two simulations are very similar, supporting the conclusion that including the effects of conductive heat transfer from the flow domain has a minor impact on the predicted atrium temperatures. Surface thermal and ignition properties are therefore not the main cause of the discrepancies between the predicted and measured atrium temperatures in the CFD model of the experimental facility. Accordingly, all remaining CFD simulations of the full-scale experimental facility and BSP behaviour at high elevations assume the fire compartment and atrium boundaries have inert thermal properties.

The fire compartment modeling study concludes that modeling the fuel injection boundary condition as a rectangular volume rather than an elevated plane may reduce heat losses from the flow domain (Section 3.2.3). To test this conclusion on the CFD model of the experimental facility, simulation B4138-0059 is conducted based on B4138-0047a but with the fuel injection boundary condition modeled as a rectangular volume extending from z = 0.000 to 0.457 m rather than as an elevated plane at z = 0.457 m. In the experimental facility modeling study, the temperature of the fuel injection boundary condition is also suspected to affect heat losses from the flow domain. Inspection of the predicted temperatures from simulations of the experimental facility shows that the fuel injection boundary condition remains at an ambient temperature of 20 °C despite surrounding fire temperatures approaching flame temperatures of 1 200 °C. It is unclear whether this is an artifact of the fuel injection boundary condition implementation in FDS or if the cool fuel injection surface acts as a heat sink and forces an artificial heat loss from the flow domain as the low surface temperature is maintained. Simulation B4138-0060 is conducted based on B4138-0047a but with the fuel injection boundary condition temperature changed from the default ambient value of 20 °C (293 K) to 1 200 °C (1 473 K), a temperature representing commonly assumed conditions within a diffusion flame [49]. Figure 43 compares the atrium CL temperature profiles from simulations B4138-0047a, 59 and 60 with that from experiment B4138-024E.

The four temperature profiles in Figure 43 are similar in shape, exhibiting an atrium smoke layer and transition region. The three simulations again underpredict the atrium smoke layer temperatures compared to the experimental data with error magnitudes ranging between 22 and 32 °C. Predicted atrium smoke layer elevations are lower than those measured in the experiment but are within the previously stated error limit of ±0.5 m. Comparison of the profiles from simulations B4138-0047a and 59 indicates that modeling the fuel injection boundary condition as a volume rather than an elevated plane slightly decreases the predicted atrium temperatures (≈ 2 °C) at elevations greater than 8.5 m above the floor. This is opposite to the impact on the fire compartment temperatures found in the fire compartment

modeling study (Section 3.2.2) but does not significantly improve the agreement between the simulation results and the experimental data. This temperature decrease may result from increased amounts of ambient air being entrained into the compartment fire in order to achieve complete combustion of the fuel, since the presence of the burner volume would obstruct the flow of air into the base of the fire. Alternatively, such a flow obstruction may prevent the fuel from achieving complete combustion, leading to a decrease in fire size and resulting BSP temperatures. The impact of an elevated fuel injection boundary condition on predicted atrium temperatures cannot be conclusively determined from the results of the experimental facility modeling study. Comparison of the profiles from simulations B4138-0047a and 60 indicates that specifying a higher temperature for the fuel injection boundary condition significantly increases the predicted atrium temperatures at every elevation (≤8 °C). This improves the correlation of the predicted and measured atrium temperatures such that their relative error is reduced by ≈ 20% and does not appreciably change the value of z_l. The effect of fuel injection boundary condition temperature on predicted atrium temperatures is identified as one of the key issues in use of FDS for this application; however, there is insufficient data to determine the best representation of this boundary condition. Therefore, subsequent CFD simulations of BSP behaviour at high elevations (Chapter 4) model the burner as a horizontal fuel injection boundary condition at an elevation of z = 0.000 m and a temperature of 20 °C in order to avoid possible uncertainties due to modeling the burner as an elevated plane.

Decreasing the value of the radiative fraction of the fire, χ, in the simulations should increase the amount of heat transferred to the gases in the fire compartment, increasing the fire compartment temperatures and therefore the temperatures of the BSP approach flow and atrium temperatures. This effect may improve the agreement between the predicted atrium temperatures and the experimental data. Simulation B4138-049 is conducted based on B4138-0047a but with the radiative fraction lowered from the default value of $\chi = 0.35$ (Table 3.1) to $\chi = 0.25$. Figure 44 plots the atrium CL temperature profiles for simulations B4138-0047a and 49 as well as that from experiment B4138-024E. Again, the predicted and measured temperature profiles are similar in shape but the atrium temperatures are underpredicted compared to the experimental data with error magnitudes up to 28 °C. Predicted atrium smoke layer elevations are lower than those measured in the experiment but are within the previously stated error limit of ±0.5 m. Decreasing the radiative fraction by 28% clearly increases the predicted atrium temperatures at every elevation (≤5 °C), reducing the relative error between predicted and measured atrium temperatures by ≈ 15%. The default value for the radiative fraction of propane used in FDS v.4.00 ($\chi = 0.35$) is within the established range for this fuel [49]. Further reduction of the discrepancies in predicted and measured atrium temperatures based on the effects of radiative heat transfer alone would require specifying a value for χ outside of this established range. Combining changes in the value for χ

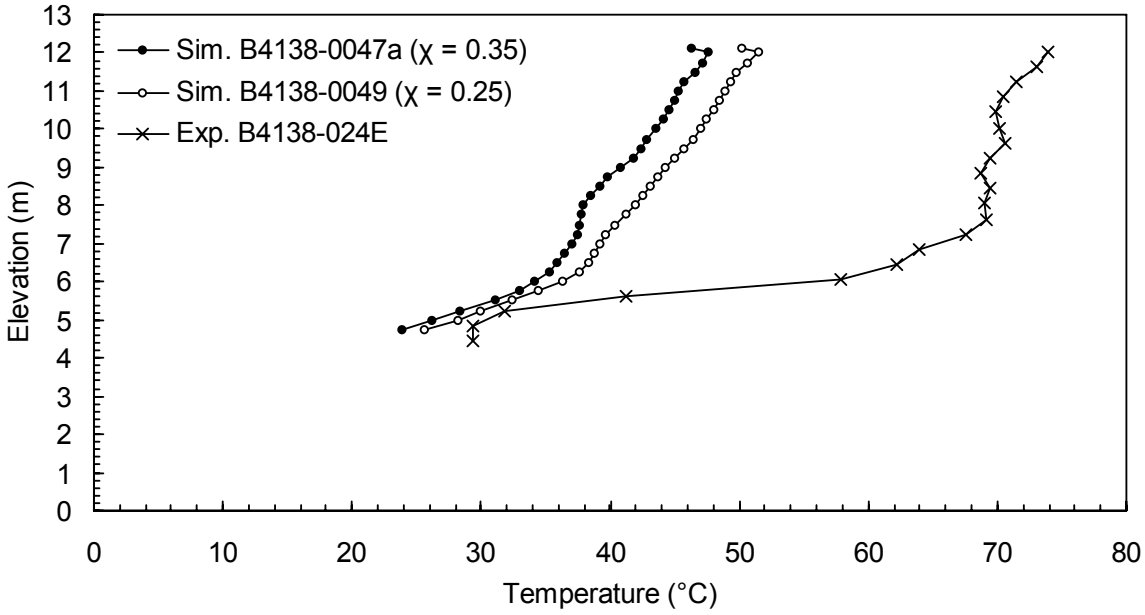

Figure 44. Atrium CL temperature profiles for selected experimental facility simulations showing the effect of different radiative fractions, χ.

with changes to the other modeling parameters listed in Table 3.3 may improve the agreement between the simulation results and the experimental data, but such a multivariate sensitivity analysis was deemed beyond the scope of the current research. Therefore, inappropriate specification of the radiative fraction of the fire is not considered the main cause of the discrepancies between the predicted and measured atrium temperatures in the CFD simulations of the experimental facility. The high sensitivity of predicted temperatures throughout the flow domain to the value of radiative fraction, however, is identified as an important issue with use of FDS for these applications. Although the radiative fractions of propane and other simple fuels are well established, the radiative fractions of more complex and/or mixed fuels typically encountered in real atria, and therefore used for atrium design fire calculations, are generally known with less certainty due to the lack of experimental measurements of χ. This suggests that CFD simulations of atrium smoke management systems conducted using software where the effects of radiation play a major role may be subject to large inaccuracies in the magnitudes of predicted temperatures when there is large uncertainty in the value of χ.

Inaccuracies in the Smagorinsky form of the LES turbulence model used in FDS could contribute to the discrepancies between the predicted results and experimental data. The main parameter affecting the accuracy of the turbulence model in FDS is the value of the Smagorinsky coefficient, C_s, an empirical constant relating the sub-grid scale eddy viscosity in the LES turbulence model to the fluid density, filter

length scale and grid-scale strain rate [11]. The technical documentation for FDS [35] suggests a value of $C_s = 0.20$ based on validation of FDS simulations using experimental data from compartment fires. This value is lower than the value of $C_s = 0.23$ originally proposed by Smagorinsky [50]. Due to the lack of guidance for selecting an appropriate value for the Smagorinsky constant for LES modeling of buoyant fire plumes, the default value of $C_s = 0.20$ suggested by FDS is used in all CFD simulations conducted as part of this thesis. It is thought that changing the value for C_s would affect the turbulence generation and dissipation rates, resulting in an effective redistribution of enthalpy throughout the flow domain rather than contributing directly to apparent additional heat loss from the flow domain. With regard to simulations of the experimental facility, such a redistribution would change the shapes of the atrium temperature profiles but not the average atrium temperature. However, these simulations instead predict atrium temperature profiles which are similar in shape to the experimental data and an average atrium temperature ≈ 30 °C lower than the measured value (for example, Figure 39), giving no indication that using a value of $C_s = 0.20$ inaccurately models the turbulence of the experimental facility airflows. The systemically low atrium temperatures predicted by the CFD simulations is therefore not suspected to be caused by errors in the choice of value for the Smagorinsky constant, C_s, in the LES turbulence model used in FDS.

Although the CFD simulations of the experimental facility all predict atrium temperature profiles with the same shape as the experiments as well as reasonably accurate values for z_l, none of the changes in modeling methodology (Table 3.3) decrease the discrepancies between predicted and measured atrium temperatures to less than 20 °C. A sensitivity analysis of some of the key parameters in these simulations indicates that these discrepancies may be caused by implementation of grid designs, heat transfer effects at boundary conditions, radiative fraction and other issues. The full-scale experimental program temperature measurements used as a basis for comparison include an inherent precision of ±2 °C [44] but may also be affected to a much larger degree (≥ 10 °C) by the effects of radiation and other errors. As noted in Section 2.6, the impact of radiation error on the atrium CL thermocouples is assumed to be negligible due to their distance from the fire and compartment boundaries. Errors in the measurements of exhaust system mass flow rate (m_{exh}) or fire size (Q) obtained during the full-scale experimental program may contribute to the atrium temperature discrepancies. However, such errors would produce discrepancies in both the average atrium smoke layer temperature and atrium smoke layer elevation; only the former is evident in Figure 39. Since the intention of the current research is to examine the behaviour of BSP mass flow rates, it is less important for the model to accurately predict atrium temperatures than it is to predict z_l, which depends primarily on m_{BSP}. Limitations may remain in the design of the CFD model of the experimental facility, including inappropriate boundary conditions, unidentified leakage paths and poor modeling of combustion chemistry. Nonetheless, the simulations have shown that the

CFD model of the experimental facility is able to accurately predict the shape of the atrium temperature profile. More importantly, its ability to predict atrium smoke layer elevations with reasonable accuracy implies that the model can predict BSP mass flow rates with the same accuracy. Based on this assessment, the FDS model of the experimental facility is considered a reasonable foundation for development of an extended model to investigate BSP behaviour at high elevations.

3.3.3 Conclusions of the Experimental Facility Modeling Study

The CFD simulations of the experimental facility predict atrium temperature profiles similar in shape to those measured in the full-scale experimental program with upper hot smoke layers and lower ambient air layers separated by transition regions possessing higher vertical temperature gradients. The predicted atrium temperatures have lower magnitudes than those measured in the experimental program. Atrium smoke layer elevations visually determined from the atrium CL temperature profiles have accuracies of ±0.5 m relative to the experimental data. Simulations conducted to investigate the effect of a number of parameters on predicted atrium temperatures (Table 3.3) do not significantly improve the prediction of atrium temperatures. Discrepancies between predicted and measured atrium temperatures are attributed to limitations in the design of the CFD model of the experimental facility and possible issues with FDS. The results from these simulations support the conclusion that CFD models developed using FDS are able to predict general trends in buoyant plume behaviour in atria such as entrainment into plumes and formation of an atrium smoke layer. Specifically, the ability of FDS to accurately predict BSP mass flow rates is supported by its ability to predict atrium smoke layer elevations with reasonable accuracy.

3.4 Conclusions

The CFD models of the full-scale experimental fire compartment and entire facility are able to predict the depth of the hot smoke layer exiting the compartment to a high degree of accuracy and the atrium smoke layer elevation to an accuracy of ± 0.5 m. These results indicate that FDS is capable of modeling some of the key physical phenomena which determine the behaviour of compartment fires and buoyant fire plumes in atria, including stratification of hot gases in the compartment and atrium and entrainment of ambient air into buoyant plumes. Predicted temperatures differed from those measured in the experimental program by as much as −750 °C in the fire compartment and −30 °C in the atrium. A series of comparative simulations identifies some issues in modeling of buoyant fire plumes in atria using FDS, including: correction of radiation effects on measured temperatures, coupling of conservation equations across grid interfaces, modeling of heat transfer through fuel injection boundary conditions and high sensitivity of predicted atrium temperatures to the value of the radiative fraction. A sensitivity analysis of various modeling methodologies and parameters related to these issues shows how each impacts predicted temperatures, although none to such a degree that the discrepancies between predicted and measured temperatures are substantially reduced. A comprehensive examination of these issues is beyond the scope of this thesis. Nonetheless, the ability of the model of the experimental facility to predict atrium smoke elevation with a reasonable degree of accuracy (± 0.5 m) implies that BSP mass flow rates are also predicted with a similar degree of accuracy. Based on this conclusion, the FDS model of the experimental facility is assumed to form a reasonably accurate basis from which to develop a CFD model of BSP behaviour at high elevations. Chapter 4 describes the development of such a model which is broadly based on the models of the experimental facility but which avoids some of their limitations.

Chapter 4 CFD Model of BSP Behaviour at High Elevations

Two of the major limitations of the existing body of BSP research identified in Chapter 1 are a general lack of data relating to mass flow rates in full-scale BSPs and, in particular, a lack of data for BSP mass flow rates in high-elevation atria i.e. $h_{atr} \geq 10$ m. Both limitations put the accuracy of existing methods used to estimate BSP mass flow rates into question. The full-scale experimental program described in Chapter 2 is designed to begin to address the first limitation, but, as discussed in Section 2.6, does not provide BSP mass flow rate data at elevations greater than 4 m above the balcony elevation. A CFD modeling study of BSP mass flow rates at both full-scale and at high elevations is therefore conducted in order to address the second limitation and extend the experimental data to the prediction of BSP behaviour in high-elevation atria. Predictions of BSP mass flow rates at higher elevations based on CFD simulations are proposed as an alternative to experimental measurements since full-scale, high-elevation atrium experimental facilities are currently unavailable. Previous numerical modeling studies of BSP behaviour (Section 1.1.4) have focused neither on prediction of BSP mass flow rates in full-scale atria nor in high-elevation atria. Therefore, the high-elevation BSP modeling study conducted in this final part of the thesis is the only parametric study of BSP mass flow rate behaviour performed either at full-scale or at high elevations.

This chapter describes the development of a CFD model of BSP behaviour at high elevations and its use in a parametric study to develop a proposed new m_{BSP} estimation method for use in the design of smoke management systems for high-elevation atria ($h_{atr} \geq 10$ m). This model is based broadly on the CFD model of the low-elevation atrium experimental facility described in Chapter 3 which was shown to predict atrium smoke layer elevations with a reasonable degree of accuracy (±0.5 m). Since atrium smoke layer elevation is directly determined by BSP mass flow rate (Table 1.1), this conclusion suggests that a similar model of BSP behaviour at high elevations should predict BSP mass flow rate with a reasonable degree of accuracy. This new model takes into account several of the limitations identified in the low-elevation atrium modeling effort (Sections 3.2.3 and 3.3.3) and incorporates some unique modeling methodologies in order to address limitations in the existing body of experimental BSP mass flow rate data. Typical simulation results are discussed to identify the strengths and limitations of the model and a grid optimization analysis is performed to increase the model's ability to accurately predict BSP behaviour at high elevations. A parametric study of BSP mass flow rate as a function of fire size, compartment geometry and elevation is conducted using the model and results are used to develop a proposed new method for estimating BSP mass flow rates at elevations higher than those addressed by the

existing BSP methods (Section 1.1.2). The new method is then compared to the existing methods to estimate BSP mass flow rates summarized in Table 1.1.

4.1 Design Considerations

Both the existing body of BSP research (Chapter 1) and the CFD models of the experimental facility (Chapter 3) have limitations related to accurate prediction of BSP mass flow rates. This section discusses how the CFD model of BSP behaviour at high elevations is designed to minimize the impact of these limitations on the accuracy of predicted BSP mass flow rates in the current modeling study.

All of the BSP experimental programs and modeling studies reviewed in Chapter 1 measure BSP mass flow rates, m_{BSP}, using the same technique, namely inferring them from an equilibrium atrium exhaust system mass flow rate, m_{exh}, for a given atrium smoke layer elevation, z_l. This reliance on the presence of an atrium to measure m_{BSP} is unavoidable in such experimental programs since the accurate, high-resolution measurement of velocities and temperatures necessary to calculate m_{BSP} directly is prohibitively expensive. In contrast, CFD simulations predict temperatures and velocities throughout the flow domain and allow mass flow rates to be calculated across any plane in that domain. CFD models of BSP flow dynamics therefore do not require the presence of a physically defined atrium in order to predict m_{BSP}. However, all of the CFD modeling studies reviewed in Section 1.1.4 do include a physical atrium and predict m_{BSP} based on equilibria with m_{exh} (as per the experimental method) rather than calculating m_{BSP} directly from predicted flow velocities and temperatures. This methodology is presumably used to allow more direct comparison of the simulation results with the experimental data. The inclusion of an atrium in the CFD geometry used to model BSP flow dynamics is therefore not required, other than to facilitate comparison of the predicted simulation results with experimental data obtained in atrium facilities. The removal of solid surfaces defining an atrium from a CFD model of BSP flow dynamics is further justified by the results of previous BSP experimental programs ([42, 43, 18, 33, 32]) which demonstrate that the atrium walls affect the accuracy of the atrium smoke layer elevation measurements, z_l. Errors in the measurement of z_l will affect the accuracy of the m_{BSP} profiles ($m_{BSP} = f(z_l)$) produced from the experimental data. Therefore, the most fundamental and physically consistent predictions of m_{BSP} would be obtained if no atrium was present, i.e. the BSP was allowed to rise through an ambient atmosphere without interacting with atrium walls or forming an atrium smoke layer.

Based on the justification outlined above, the current CFD model of BSP behaviour at high elevations is developed without an atrium; the flow domain ceiling and walls are modeled as open boundary conditions rather than as solid surfaces. BSP mass flow rates are predicted at discrete elevations over a

range typical of high-elevation atria using a method described in Section 4.2 below. This modeling methodology is unique amongst published BSP modeling studies (Section 1.1.4) and is proposed to minimize the effects on predicted values for m_{BSP} caused by the presence of atrium walls and atrium smoke layer. The removal of the physical definition of an "atrium" from the model allows BSP mass flow rate data to be recorded as a function of elevation over the entire range of typical atrium elevations in a single simulation. In contrast, experimental programs and modeling studies which infer m_{BSP} can measure or predict only a single value for m_{BSP} at a specific elevation z_l in each experiment or simulation. Multiple experiments or simulations are therefore required to define a $m_{BSP} = f(z_l)$ profile over the entire atrium elevation. One of the strengths of the current model is then that the number of simulations required for the parametric study of BSP mass flow rate (Section 4.4) is greatly reduced.

The modeling studies described in Chapter 3 identified a number of issues related to the use of single transformed grid designs, the implementation of multiple grids and modeling of heat transfer through fuel injection boundary conditions (Sections 3.2.3 and 3.3.3) as implemented in the CFD models of the full-scale experimental facility. The effects of these issues were minimized in the previous modeling studies by avoiding the use of multiple grid designs and placing fuel injection boundary conditions on flow domain boundaries (Section 3.3.2). Therefore, these modeling methodologies are incorporated into the CFD model of high-elevation BSP behaviour described in Section 4.2 below. The use of a single, non-transformed grid design limits the accuracy of the predictions of fire dynamics in the compartment and may also affect the accuracy of the predicted BSP flow dynamics under the balcony and in the turning region[2]. However, inaccuracies in the predicted flow dynamics in the fire compartment, approach flow region or turning region are expected to have a small impact on the predicted values of m_{BSP}, especially at higher elevations. This issue is discussed in more detail in Section 4.2.

The design of the CFD model described in the following section takes into consideration limitations in both the CFD software and the existing body of BSP research described above. The removal of atrium wall effects from this model is unique amongst the published BSP modeling studies and is proposed to minimize the effects of the atrium walls and atrium smoke layer on the predicted m_{BSP} profiles.

4.2 CFD Model of BSP Behaviour at High Elevations

This section describes a CFD model developed to predict BSP mass flow rates over a larger range of elevations than that existing in the current body of BSP research (Chapter 1). A fire compartment similar

[2] Section 5.2 refers to a modeling study currently being conducted by a graduate student at Carleton University which focuses on the BSP flow dynamics below the balcony elevation [21].

to that used in the full-scale experimental program (Chapter 2) is modeled in a flow domain with an elevation of 50.0 m. This elevation represents an atrium of approximately 13 storeys, compared to the 4 storey atrium simulated in the CFD model developed in parallel with the full-scale experimental program (Section 2.3.1). The maximum BSP elevation quoted in the reduced-scale experimental programs reviewed in Chapter 1 is 9.2 m ([32]), similar to the maximum value of 9 m measured during NRC's full-scale experimental program. Prediction of BSP mass flow rates for elevations up to 50.0 m is therefore a significant extension to the existing body of BSP research. Once the grid design for the high-elevation BSP model is optimized (Section 4.3), this model is used to conduct a parametric study of BSP mass flow rates at high elevations as a function of fire size, compartment geometry and elevation (Section 4.4).

Figure 45 illustrates the geometry for the CFD model. A 12.0 m wide by 5.0 m deep by 5.0 m high fire compartment is located at floor level in a 50.0 m cubic flow domain. The co-ordinate system origin is located at the compartment opening centerline at ground level with the positive x-axis oriented outward from the fire compartment, the positive z-axis oriented vertically and the positive y-axis oriented relative to both according to the right-hand rule, as shown in Figure 45. The fire compartment opening is located −15.0 m in the x-direction from the flow domain centerline with the opening centerline aligned with the flow domain centerline in the x-z plane. The fire compartment position is selected to allow the BSP to project into the flow domain as far away as possible from the flow domain walls. The flow domain dimensions were selected based on preliminary simulations described in Section 4.3 in order to fully contain the largest BSPs modeled as part of the parametric study (Section 4.4). The flow domain walls and ceiling are specified as open boundary conditions; the flow domain floor is specified as a solid surface with thermal and ignition properties of an inert material (Table 3.2).

Figure 46 illustrates the geometry of the fire compartment in the high-elevation BSP model. The fire compartment is 12.0 m wide by 5.0 m deep by 5.0 m high with an opening which varies between W = 5.0 and 12.0 m. A 12.0 m wide by 5.0 m deep balcony is attached to the fire compartment. Draft curtains with depths of h_{draft} = 0.0 and 2.0 m located at the edges of the fire compartment opening are specified along the full depth of the balcony. Compartment fascia depths of h_{fasc} = 0.0 and 1.5 m are specified. Figure 46 illustrates a typical fire compartment geometry where W = 5.0 m, h_{draft} = 2.0 m and h_{fasc} = 1.5 m. The fire compartment boundaries are specified as solid surfaces with zero thickness and thermal and ignition properties of an inert material (Table 3.2). The fire compartment dimensions were based on those used in the full-scale experimental program (Section 2.3.2) since this facility was designed to simulate typical fire compartment geometries occurring in real atria (Section 2.2). These fire compartment dimensions were rounded off to a resolution of 0.5 m to allow for control volumes of this size to be applied to the flow domain without requiring grid transformations to align the control volume edges exactly with the fire compartment surfaces.

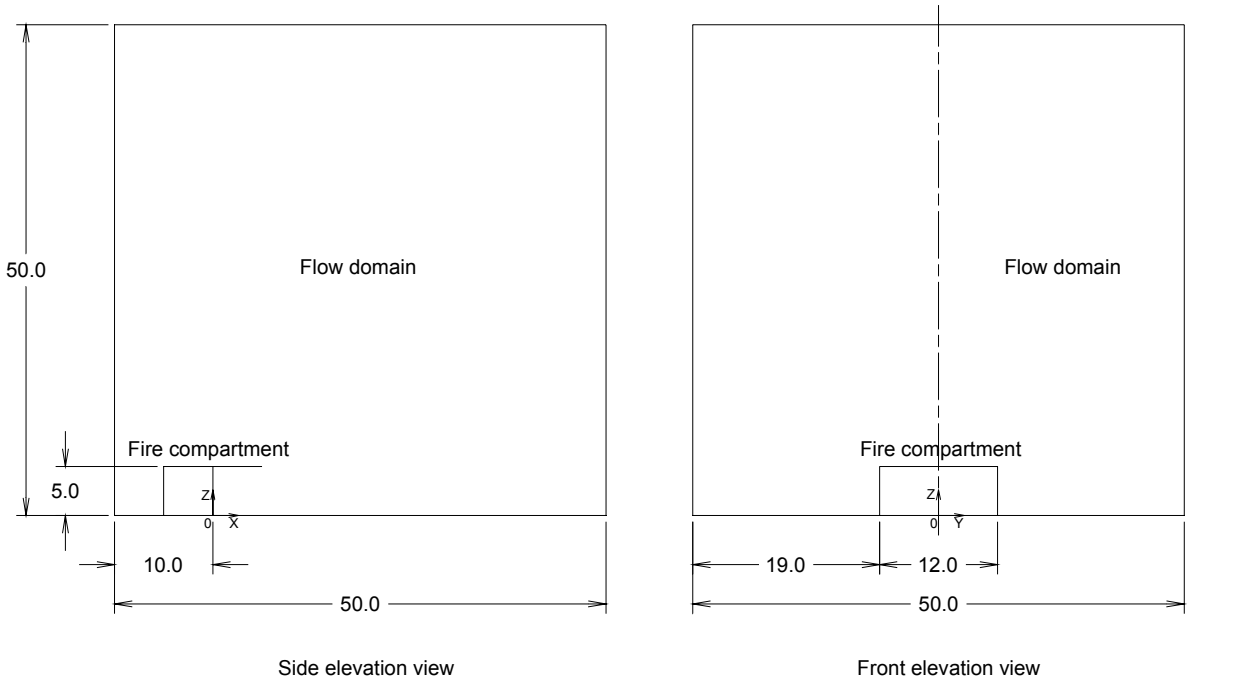

Figure 45. Geometry of the high-elevation BSP model.

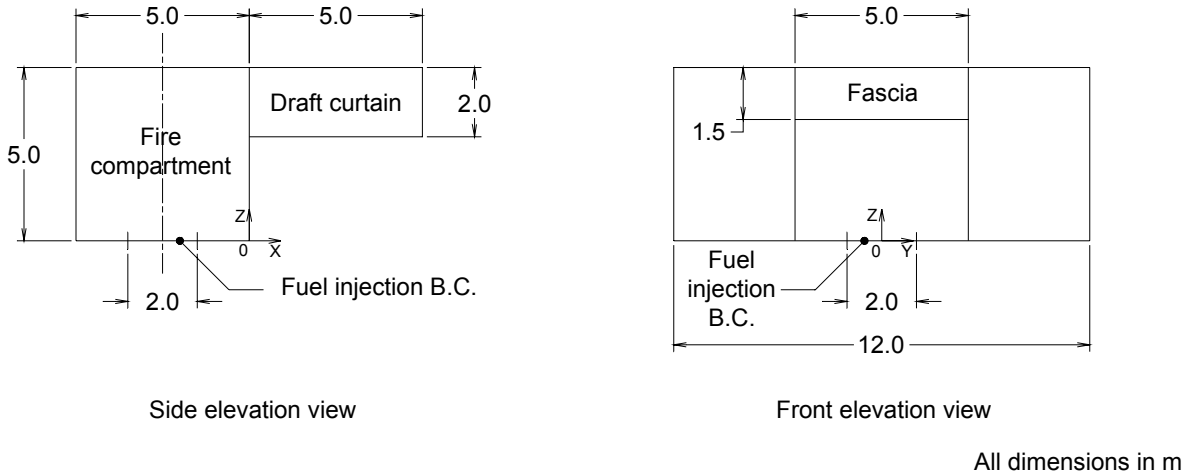

Figure 46. Geometry of the fire compartment in the high-elevation BSP model.

The fire is modeled as a steady release of propane from a square fuel injection surface located at the center of the fire compartment (Figure 46). Default values were used for the propane combustion properties, radiation model and ambient conditions (Table 3.1). Based on the conclusions of the fire compartment modeling study (Section 3.2.3), the fuel injection boundary condition is specified along the bottom flow domain boundary (i.e. at an elevation of z = 0.0 m) in order to minimize heat losses from the flow domain through the boundary condition. The size of the fuel injection boundary condition varies from 1 to 9 m^2 to maintain fire densities in the range of Q/A_{burner} = 0.25 to 0.75 MW/m^2. This range is typically assumed to accurately represent fires occurring in real atria (Section 2.3.3). Figure 46 illustrates a typical fuel injection boundary condition area of 2.0 by 2.0 m.

The experimental facility modeling studies conclude that multiple grid designs in FDS simulations may lead to inconsistencies in predicted results due to inappropriate coupling of conservation equations between grids (Section 3.3.2). The fire compartment modeling study concludes that fire compartment temperatures predicted using single transformed grid designs do not agree as well with measured temperatures as predictions using single grids (Section 3.2.3). Based on these results, the simplest possible grid design consisting of a single grid with constant control volume size (i.e. no grid transformation) was chosen to avoid potential inconsistencies caused by other grid designs. Therefore, a single grid design is used here, with a single grid of isometric control volumes (i.e. $\Delta x = \Delta y = \Delta z$) defined over the entire flow domain. This grid design does not assign smaller control volumes over the combustion zone in the fire compartment and may therefore lead to inaccuracies in prediction of the detailed fire dynamics in the compartment. However, the focus of this modeling study is the prediction of BSP mass flow rates at elevations typical of those found in high-elevation atria, not accurate prediction of the underlying compartment fire dynamics. Although the compartment fire dynamics are expected to affect the BSP approach flow and turning regions, accurate prediction of temperatures and velocities in the combustion zone may not be required to accurately predict BSP mass flow rates in the atrium, particularly at the higher elevations. This proposition is assessed further in the grid sensitivity analysis described in Section 4.3.

All data from the simulations is recorded at 1 s intervals throughout the flow domain. Mass flow rates are calculated based on velocities and temperatures across horizontal planes spanning the entire flow domain every 0.5 m in elevation from z = 0.0 to 50.0 m. These predicted values of mass flow rate are assumed to give a close approximation to the BSP mass flow rate, m_{BSP}, at each elevation even though they include a small contribution from the mass flow rate of ambient air which is not generally included as part of the BSP mass flow rate. Measurement of m_{BSP} by itself, without contributions from movements in the ambient air, would require a BSP perimeter to be identified based on either temperature rise or velocity, and m_{BSP} to be calculated based on velocities and temperatures within this boundary. Definition

of a BSP perimeter forms a complicated and somewhat arbitrary data processing procedure. Also, above some critical elevation, ambient air outside of the BSP exhibits no net movement over a period of time by definition, so the mass flow rate of ambient air across a horizontal plane can be assumed to be zero. This assumption may be invalid at elevations below the balcony ($z \leq 5.0$ m) due to the significant flow of ambient air into the fire compartment to react with fuel in the combustion zone. Therefore, although mass flow rates across horizontal planes below the balcony elevation of $z = 5.0$ m are recorded, their accuracy is understood to be limited.

Mass flow rates across the five flow domain open boundary conditions are recorded in order to determine if significant amounts of air are exiting or entering the flow domain, indications that the BSP is intersected by the flow domain boundaries. Analysis of the leakage through the flow domain boundaries was initially conducted as part of the grid optimization analysis described in Section 4.3. Results were used to determine the optimal flow domain area of 50.0 by 50.0 m.

4.3 Grid Optimization Analysis

The CFD model for predicting BSP flow dynamics at high elevations is developed mainly for use in a parametric study of mass flow rates in BSPs typical of those produced by fires in high-elevation atria (Section 4.4). Prior to conducting the parametric study, an analysis is performed to optimize the grid design of the CFD model based on a number of criteria related to the nature of the BSP mass flow rate profiles in the flow domain. A series of simulations are conducted with different grids designed to assess three important parameters: the use of symmetry boundary conditions, the grid sensitivity to control volume size and the overall flow domain area. Some typical, yet preliminary, results from the new CFD model are presented and discussed as an introduction to their use in the grid optimization analysis and parametric study.

The parameters used in each of the simulations performed as part of the grid optimization analysis are listed in Appendix C. Figure 47 is a typical BSP visualization based on the predicted instantaneous temperature field in the flow domain from simulation B4138-0077 at $t = 300$ s. The BSP is predicted to project horizontally into the atrium once it passes the balcony elevation. Note that no atrium smoke layer is evident, as compared to a similar visualization from experimental facility simulation B4138-0047a (Figure 37), due to the absence of a physically defined “atrium” in the high-elevation BSP simulation. Figure 48 is a typical three-dimensional BSP visualization from simulation B4138-0077 at $t = 300$ s, with the BSP boundary defined based on an isothermal surface with $T_{surf} = 22$ °C. This visualization indicates that the BSP perimeter is defined by a series of highly complex flow features, similar to those seen in the visualization from simulation B4138-0047a (Figure 38) using the CFD model of the full-scale

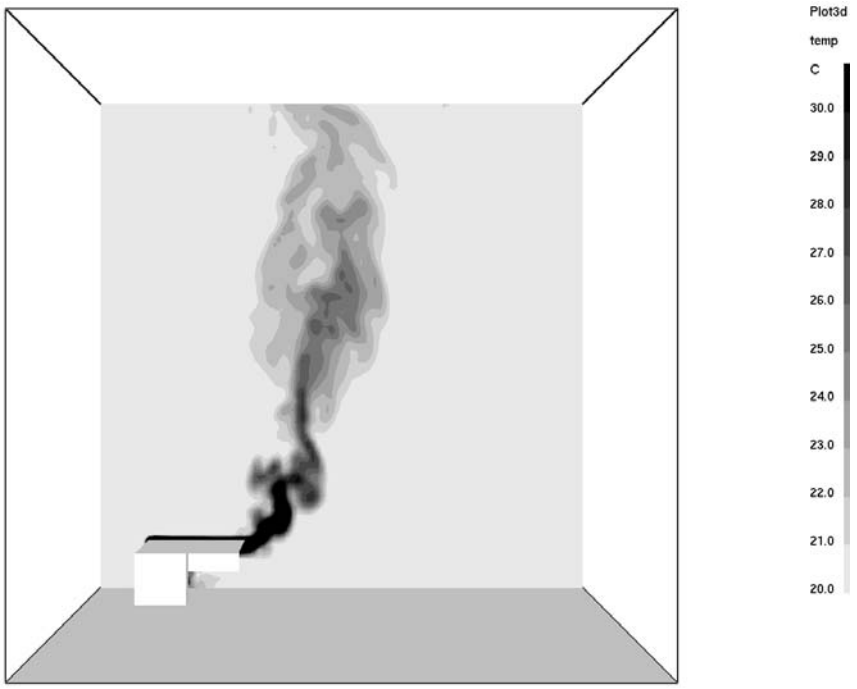

Figure 47. Typical visualization of a BSP based on an instantaneous temperature field from high-elevation BSP simulation B4138-0077 (t = 300 s).

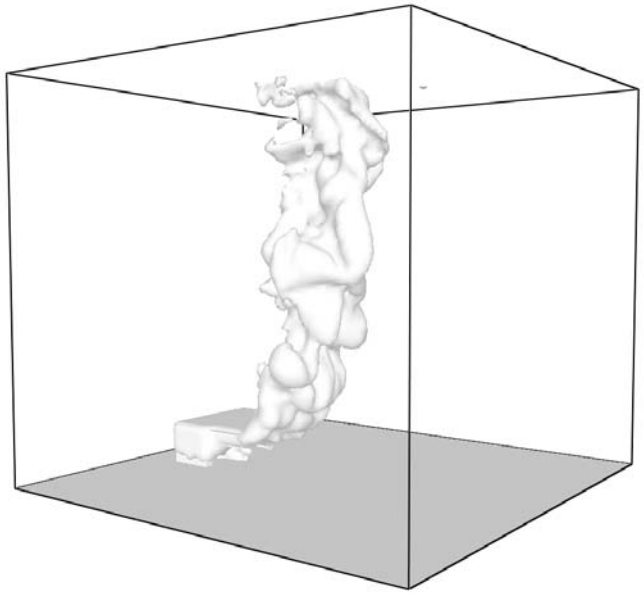

Figure 48. Typical three-dimensional visualization of a BSP based on an isothermal surface from high-elevation BSP simulation B4138-0077 (T_{surf} = 22 °C, t = 300 s).

experimental facility. In the present simulations, the absence of an atrium smoke layer having a temperature comparable to that of the BSP allows much clearer visualization of the BSP perimeter (based on isothermal surfaces) than in the previous simulations of the experimental facility (Figure 48 vs. Figure 38). It should be noted here that while temperatures are predicted in all of the present simulations, the emphasis is on prediction of BSP mass flow rates, so the temperatures are used solely for visualization and diagnostic purposes and are not analyzed further in this thesis.

Figure 49 plots the BSP mass flow rates recorded at every 0.5 m in elevation from z = 0.5 to 50.0 m above the floor for a typical simulation (B4138-0077: Q = 2.0 MW, W = 10.0 m, h_{fasc} = 0.0 m, h_{draft} = 2.0 m). The highest BSP mass flow rates occur at the highest elevations; the lowest BSP mass flow rates occur near the bottom of the flow domain. This trend agrees with that expected based on existing expressions for the prediction of m_{BSP} (Table 1.1) which estimate that $m_{BSP} \propto z$. The predicted values of m_{BSP} at every elevation are transient until $t \approx 45$ s due to the time required for the BSP to rise to the flow domain upper open boundary condition and then stabilize over the entire flow domain. After $t \approx 45$ s, values of m_{BSP} at each elevation exhibit considerable fluctuation about an average, steady value due to the turbulent nature of the BSP. In general, fluctuations about the average value are greater in magnitude at higher elevations due to an increase in characteristic eddy length scale as the BSP rises. This premise is supported by the BSP visualizations shown in Figure 47 and Figure 48 which indicate that variations in predicted BSP temperatures are characterized by larger two- and three-dimensional structures at higher elevations. A steady-state time of t = 120 s is conservatively assumed for all of the high-elevation CFD simulations based on visual inspection of plots similar to Figure 49 from a number of preliminary simulations. The results from preliminary simulations indicated that predicted BSP mass flow rates at all elevations reach steady-state values after $t \approx 120$ s when turbulent fluctuations are neglected, as demonstrated in Section 4.3. Based on this value, simulation times of 300 s are specified for all of the high-elevation BSP simulations, a lower value than the assumed steady-state time of t = 500 s for the full-scale experimental program (Section 2.4) due to the additional time required for a stable atrium smoke layer to form during the experiments.

The predicted m_{BSP} data at every elevation is averaged over the period t = 120 to 300 s to average across the fluctuations illustrated in Figure 49. This temporal averaging yields a single average m_{BSP} profile ($m_{BSP} = f(z_l)$) for each simulation. Figure 50 plots vertical profiles of temporally averaged m_{BSP} predictions from a number of typical simulations as well as the profile plotted in Figure 49. These simulation all have the same compartment geometry (W = 10.0 m, h_{fasc} = 0.0 m, h_{draft} = 2.0 m) but simulate fire sizes ranging from Q = 1.0 to 5.0 MW. The balcony elevation of z = 5.0 m is also plotted as a dashed line in Figure 50 to illustrate the lower limit below which the m_{BSP} data is not expected to be accurate (Section 4.2). Due to the large vertical scale of Figure 50, only a slight irregularity in the m_{BSP}

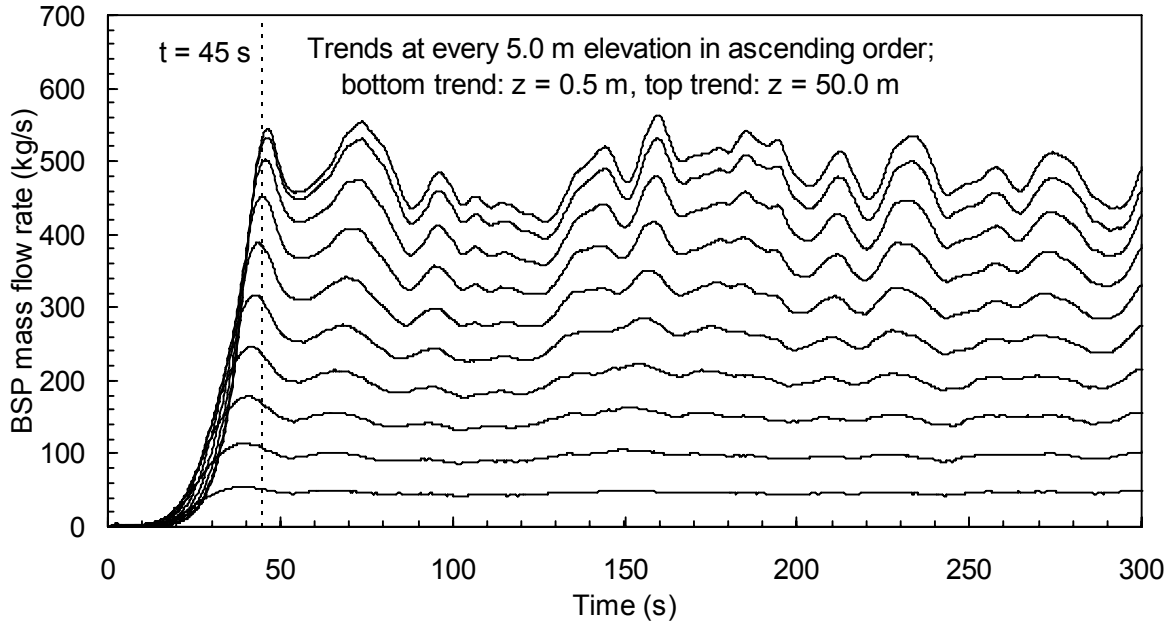

Figure 49. Typical BSP mass flow rate predictions from the high-elevation BSP simulations (B4138-0077: Q = 2.0 MW, W = 10.0 m, h_{fasc} = 0.0 m, h_{draft} = 2.0 m).

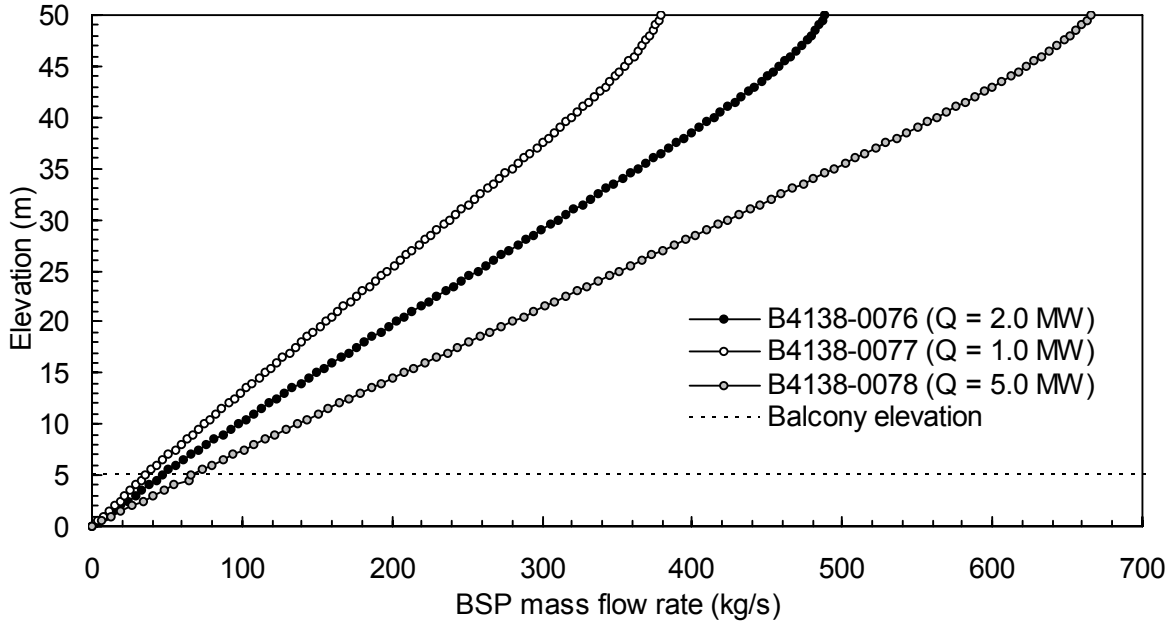

Figure 50. Typical BSP mass flow rate profiles from the high-elevation BSP simulations with various fire sizes, Q (W = 10.0 m, h_{fasc} = 0.0 m, h_{draft} = 2.0 m).

profile predicted by simulation B4138-0078 is evident below the balcony elevation. Comparison of the transient (Figure 49) and temporally averaged (Figure 50) m_{BSP} data from simulation B4138-0077 demonstrates how temporal averaging yields a more easily interpreted version of the m_{BSP} data for each simulation. The profiles plotted in Figure 50 show that m_{BSP} varies nearly linearly with elevation ($m_{BSP} \propto z$) over the majority of the flow domain with some nonlinearities at elevations below the balcony ($z \approx [0.0, 5.0]$ m) and near the top of the flow domain ($z \approx [40.0, 50.0]$ m). Nonlinearities near the top of the flow domain occur in all of the present simulations and appear to span a larger range of elevations as the control volume size increases, therefore discussion of this effect is deferred until the discussion of the grid optimization study below. The overall linear variation of m_{BSP} with elevation throughout most of the flow domain matches the functional form employed for estimation of m_{BSP} in the existing BSP methods (Table 1.1), a fact which supports the conclusion that the present CFD model accurately predicts (at a minimum) trends in BSP behaviour at high elevations. Further, each of the three m_{BSP} profiles plotted in Figure 50 also exhibits a different slope since each models BSP development from the same fire compartment but for a different fire size, Q. As expected from the functional form of the existing expressions for estimation of m_{BSP} as a function of fire size ($m_{BSP} \propto Q^{1/3}$) (Table 1.1), larger values of Q increase the vertical gradient in m_{BSP} (dm_{BSP}/dz) and decrease the slope of the m_{BSP} profiles (dz/dm_{BSP}), again suggesting that the present CFD model accurately captures the major trends embodied in existing m_{BSP} estimation methods.

The BSP mass flow rate profiles predicted by the high-elevation CFD simulations are generally of good quality and appear to capture expected trends in BSP behaviour based on existing methods to estimate m_{BSP}. The predicted profiles are analyzed further in the grid optimization analysis below and in the parametric study (Section 4.4), before being used in development of a proposed new method for estimating BSP mass flow rates at high elevations for application in atrium smoke management system design (Section 4.5).

One of the modeling methodologies assessed in the grid optimization analysis is the use of symmetry boundary conditions. Symmetry boundary conditions are applied to CFD grid designs in order to reduce the number of control volumes needed in the model and thereby either reduce the required computation time or allow additional refinement of key regions of the flow domain. To test the use of symmetry boundary conditions in the current CFD model, simulations of BSP behaviour are conducted using a symmetry boundary condition located at $y = 0.0$ m. This symmetry boundary condition exactly bisects the flow domain, fire compartment and BSP along their coincident planes of symmetry and may be expected to predict simulation results identical to those using a grid design over the full flow domain but requiring half the number of control volumes for each simulation. Figure 51 plots the predicted m_{BSP} profiles from simulations with and without the symmetry boundary condition for the same fire size,

compartment geometry, overall flow domain dimensions and control volume size. The values of m_{BSP} predicted by the simulation with a symmetry boundary condition are doubled since only one half of the BSP is modeled. Comparison of the predicted m_{BSP} profiles in Figure 51 shows that the application of a symmetry boundary condition at the fire compartment and BSP centerline results in significantly lower predicted m_{BSP} values ($\approx -7\%$) over the entire flow domain elevation. This is attributed to inaccuracies in the prediction of three-dimensional turbulence and mixing effects across the symmetry plane, which in turn affects the accuracy of the predicted entrainment rate into the BSP and BSP mass flow rate. This seems consistent with the fact that the structure of buoyant fire plumes well away from the fire may be characterized by large eddies which are not symmetrically distributed about the plume centerline at any instant in time. Therefore, specification of a symmetry boundary condition along the BSP centerline is not recommended as a technique for reducing computation times for CFD simulations of buoyant fire or balcony spill plumes and the final optimized grid design for the present CFD model (Section 4.2) does not make use of symmetry boundary conditions.

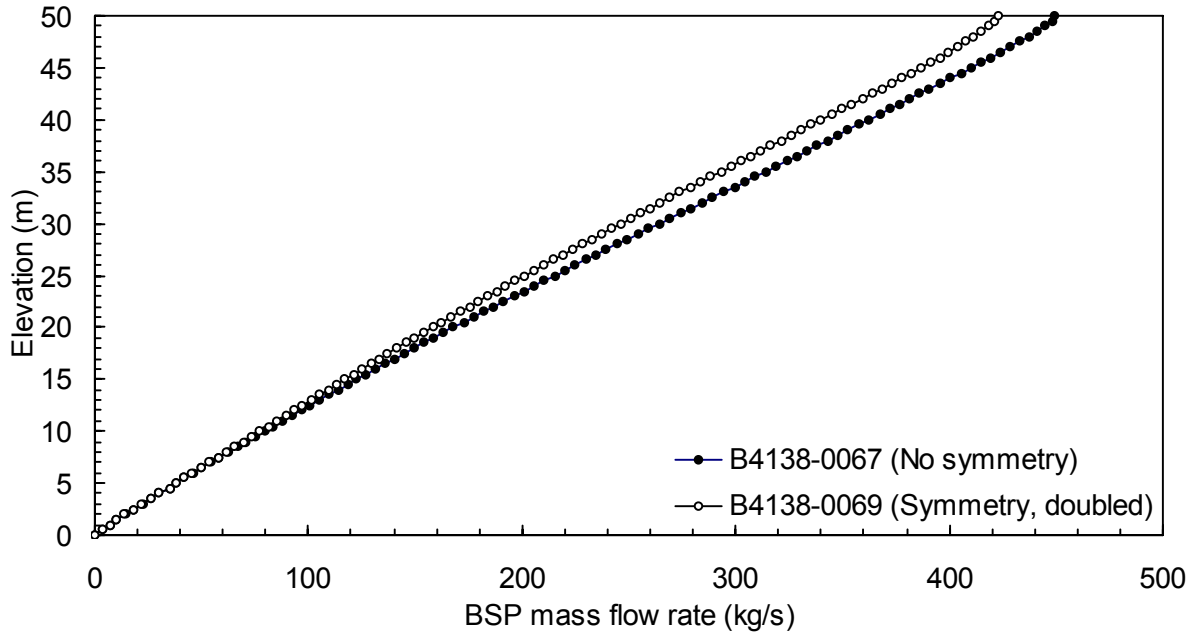

Figure 51. Comparison of predicted BSP mass flow rates with and without a symmetry boundary condition applied at y = 0.0 m (Q = 2.0 MW, W = 5.0 m, h_{fasc} = 0.0 m, h_{draft} = 0.0 m, Δ = 0.5 m).

The second stage in optimization of the computational grid for the current CFD model is to determine the largest control volume size for which predicted values of m_{BSP} are insensitive to the choice of control volume size. It was demonstrated in Chapter 3 that the accuracy of LES-based CFD simulations of buoyant fire plumes depends primarily on the control volume sizes in the combustion zone; however, it is recognized in the high-elevation BSP study that due to the large volumes to be modeled, accurate modeling of the combustion zone may be limited by the total number of control volumes practical with respect to computational requirements as well as limitations of the multiple and/or single transformed grid capabilities of FDS. Determination of the optimized control volume size that affords grid-insensitive predictions for the high-elevation CFD model is therefore based on the model's efficacy with regards to predicted BSP mass flow rates above the balcony elevation. In Chapter 3 and in previous work [16], it is shown that control volume sizes in the range of Δ = 0.1 to 1.0 m are needed to yield reasonably grid-insensitive predictions of buoyant fire plume dynamics in fire compartments and for atria fire scenarios. As part of the current analysis, three high-elevation BSP simulations are conducted, each with a different control volume size in this range: Δ = 0.25, 0.50 and 1.00 m. A fire size of Q = 2.0 MW and an opening width of W = 10.0 m are chosen as being in the middle of their respective ranges. Specification of draft curtain and fascia depths are omitted from the grid sensitivity analysis i.e. h_{fasc} = 0.0 m and h_{draft} = 0.0 m in all simulations. Further, the flow domain height is reduced from 50.0 to 25.0 m for all three simulations in order to reduce the total number of control volumes needed to model the entire flow domain to a practical amount for the simulations using smaller control volumes.

Figure 52 compares the predicted m_{BSP} profiles from the three simulations with different control volume sizes. The profile from simulation B4138-0073 (Δ = 1.00 m) exhibits a stepped trend since the same value of m_{BSP} is predicted for the two mass flow rate measurement planes (Δz = 0.5 m) defined in each control volume (Δz = 1.0 m). All three profiles demonstrate the generally linear behaviour expected from profiles of BSP mass flow rate with elevation (Figure 50). As the control volume size decreases, the non-linear portions of the profiles near the flow domain upper open boundary condition span a smaller elevation. These nonlinearities are not particular to any single cut-off value for the flow domain height, since a simulation with an increased flow domain height of 50.0 m resulted in similar nonlinearities. These nonlinearities are not due to part of the BSP mass flow rate escaping from the flow domain near its ceiling since such leakage was determined to be low for each simulation as part of the grid optimization analysis. Nonlinearities in the m_{BSP} profiles are instead attributed to the propagation of the open boundary condition at the top face of the flow domain back into the computational grid. In essence, the zero pressure requirement imposed along this open boundary condition forces the flow near the ceiling to adapt, whereas in reality, a small pressure difference would be present in this flow region due to buoyancy effects in the plume. Therefore, the nonlinearities in the m_{BSP} profiles near the top face of the

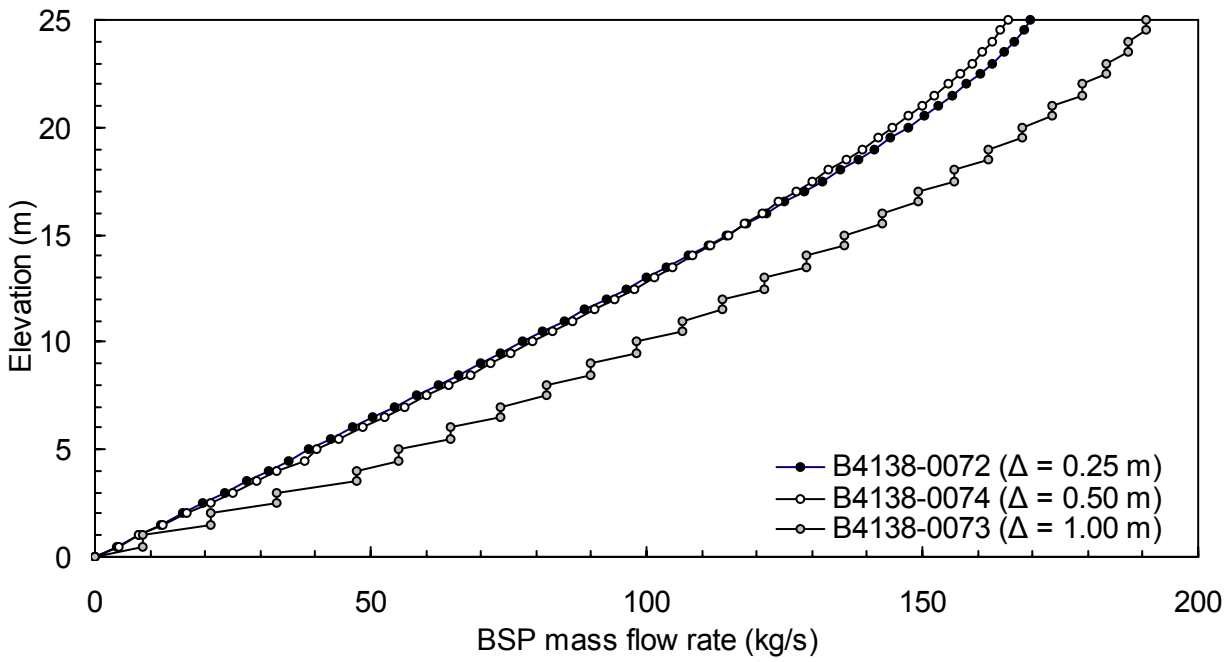

Figure 52. Comparison of predicted BSP mass flow rates with different control volume sizes, Δ.

flow domain are considered a modeling error which is assumed to not significantly affect the BSP flow dynamics in the rest of the flow domain. The method for omission of these nonlinear portions of the m_{BSP} profiles during the parametric study is described further in Section 4.4. Simulation B4138-0073 (Δ = 1.00 m) predicts significantly larger BSP mass flow rates (≈ 20%) over the entire flow domain elevation than those predicted by simulation B4138-0074 (Δ = 0.50 m). In contrast, simulation B4138-0074 (Δ = 0.50 m) predicts values for m_{BSP} which are only slightly larger (≈ 3%) over most of the flow domain elevation than those predicted by simulation B4138-0072 (Δ = 0.25 m). This trend is reversed in the non-linear region near the top face of the flow domain due to the larger size of this region in simulation B4138-0074. Since the predicted m_{BSP} profiles from simulations using control volume sizes of Δ = 0.50 and 0.25 m are approximately equal over the entire flow domain elevation (±4%), a control volume size of Δ_{opt} = 0.50 m is recommended as being optimal for the current high-elevation CFD model. This control volume size is used in all subsequent simulations, including those conducted as part of the parametric study of BSP mass flow rates at high elevations (Section 4.4).

The final parameter examined in the grid optimization analysis is the plan area of the flow domain. The main criterion for selecting the optimal flow domain area is full containment of the BSP within the flow domain in all directions over the full elevation of 50 m. Too small a flow domain will cause the BSP to intersect the flow domain walls at a certain elevation, causing predictions of m_{BSP} above this

elevation to be low due to loss of BSP mass from the flow domain. Too large a domain will unnecessarily increase the total number of control volumes, and therefore the solution time. A series of simulations using flow domains of various sizes and the optimal control volume size of Δ_{opt} = 0.5 m is conducted to determine the minimum flow domain area required to fully contain the BSP. Figure 53 shows predicted mass flow leakage rates through the four vertical flow domain faces, at elevations near the upper face of the domain (z = [45.0, 50.0] m), for a typical simulation with the largest fire size and therefore highest BSP mass flow rate (B4138-0084: Q = 5.0 MW, W = 8.0 m, h_{fasc} = 0.0 m, h_{draft} = 2.0 m). Positive leakage mass flow rates are in the direction of the positive x- or y-axis (Figure 45). The predicted mass flow leakage rates exhibit the same transient trend as the m_{BSP} data described above due to the time required for the BSP to stabilize over the entire flow domain elevation. Mass flow rates leakage rates through all four vertical domain boundaries at this elevation are actually directed into the flow domain to compensate for the BSP mass flow rate exiting the flow domain through the upper boundary. Therefore, no net mass flow rate out of the domain occurs through the four vertical boundaries, indicating that the BSP is fully contained within the flow domain. Based on these results, a minimum flow domain area of 50.0 m by 50.0 m is recommended for the CFD model of BSP behaviour at high elevations and is used in all subsequent simulations. The choice of flow domain area also affects the degree to which the open boundary conditions along the flow domain walls affect the BSP flow near the top of the domain (i.e. where the widening plume most closely approaches the walls). As with the impact of the top boundary condition on the BSP flow described above, any effects of the side boundary conditions on the BSP flow are considered a modeling error which are assumed to not significantly affect the BSP flow dynamics in the rest of the flow domain.

The grid optimization analysis indicates that a 50.0 m cubic flow domain should be used in the simulations of BSP mass flow rates at high elevations. A control volume size of Δ_{opt} = 0.5 m should be adopted for a total of 10^6 control volumes. Symmetry boundary conditions are not recommended and therefore are not included in the final CFD model. The optimized CFD model (Section 4.2) is used to conduct the parametric study described in Section 4.4.

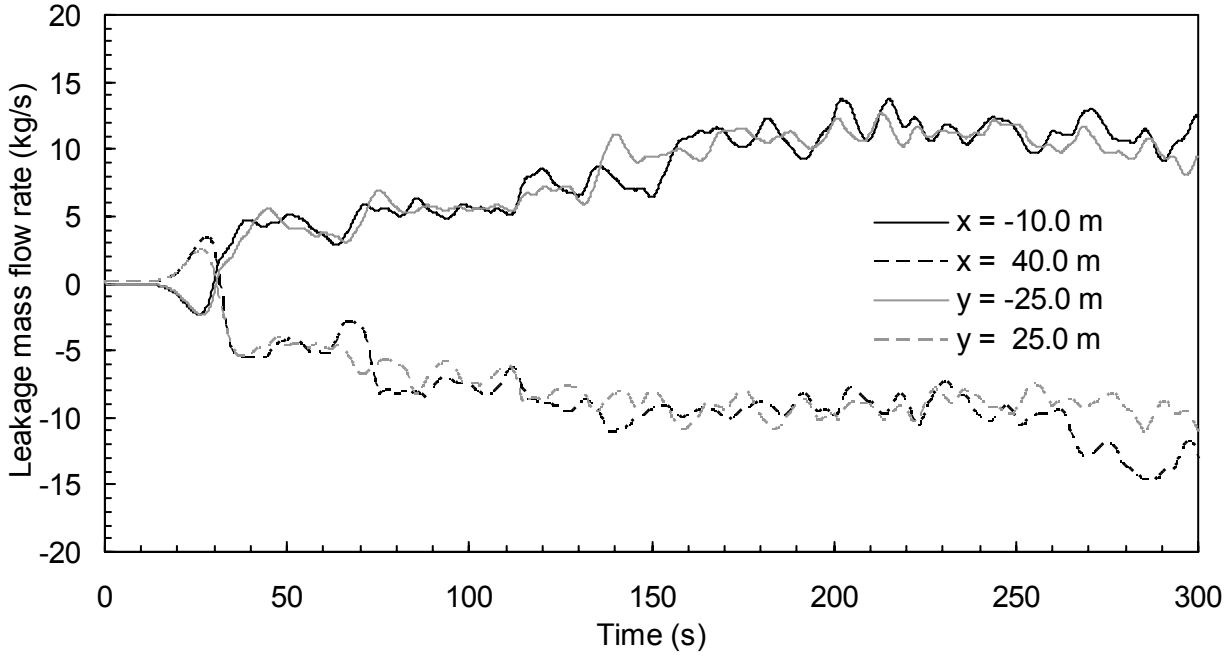

Figure 53. Typical leakage mass flow rates through flow domain walls from the high-elevation BSP simulations, z = [45.0, 50.0] m (B4138-0084: Q = 5.0 MW, W = 8.0 m, h_{fasc} = 0.0 m, h_{draft} = 2.0 m).

4.4 Parametric Study of BSP Mass Flow Rates at High Elevations

This section describes a parametric study of BSP behaviour at high elevations conducted using the CFD model described in the previous sections. The objective is to predict BSP mass flow rate profiles for a range of fire sizes and fire compartment geometries typically found in real, high-elevation atria and use them in the development of a new method for estimating BSP mass flow rates appropriate for the design of smoke management systems in high-elevation atria (Section 4.5).

The parametric study is conducted using the same independent parameters as used in the full-scale experimental program (Chapter 2): fire size (Q), compartment opening width (W), compartment opening fascia depth (h_{fasc}) and draft curtain depth (h_{draft}). The parameter ranges used in the full-scale experimental program are chosen based on typical values found in real atria (Section 2.2). Since the objective of the parametric study is to develop a new BSP estimation method for use in designing atrium smoke management systems, the parameter ranges used for the full-scale experimental program remain valid and are mirrored in this study. Table 4.1 summarizes the values of the parameters used in the parametric study. A compartment opening width of W = 8.0 m is substituted for the value of W = 7.5 m

used in the experimental program because the grid-insensitive control volume size of $\Delta = 0.5$ m used in the high-elevation BSP model does not allow a 7.5 m wide opening to be centered on the wall of the fire compartment. The 8.0 m width is an intermediate value in the range of compartment opening widths and its exact value is not critical to the study. The fascia depth $h_{fasc} = 1.6$ m and draft curtain depth $h_{draft} = 2.9$ m used in the experimental program (Section 2.3.2) are replaced with the values $h_{fasc} = 1.5$ m and $h_{draft} = 2.0$ m, again in order to conform to the optimized control volume size of $\Delta = 0.5$ m in the high-elevation BSP model.

Parameter	Units	Values
Fire size, Q	kW	1 000, 2 000, 5 000
Compartment opening width, W	m	5.0, 8.0, 10.0
Compartment opening fascia depth, h_{fasc}	m	0.0, 1.5
Draft curtain depth, h_{draft}	m	0.0, 2.0

Table 4.1. Parameter values for the parametric study of BSP mass flow rates at high elevations.

Table 4.2 lists the parameters used in each of the simulations conducted for the parametric study. All simulations are conducted using the optimized high-elevation BSP model described in Section 4.2. Simulation times of 300 s are chosen to achieve steady-state conditions. When conducted on a workstation with a Pentium IV 2.5 GHz processor and 1.0 GB of RAM, the simulations require an average of 12.1 h to solve a simulation time of 300 s for an average efficiency ratio of 1:145. Each simulation in the parametric study produces an average BSP mass flow rate profile similar to those shown in Figure 50 above, obtained by averaging the m_{BSP} data at each elevation over the period t = 120 to 300 s. Some simulations where draft curtains were absent ($h_{draft} = 0.0$ m) predicted an approach flow which was visually noted to spill past the ends of the 12.0 m wide balcony in addition to the edge of the balcony parallel to the compartment opening. Since all of the existing methods to estimate m_{BSP} (Section 1.1.2) assume that the approach flow does not spill past the ends of a balcony, these simulations were repeated with a 50.0 m wide balcony to prevent this flow scenario from occurring. Some simulations where draft curtains were present ($h_{draft} = 2.0$ m) predicted a BSP which was visually noted to spill under the draft curtains. These simulations were not repeated and were considered invalid since draft curtains deeper than $h_{draft} = 2.0$ m are assumed to impede egress routes under the balcony. The full dataset from the parametric study is available from the author upon request.[3]

To develop a new BSP estimation method based on the results of the parametric study, it is desirable to express the predicted m_{BSP} profiles using as few independent parameters as possible. For example, m_{BSP}

[3] The author can be contacted via e-mail at: cameron_mccartney@hotmail.com.

Sim.	Fire size, Q (kW)	Opening width, W (m)	Draft curtain depth, h_{draft} (m)	Comp. open. fascia depth, h_{fasc} (m)	C (kg/s-m)	m_0 (kg/s)
76	2 000	10.0	2.0	0.0	10.7	42.2
77	1 000	10.0	2.0	0.0	8.24	32.2
78	5 000	10.0	2.0	0.0	14.4	64.3
79	2 000	5.0	2.0	0.0	9.02	25.3
80	1 000	5.0	2.0	0.0	7.08	19.2
81	5 000	5.0	2.0	0.0	12.9	45.9
82	2 000	8.0	2.0	0.0	10.0	33.1
83	1 000	8.0	2.0	0.0	7.92	26.2
84	5 000	8.0	2.0	0.0	13.2	53.1
86	5 000	8.0	0.0	0.0	17.9	102
87	5 000	5.0	0.0	0.0	20.3	177
90	5 000	5.0	0.0	1.5	22.2	182
91	5 000	5.0	2.0	1.5	12.2	48.7

Table 4.2. Linear regression parameters for parametric study simulations ($m_{BSP} = C\ (z - z_{balc}) + m_0$).

profiles could be described by the slope and intercept of a plot of m_{BSP} with elevation since such profiles have previously been shown to be linear over most of the flow domain elevation (Figure 50) and a linear trend matches the functional form of the existing m_{BSP} estimation methods (Table 1.1) which generally express m_{BSP} as a linear function of elevation. Accordingly, a linear equation is fit to each m_{BSP} profile predicted by the parametric study simulations using linear regression:

$$m_{BSP} = C\ (z - z_{balc}) + m_0 \qquad \text{(Eq. 1)}$$

where m_{BSP} is the BSP mass flow rate (kg/s), C is a proportionality constant (kg/s-m), z is the plume elevation above the atrium floor (m) and m_0 is an offset term representing the BSP mass flow rate at the balcony elevation, z_{balc} (kg/s). The proportionality constant C in Equation 1 is the inverse of the slope of m_{BSP} profiles such as those shown in Figure 50 above i.e. C has units of kg/s-m whereas the slopes of the m_{BSP} profiles have units of m-kg/s. When performing the linear regressions, nonlinear m_{BSP} data near the upper flow domain boundary and below the balcony elevation are not considered. Instead, based on an examination of all m_{BSP} profiles predicted in the parametric study, only m_{BSP} data between z = 15.0 and 35.0 m was considered. Figure 54 illustrates a typical linear fit to the predicted data from simulation B4138-0076. This fit exhibits a high degree of correlation with the data; the coefficient of determination has a value of $R^2 = 0.999996$. The proportionality constant is $C \approx 10.7$ kg/s-m; the offset term, m_0, is calculated as the value of the m_{BSP} linear equation evaluated at the balcony elevation of z = 5.0 m, or

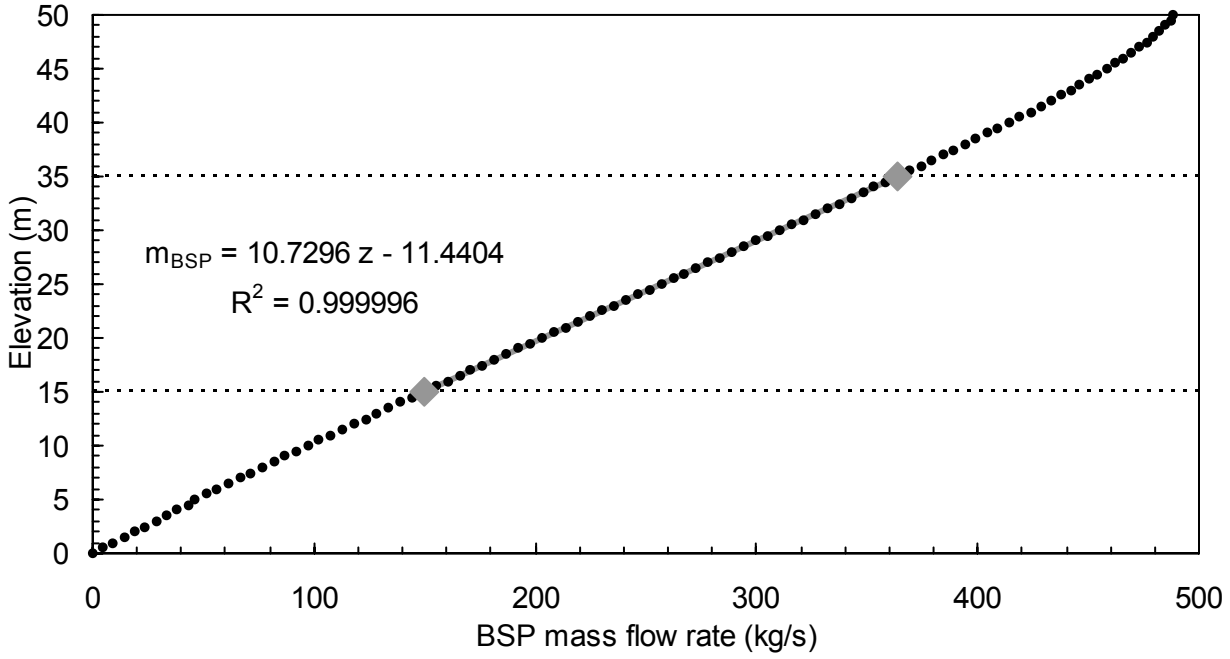

Figure 54. Typical linear regression to m_{BSP} profile predicted by parametric study simulation B4138-0076.

$m_0 \approx 42.2$ kg/s. Taken together, such a pair of values for C and m_0 accurately represent the m_{BSP} profile predicted by a single simulation in the parametric study. Across all simulations conducted in the parametric study, the minimum value of the coefficient of determination is $R^2 = 0.999$, indicating that all of the m_{BSP} profiles are described by Equation 1 to a high degree of accuracy. Table 4.2 lists the proportionality constants, C, and offset terms, m_0, calculated for each of the simulations in the parametric study. Both C and m_0 correlate strongly with fire size, Q, and compartment opening width, W i.e. C, $m_0 \propto Q^n W^m$ ($n > 0$, $m > 0$). This agrees with the functional forms incorporated into existing BSP estimation methods where $C \propto Q^{1/3} W^{2/3}$ (Table 1.1). Examination of the parameters listed in Table 4.2 also allows the dependence of m_{BSP} on the two secondary independent parameters, h_{draft} and h_{fasc}, to be evaluated. This issue is discussed in Section 4.5 with regards to the inclusion of these two parameters in the new BSP estimation method.

The values for the proportionality constant, C, and the offset term, m_0, calculated from the simulations in the parametric study (listed in Table 4.2) are used in the development of a new method to estimate BSP mass flow rates for use in smoke management system design for high-elevation atria (Section 4.5).

4.5 Development of a New BSP Method

The objective of the high-elevation BSP modeling study is to develop a proposed new method by which to estimate BSP mass flow rates at high elevations. The current lack of such a method hinders the design of effective smoke management systems for high-elevation atria. Since the proposed method is based on CFD predictions of BSP mass flow rates at high elevations, it is expected to be more accurate than extension of existing BSP methods based on low-elevation experimental data (Section 1.1.2) to higher elevations. This section describes the development of a method to estimate BSP mass flow rates at high elevations based on the m_{BSP} data provided by the parametric study (Section 4.4). BSP mass flow rates estimated using the proposed method are compared to those estimated using the existing BSP methods (Section 1.1.2) in order to partially evaluate the new method for use in atrium smoke management system design.

The first step in the development of a new m_{BSP} estimation method for high-elevation atria is to specify its functional form. Results from the parametric study (Section 4.4) demonstrate how the BSP mass flow rate profiles predicted by the parametric study simulations are accurately described by linear equations of the form given by Equation 1. The existing BSP methods summarized in Table 1.1 also express BSP mass flow rate as a linear function of elevation. Therefore, the functional form of the new method is specified as a linear function of elevation:

$$m_{BSP} = C(z - z_{balc}) + m_0 \qquad \text{(Eq. 2)}$$

where C is a proportionality constant (kg/s-m), z is the plume elevation above the atrium floor (m), z_{balc} is the balcony elevation (m) and m_0 represents the BSP mass flow rate at the balcony elevation (kg/s). As previously discussed in Section 4.2, the use of relatively large control volume sizes in the simulations of BSP behaviour at high elevations limits the accuracy of predicted compartment fire plume dynamics, as well as that of the approach flow and turning region. These, in turn, limit the accuracy of predicted values of m_0. The high degree of uncertainty in the values of m_0 calculated from the parametric study simulations complicates the development of an accurate expression for m_0 in terms of the independent parameters which affect BSP mass flow rate (i.e. Q, W, etc.). If m_0 is left as an unspecified term in the new BSP method, suitable estimates for this quantity based on compartment fire expressions or empirical data will be required in future to calculate m_{BSP}. Uncertainties in estimated values for m_0, however, will not significantly affect the total accuracy of the new BSP method since the BSP mass flow rate at the balcony elevation (m_0) represents a small fraction of the total BSP mass flow rate (m_{BSP}), especially at higher elevations. Determination of an expression for m_0 in terms of the independent parameters investigated as part of the parametric study is therefore omitted from the current research effort. Guidance for estimating m_0 for use with the new BSP method is given later in this section. The

development of the new BSP method focuses on expressing the proportionality constant, C, in terms of the independent parameters which affect m_{BSP}.

The proportionality constant, C, in Equation 2 represents the increase in BSP mass flow rate per unit height above the balcony and has a particular value for each unique combination of fire size and fire compartment geometry. A general method for estimating BSP mass flow rates at high elevations requires C to be expressed in terms of the independent parameters affecting m_{BSP}: Q, W, h_{fasc} and h_{draft}. The following expression for C in terms of Q and W is assumed based on the existing BSP methods (Table 1.1):

$$C = C_m (Q^n W^m) \qquad \text{(Eq. 3)}$$

where C_m is a proportionality constant characteristic of BSPs (kg/s-kW^n-m^{m+1}), Q is the fire size (kW), W is the compartment opening width (m) and n and m are exponents (-). Neither of the secondary independent parameters, h_{fasc} and h_{draft}, are included in Equation 3 since their impact on m_{BSP} could not be conclusively determined from the limited number of simulations conducted during the parametric study (Table 4.2). Further, an accurate and comprehensive analysis of the variation of m_{BSP} with h_{fasc} and h_{draft} using the high-elevation BSP model is unfeasible due to the aforementioned uncertainties in prediction of approach flow and turning region properties. Therefore, the values of the proportionality constant, C_m, and the exponents n and m in Equation 3 are determined using only values of C, Q and W from those simulations where h_{fasc} = 0.0 m and h_{draft} = 2.0 m (Table 5.2). Ideally, a single value for C_m which is characteristic of BSPs should be calculated from the parametric study data. In reality, slight inconsistencies and/or modeling errors requires an average value to be calculated for C_m based on an optimization criterion. An iterative regression method is used to calculate optimal values for C_m, n and m based on statistical quantities. Initial values of n = 1 and m = 1 were substituted into Equation 3 along with values for C, Q and W from Table 4.2 to calculate initial values for C_m:

$$C_m = C / Q^n W^m \qquad \text{(Eq. 4)}$$

The iterative regression method was initially performed with the criterion of minimizing the standard deviation of the set of values for C_m (σ_{Cm}) determined using the data from the parametric study. However, the use of this criterion predicts optimized values of n and m which approach infinity since such values cause both C_m and σ_{Cm} to approach zero (Equation 4). Instead, a second optimization criterion is used based on minimizing the ratio of σ_{Cm} and the average of the set of values for C_m calculated from the parametric study data i.e. $\sigma_{Cm}/C_{m,ave}$. Normalization of σ_{Cm} by $C_{m,ave}$ removes the tendency for the iterative method to predict optimized values of n and m which approach infinity. The optimal values for n and m are found using a simple iterative procedure where values of both exponents

are varied manually to minimize the quantity $\sigma_{Cm}/C_{m,ave}$. Based on the proportionality constants, C, calculated using data from the CFD simulations with draft curtains ($h_{draft} = 2.0$ m) and without a compartment opening fascia ($h_{fasc} = 0.0$ m), the optimal values of C_m, n and m in Equation 3 are:

$$n = 0.35 \; ; \; m = 0.20 \; ; \; C_m = C_{m,ave} = 0.46 \text{ kg/s-kW}^{0.35}\text{-m}^{1.20} \; (\sigma_{Cm} = 0.020 \text{ kg/s-kW}^{0.35}\text{-m}^{1.20})$$

The value of the fire size exponent, n, in most existing m_{BSP} estimation methods is n = 1/3 (Table 1.1). This is an established value based on fundamental dimensional analysis [25] and can reasonably be assumed to be the same for BSP behaviour as predicted by the parametric study. Forcing n = 0.333 and optimizing the value of m to minimize the ratio $\sigma_{Cm}/C_{m,ave}$ yields:

$$n = 0.333 \; ; \; m = 0.20 \; ; \; C_m = C_{m,ave} = 0.52 \text{ kg/s-kW}^{0.33}\text{-m}^{1.20} \; (\sigma_{Cm} = 0.022 \text{ kg/s-kW}^{0.33}\text{-m}^{1.20})$$

The value of the proportionality constant, C_m, varies greatly with small changes in the value of the fire size exponent, n. The value of C_m with the forced value of n = 1/3 is approximately 13% percent higher than that with the unforced value of n = 0.35. Forcing the value of n to be equal to n = 1/3 causes the magnitude of the standard deviation of the proportionality constant C_m to increase slightly from $\sigma_{Cm} = 0.020$ to 0.022, indicating that Equation 2 with the forced value of n fits the simulation data slightly worse than with the unforced value. Nonetheless, in order to preserve physical consistency, the forced value of n = 0.333 is considered more suitable in the present work and the following new method for estimating BSP mass flow rates at high elevations is proposed based on the best fit of a linear equation for m_{BSP} as a function of elevation, fire size and compartment geometry (Equation 2, Equation 3) to data from the parametric study CFD simulations (Table 4.2):

$$m_{BSP} = 0.52 \, Q^{1/3} W^{0.20} \, z + m_0 \qquad \text{(Eq. 5)}$$

Equation 5 is developed using fire sizes in the range Q = [1.0, 5.0] MW, fire compartment widths in the range W = [5.0, 10.0] m and elevations in the range $z \leq 50.0$ m. This method is applicable only to fire scenarios where the approach flow is channelled by draft curtains. Equation 5 may or may not be accurate if a fire compartment fascia is present. The fire size exponent in Equation 5 is expressed as a fraction to emphasize that it is equal to the exact value of one-third obtained from fundamental dimensional analysis [25]. Conversely, the value of the compartment opening width exponent is expressed to two significant digits to emphasize that it is calculated based on a correlation to CFD simulation data. Since the current research effort has not developed an expression for m_0 as a function of the independent parameters Q and W, m_0 should be estimated in a manner that is both conservative and consistent with existing guidance. For example, Morgan and Hansell [41] suggest that either a) the absence of a compartment opening fascia ($h_{fasc} = 0$) will cause no entrainment to occur into the approach

flow between the compartment opening and balcony edge and m_0 should therefore be approximated as equal to the approach flow mass flow rate at the compartment opening, m_o; or b) the presence of a compartment opening fascia ($h_{fasc} > 0$) will cause significant entrainment to occur into the approach flow and m_0 should therefore be conservatively estimated as equal to twice m_o based on unpublished research by Marshall which examined this flow scenario in a limited number of experiments. In either case, the mass flow rate of the approach flow at the compartment opening, m_o, can be calculated using established expressions for the mass flow rate of hot gases from compartment fires [49].

Validation of the new m_{BSP} estimation method given in Equation 5 is not currently possible due to the lack of experimental measurements of BSP mass flow rates at high elevations. However, a limited form of evaluation may be achieved by comparing Equation 5 to the existing BSP methods summarized in Table 1.1. Table 4.3 repeats selected information on the functional forms of the existing BSP estimation methods originally given in Table 1.1, including the equivalent proportionality constant, C, for each method. The expression for the proportionality constant from Equation 5 ($C = 0.52\ Q^{1/3}W^{0.20}$) is divided by the expressions for C from each existing method to illustrate the differences between the methods.

Method	$C = C_m Q^n W^m$ (kg/s-m)	BSP end entrainment	C_{McC}/C (-)	C_{McC}/C, W = [5.0, 10.0] m (-)
BRE [40]	Not included	Yes	N/A	N/A
Law [22]	$0.38\ (QW^2)^{1/3}$	Yes	$1.37W^{-0.467}$	[0.467, 0.647]
Thomas [51]	$0.21\ (QW^2)^{1/3}$	Yes	$2.48W^{-0.467}$	[0.846, 1.17]
Law [24]	$0.35\ (QW^2)^{1/3}$	Yes	$1.48W^{-0.467}$	[0.505, 0.698]
CIBSE [7]	$0.36\ (QW^2)^{1/3}$	Yes	$1.44W^{-0.467}$	[0.491, 0.680]
Poreh et al. [45]	$0.16\ (QW^2)^{1/3}$	No	$3.25W^{-0.467}$	[1.11, 1.53]
Thomas et al. [54]	$0.159\ (QW^2)^{1/3} + 0.09\ (Q/W)^{1/3}$	Yes	$0.52W^{0.20}/(0.159W^{2/3}+0.09W^{-1/3})$	[1.09, 1.39]
Harrison [19] after Poreh et al. [45]	$0.20\ (QW^2)^{1/3}$	Yes	$2.60W^{-0.467}$	[0.887, 1.23]
Harrison [19] after Thomas et al. [54]	$0.20\ (QW^2)^{1/3}$	Yes	$2.60W^{-0.467}$	[0.887, 1.23]
NFPA [14]	$0.41\ (QW^2)^{1/3}$	Yes	$1.27W^{-0.467}$	[0.433, 0.599]
McCartney	$0.52\ Q^{1/3}W^{0.20}$	Yes	1	[1, 1]

Table 4.3 Comparison of proportionality constants, C, from proposed new and existing BSP methods.

Since each of these ratios, C_{McC}/C, is a function of compartment opening width, W, the two endpoints of the range of values for W used in the parametric study, W = [5.0, 10.0] m, are used to calculate the range of value for these ratios. Comparison of the offset terms, m_0, from the proposed new and existing BSP methods is not performed here due to the previously stated inaccuracy in the predictions of this quantity.

Table 4.3 shows that the values of the fire size exponent, n, in the new and existing BSP methods are both n = 1/3 since the value from the existing methods as based on theory was used in the development of Equation 5. The value of C_m = 0.52 kg/s-m in the new method is much larger than all of the values for C_m reported in the existing BSP methods. This is due primarily to the smaller value for the compartment opening width exponent, m. The value of the compartment opening width exponent, m, is the main difference between the proposed new and existing BSP methods with the value of m in the new method being one-third the values of m in all of the existing methods. The implications of this difference are discussed later in this section. The values of the ratio C_{McC}/C vary considerably for the range of compartment opening widths, W, used in the parametric study, ranging from C_{McC}/C = 0.433 to 1.53. This indicates that the new BSP method will estimate values for m_{BSP} which are between −67% and +53% of those estimated by the existing methods. As discussed in Section 1.1.3, the mutual variance of the existing BSP methods is one of their major limitations. The fact that the new BSP method predicts values for m_{BSP} in the middle of the range estimated by the existing BSP methods supports the validity of the new method in a limited fashion. The value of C_{McC}/C is less than unity for all but three of the existing BSP methods, indicating that they will predict a greater value for m_{BSP} at a given elevation than the proposed new method. The value of C_{McC}/C for Thomas' method [51] varies around an average value of 1.01, indicating that it will predict approximately the same m_{BSP} at a given elevation as the new BSP method, depending on the compartment opening width, W. The values of C_{McC}/C for Poreh et al.'s [45] and Thomas et al.'s [54] methods are greater than unity, indicating that they will predict a lower value for m_{BSP} at a given elevation than the proposed new method. This may be explained by the fact that the experimental data used in the development of these two methods ([32]) was measured in a substantially atrium geometry than the data used in the development of the other BSP methods. It is of particular interest than the new BSP method will predict a value of m_{BSP} at a given elevation which is approximately half of that predicted by the NFPA method [14], which is the current guidance for North American atrium smoke management system designers [14]. The results of the parametric study of BSP mass flow rates at high elevations may indicate that atrium smoke management systems designed using the current North American guidance are overspecifying their fan capacities by up to a factor of two, incurring a major added expense in system installation.

Comparison of the proposed new and existing BSP methods (Table 4.3) indicates that one major difference between them is the value of the compartment opening width exponent, m. The value of

m = 2/3 in the existing BSP methods is based on fundamental dimensional analysis of the development of buoyant line plumes from heated sources. The reduced value for m based on the results of the present parametric study may indicate that BSPs are not accurately represented as equivalent buoyant line plumes. BSPs are known to degenerate from a finite length buoyant line plume at the balcony edge to an axisymmetric plume at higher elevations. For example, Yokoi's experiments [58] showed that window plumes behaved less like line plumes and more like axisymmetric plumes at higher elevations above their virtual sources. Thomas' [51] expression for BSP mass flow rate (Table 1.1) combines mass flow rate expressions from line and axisymmetric plumes such that the former dominates at lower elevations and the latter dominates at higher elevations. After passing the balcony edge, the BSP ends will experience higher entrainment relative to the front and back of the plume because of their larger available area for entrainment. This will tend to enlarge the BSP ends and increase the curvature of the plume at the ends. Given sufficient elevation to complete this degeneration process, the BSP will naturally tend towards a circular cross-sectional area i.e. an axisymmetric plume. Established expressions for the mass flow rate of axisymmetric plumes take the form $m_{axi} = C_m Q^{1/3} z^{5/3}$ [49]. This is equivalent to a compartment opening width term exponent of m = 0, since the axisymmetric plume is assumed to originate from a point source. Given that the value of m = 0.20 in the new BSP method falls between the values of m = 2/3 for a buoyant line plume and m = 0 for an axisymmetric plume, the proposition than BSPs are most accurately described as a hybrid between line and axisymmetric plumes is supported. Further research into the degeneration of BSPs from line plumes to axisymmetric plumes is required to determine whether the exponent proposed in this research is valid, as well as to determine the best way to incorporate the effects of BSP degeneration into a method for estimation of BSP mass flow rates.

4.6 Conclusions

A modeling study of BSP mass flow rates at high elevations is conducted using a CFD model of a BSP issuing into a large volume flow domain. This model is unique in that the flow domain boundaries are specified as open boundary conditions rather than solid surfaces in order to reduce the impact of the atrium walls on the accuracy of the predicted values of m_{BSP} (Section 1.1.2). The flow domain size and control volume size for the CFD model are selected based on a grid optimization analysis. The optimized model is then used in a parametric study to provide vertical profiles of BSP mass flow rate with elevation, at elevations higher than those currently provided by BSP experimental programs and modeling studies. These data are analyzed to yield a new method for estimating BSP mass flow rates at high elevations (Equation 5). Comparison of this method with existing BSP methods shows that the new method estimates values for m_{BSP} which are bounded by those predicted by existing methods.

Chapter 5 Conclusions

Two CFD modeling studies of a full-scale experimental BSP facility and one of BSP behaviour at high elevations ($z \leq 50$ m) were conducted to develop a new method to estimate BSP mass flow rate at elevations typical of those found in modern atria. The CFD models of the full-scale experimental fire compartment and entire facility were able to predict, with reasonable accuracy, the general shape of the vertical temperature profiles at the compartment opening and in the atrium. Specifically, these models were able to predict the depth of the hot smoke layer exiting the compartment with a high degree of accuracy and values of the atrium smoke layer elevation with an accuracy of ± 0.5 m. Predicted temperatures differed from those measured in the experimental program by as much as −750 °C in the fire compartment and −30 °C in the atrium. These discrepancies were attributed to radiation effects inherent in the experimental data and issues with the software used to implement the models, including the coupling of conservation equations across grid interfaces and modeling of heat transfer through fuel injection boundary conditions. A sensitivity analysis of these issues was unable to substantially reduce the discrepancies between predicted and measured temperatures. Nonetheless, the ability of the model of the experimental facility to predict atrium smoke layer elevation with a reasonable degree of accuracy (± 0.5 m) implies that BSP mass flow rates may be accurately predicted in similar models.

Based on the results of the first two modeling studies, a CFD model of BSP behaviour at high elevations was developed to predict BSP mass flow rates at elevations up to 50 m. Physical boundaries representing an atrium were not specified in this model in order to reduce the impact of the atrium walls on the accuracy of predicted values of m_{BSP}. A parametric study of the variation of BSP mass flow rate with fire size, compartment geometry and elevation produced data from which a new method for estimating BSP mass flow rates in high-elevation atria was developed, as summarized in Section 5.1.

The results from this research effort demonstrate the utility of combining full-scale experimental data on buoyant plume flow dynamics with results from CFD simulations to develop engineering correlations appropriate for use in design of atrium smoke management systems. This research also identifies and suggests methods to address some of the limitations that should be considered when using CFD techniques in the design and evaluation of atrium smoke management systems.

5.1 New BSP Method

The following new method for estimating BSP mass flow rates in high-elevation atria is proposed based on the best fit of a linear equation for m_{BSP} as a function of elevation, fire size and compartment opening width to data from the CFD simulations conducted during the parametric study:

$$m_{BSP} = 0.52\, Q^{1/3} W^{0.20}\, z + m_0 \qquad \text{(Eq. 6)}$$

The new BSP method is developed using fire sizes in the range Q = [1.0, 5.0] MW, fire compartment widths in the range W = [5.0, 10.0] m and elevations in the range $z \leq 50.0$ m. This method is applicable only to fire scenarios where the approach flow is channelled by draft curtains and may or may not be accurate if a fire compartment fascia is present. Since the current research effort does not express m_0 as a function of the independent parameters Q and W, m_0 should, for lack of a proven alternative, be estimated in a manner consistent with existing guidance [41, 49] (Section 4.5).

Comparison of predicted BSP mass flow rates using the new BSP method with those predicted using existing BSP methods shows that the former predicts values for m_{BSP} in the middle of the range estimated by existing methods. Specifically, the new BSP method estimates values for m_{BSP} which are between −67% and +53% of those estimated by the existing methods. This supports the general validity of the new method in a limited fashion. The new m_{BSP} estimation method predicts a value of m_{BSP} at a given elevation which is approximately half of that predicted by the NFPA method [14], which is the current guidance for North American atrium smoke management system designers.

5.2 Future Work

The new BSP mass flow rate estimation method is limited in that it does not provide an expression for the BSP mass flow rate at the balcony elevation, m_0. Further, the impact of a compartment opening fascia on the estimated value of m_{BSP} using the new method is believed to be small according to limited results from the parametric study but cannot be definitively stated. Additional characterization of the compartment fire dynamics and the BSP approach flow and turning region flow dynamics is required to address these limitations. Current research by Ko [21] at Carleton University focuses on modeling the BSP approach flow and turning region using CFD techniques with the objective of deriving new expressions for the BSP mass flow rate at various locations, including the compartment opening, balcony elevation, and upper limit of the turning region. Results from this study should supplement the research presented here and may quantify the m_0 term in the new BSP method.

The new BSP method has not been validated using experimental data due to the lack of full- or model-scale BSP mass flow rate data for high-elevation atria. Future experimental programs or CFD modeling

studies are required to provide additional data for validation of this method. These could potentially be conducted in the new ten-storey, full-scale atrium facility recently constructed by Carleton University in Almonte, Ontario. This facility was not available for use in the experimental program described in Chapter 2 but may be used in future programs to provide data for validation of methods to estimate buoyant plume properties for high-elevation atria applications.

References

1. ASTM E 2067-03 Standard practice for full-scale oxygen consumption calorimetry. American Society of Testing and Materials, West Conshohocken, PA. 2003.

2. Bilger, R.W. Turbulent diffusion flames. Annual Review of Fluid Mechanics, v.21, pp.101–135. 1989.

3. Chow, W. K. Numerical simulations on balcony spill plume. Fire and Materials v.23(6), pp.91-99. 1999.

4. Chow, W. K., Cui, E. CFD simulations on balcony spill plume. Journal of Fire Sciences, v.16(6), pp.468-485. 1998.

5. Chow, W. K., Li, J. Simulation on natural smoke filling in atrium with a balcony spill plume. Journal of Fire Sciences, v.19(4), pp.258-277. 2001.

6. Chow, W. K., Yin, R. Discussion on two plume formulae with computational fluid dynamics. Journal of Fire Sciences, v.20, pp.179–201. 2002.

7. CIBSE Guide Volume E: Fire Engineering. Chartered Institution of Building Services Engineers, London. 1997.

8. Cooper, L., Harkleroad, M., Quintiere, J., Rinkinen, W. An experimental study of upper hot layer stratification in full-scale multiroom scenarios. Journal of Heat Transfer, v.104, pp.741-749. 1982.

9. Drysdale, D. An Introduction to Fire Dynamics (2nd ed.). Wiley Press, ISBN 0-471-97291-6. 1998.

10. FDS/Smokeview examples (http://fire.nist.gov/fds/docs/FDS_SV_Survey_2005_7.pdf). National Institute of Standards and Technology, McGrattan, K. (ed.). 2005.

11. Ferziger, J. H., Perić, M. Computational methods for fluid dynamics (3rd ed.). Springer Verlag, ISBN 3-540-42074-6. 2002.

12. Forney, G. P., McGrattan, K. B. User's guide for Smokeview version 3.1 – a tool for visualizing fire dynamics simulation data, NISTIR 6980. National Institute of Standards and Technology. 2003.

13. Grove, B. S., Quintiere, J. G. Calculating entrainment and flame height in fire plumes of axisymmetric and infinite line geometries. Journal of Fire Protection Engineering, v.12, pp.117–137. 2002.

14. Guide for smoke management systems in malls, atria and large area (1991 ed.), Publication No. 92B. National Fire Protection Association, Quincy, MA, USA. 1991.

15. Guide for smoke management systems in malls, atria and large areas (2000 ed.), Publication No. 92B. National Fire Protection Association, Quincy, MA, USA. 2000.

16. Hadjisophocleous, G. V., McCartney, C. J. Guidelines for the use of CFD simulations for fire and smoke modeling. ASHRAE Transactions. 2005.

17. Hansell, G. O., Morgan, H. P. Design approaches for smoke control in atrium buildings. Building Research Establishment Report BR 258. Building Research Establishment, UK. 1994.

18. Hansell, G. O., Morgan, H. P., Marshall, N. R. Smoke flow experiments in a model atrium. Building Research Establishment Occasional Paper OP55. Building Research Establishment, Borehamwood, UK. 1993.

19. Harrison, R. Smoke control in atrium buildings: a study of the thermal spill plume, Fire Engineering Research Report 04/1. University of Canterbury, Christchurch, NZ. 2004.

20. Klote, J. H., Milke, J.A. Principles of smoke management. American Society of Heating, Refrigerating and Air-Conditioning Engineers, Atlanta, GA. 2002.

21. Ko, Y. J. CFD Study of the balcony spill plume: focused on the balcony area. Master of Engineering in Civil Engineering Thesis, Carleton University, Ottawa, Canada. 2006.

22. Law, M. A note on smoke plumes from fires in multi-level shopping malls. Fire Safety Journal, v.10, pp.197-202. 1986.

23. Law, M. Reply to Comments on "A note on smoke plumes from fires in multilevel shopping malls". Fire Safety Journal, v.12, p.85. 1987.

24. Law, M. Measurements of balcony smoke flow. Fire Safety Journal v.24, pp.189-195. 1995.

25. Lee, S. L., Emmons, H. W. A study of natural convection above a line fire. Journal of Fluid Mechanics, v.11(3), pp.353-368. 1961.

26. Li, J., Chow, W. K. Line plume approximation on atrium smoke filling with thermal stratified environment. Journal of Heat Transfer v.125, pp.289-300. 2003.

27. Lougheed, G. D. Expected size of shielded fires in sprinklered office buildings. ASHRAE Transactions, v.103(1), pp.395-410. 1997.

28. Lougheed, G. D., Hadjisophocleous, G. V., McCartney, C. J., Taber, B. C. Large-scale physical model studies for an atrium smoke exhaust system. ASHRAE Transactions, v.105(1), pp. 676-698. 1999.

29. Lougheed, G. D., McCartney, C. J., Taber, B. C. Smoke movement for sprinklered fires. ASHRAE Transactions, v.106(1), pp. 605-619. 2000.

30. Lougheed, G. D., McCartney, C. J., Taber, B. C. Sprinklered mercantile fires. ASHRAE Transactions, v.107(1), pp.730-743. 2001.

31. Madrzykowski, D., Vettori, R. A sprinkler fire suppression algorithm. Journal of Fire Protection Engineering, v.4, pp.151-164. 1992.

32. Marshall, N. R., Harrison, R. Experimental studies of thermal spill plumes. Building Research Establishment Occasional Paper OP1. Building Research Establishment, Borehamwood, UK. 1996.

33. Marshall, N. R., Harrison, R., Morgan, H. P. A study of the mechanisms that govern the entrainment of air into a thermal line plume. Building Research Establishment Building Research Note N65/93. Building Research Establishment, Borehamwood, UK. 1993.

34. McGrattan, K. B., Forney, G. Fire Dynamics Simulator (Version 4) – User's Guide, NIST Special Publication 1019. National Institute of Standards and Technology. 2006.

35. McGrattan, K. B. et al. Fire Dynamics Simulator (Version 4) – Technical Ref. Guide, NIST Special Publication 1018. National Institute of Standards and Technology. 2006.

36. Miles, S., Kumar, S., Cox, G. The balcony spill plume – some CFD simulations. Proceedings of the Fifth International Symposium on Fire Safety Science, pp.237-247. International Association of Fire Safety Science. Melbourne, Australia. 1997.

37. Milke, J. A. Smoke management in covered malls and atria. The SFPE Handbook of Fire Protection Engineering, Chapter 13. Society of Fire Protection Engineers, DiNenno, P. J. (ed.) 2002.

38. Morgan, H. P. The horizontal flow of buoyant gases toward an opening. Fire Safety Journal v.11, pp.193-200. 1986.

39. Morgan, H. P. Comments on 'A note on smoke plumes from fires in multi-level shopping malls'. Fire Safety Journal v.12, pp.83-84. 1987.

40. Morgan, H. P., Ghosh, B. K., Garrad, G., Pamlitschka, R., De Smedt, J-C., Schoonbaert, L. R. Design methodologies for smoke and heat exhaust ventilation, BRE Report 368. Building Research Establishment, Garston, UK. 1999.

41. Morgan, H. P., Hansell, G. O. Atrium buildings: calculating smoke flows in atria for smoke control design. Fire Safety Journal, v.12, pp.9-35. 1987.

42. Morgan, H. P., Marshall, N. R. Smoke hazards in covered, multi-level shopping malls: an experimentally-based theory for smoke production, BRE Current Paper CP48/75. Building Research Establishment, Borehamwood, UK. 1975.

43. Morgan, H. P., Marshall, N. R. Smoke control measures in a covered two storey shopping mall having balconies as pedestrian walk ways, BRE Current Paper CP11/79. Building Research Establishment, Borehamwood, UK. 1979.

44. Omega temperature handbook, The (5th ed.). Omega Engineering Inc. 2005.

45. Poreh, M., Morgan, H. P., Marshall, N. R., Harrison, R. Entrainment by two-dimensional spill plumes. Fire Safety Journal, v.30(1), pp.1-19. 1998.

46. Quintiere, J., Steckler, K., Corley, D. An assessment of fire induced flows in compartments. Fire Science and Technology, v.4, pp.1-14. 1984.

47. Rehm, R. G., Baum, H. R. The equations of motion for thermally driven buoyant flows. Journal of Research of the NBS, v.83, pp.297–308. 1978.

48. Relationships for smoke control calculations. Technical Memoranda TM19:1995, Chartered Institute of Building Services Engineers, London. 1995.

49. SFPE Handbook of Fire Protection Engineering, The. Society of Fire Protection Engineers, DiNenno, P. J. (ed.) 2002.

50. Smagorinsky, J. General circulation experiments with the primitive equations - I. The basic experiment. Monthly Weather Review, v.91(3), pp. 99–164. 1963.

51. Thomas, P. H. On the upward movement of smoke and related shopping mall problems. Fire Safety Journal, v.12, pp.191-203. 1987.

52. Thomas, P. H. Discussion of ‘Measurements of balcony smoke flow’ (Comment). Fire Safety Journal v.24, p.201. 1995.

53. Thomas, P. H., Hinkley, P. L., Theobald, C. R., Simms, D. L. Investigation of the flow of hot gases in roof venting, Fire Research Technical Paper No. 7. The Stationary Office, London, UK. 1963.

54. Thomas, P. H., Morgan, H. P., Marshall, N. R. The spill plume in smoke control design. Fire Safety Journal, v.30, pp.21-46. 1998.

55. Walatka, P. P., Buning, P. G. PLOT3D User's Manual (Version 3.5), NASA Technical Memorandum 101067. National Aeronautics and Space Administration. 1989.

56. Welsh, S., Rubini, P. Three-dimensional simulation of a fire-resistance furnace. Proceedings of the Fifth International Symposium on Fire Safety Science. International Association for Fire Safety Science. Melbourne, Australia. 1997.

57. Yii, E. H. Exploratory salt water experiments of balcony spill plume using laser induced fluorescence technique. Fire Engineering Research Report 98/7. University of Canterbury, Christchurch, NZ. 1998.

58. Yokoi, S. Study on the prevention of fire spread by hot upward current. Building Research Institute Report 34. Japan. 1960.

Appendix A List of Full-Scale Experiments

Test	Step	Start time (s)	End time (s)	Fire size (MW)	Comp. open. width (m)	Comp. open. fascia	Draft curtains	Exhaust fan speed (Hz)	Exhaust system mass flow rate (kg/s)	Curtain opening depth (m)	Louvers
B4138-007	A	0	1006	0.75	12.0	N	N	12	6.26	0.0	None
	B	1006	1539					24	11.83		
	C	1539	2093					36	17.93		
	D	2093	2626					48	23.92		
	E	2626	3170					60	29.33		
B4138-008	A	0	1094	0.5	12.0	N	N	12	6.17	0.0	None
	B	1094	1637					24	12.62		
	C	1637	2180					36	18.35		
	D	2180	2711					48	23.96		
	E	2711	3260					60	29.76		
B4138-010	A	0	885	1.0	5.0	Y	N	12	5.14	0.0	None
	B	885	1480					24	10.77		
	C	1480	2061					36	16.34		
	D	2061	2657					48	21.65		
	E	2657	3240					60	27.32		
B4138-011	A	0	902	2.0	5.0	Y	N	12	4.64	0.0	None
	B	902	1483					24	9.89		
	C	1483	2094					36	14.88		
	D	2094	2683					48	20.28		
	E	2683	3270					60	25.14		
B4138-012	A	0	900	0.5	5.0	Y	N	12	5.21	0.0	None
	B	900	1500					24	11.03		
	C	1500	2110					36	16.75		
	D	2110	2679					48	22.52		
	E	2679	3270					60	27.68		
B4138-013	A	0	1082	0.75	5.0	Y	N	12	4.27	0.0	None
	B	1082	1694					24	10.02		
	C	1694	2286					36	15.90		
	D	2286	2884					48	21.05		
	E	2884	3490					60	26.25		
B4138-014	A	0	921	1.5	5.0	Y	N	12	4.29	0.0	None
	B	921	1513					24	9.37		
	C	1513	2108					36	14.76		
	D	2108	2707					48	19.97		
	E	2707	3330					60	24.52		
B4138-015	A	0	1029	0.5	7.5	Y	N	12	5.21	0.0	None
	B	1029	1607					24	10.71		
	C	1607	2231					36	16.63		
	D	2231	2832					48	21.97		
	E	2832	3420					60	27.24		
B4138-016[1]	A	0	856	1.0	7.5	Y	N	12	5.11	0.0	None
	B	856	1440					24	10.14		
	C	1440	2062					36	15.54		
	D	2062	2654					48	20.92		
	E	2654	3840					60	26.35		
B4138-017[2]	A	0	2690	1.5	7.5	Y	N	30	12.91	0.0	None
	B	2690	3630					60	23.03		

Test	Step	Start time (s)	End time (s)	Fire size (MW)	Comp. open. width (m)	Comp. open. fascia	Draft curtains	Exhaust fan speed (Hz)	Exhaust system mass flow rate (kg/s)	Curtain opening depth (m)	Louvers
B4138-018[3]	A	0	945	2.0	7.5	Y	N	12	4.53	0.0	None
	B	945	1563					24	9.61		
	C	1563	2241					36	14.63		
	D	2241	2815					48	20.04		
	E	2815	4020					60	24.85		
B4138-019	A	0	2630	2.0	7.5	Y	N	60	25.01	0.0	Open @ 1500 s
B4138-020	A	0	1195	1.5	7.5	Y	N	12	4.81	0.0	None
	B	1195	1791					24	10.09		
	C	1791	2363					36	15.42		
	D	2363	2969					48	24.92		
	E	2969	3570					60	25.04		
B4138-021	A	0	1545	0.75	5.0	Y	N	60	27.15	0.0	E, S
	B	1545	2893	1.0					26.16		
	C	2893	3970	1.5					25.58		
	D	3970	5158	2.0					24.93		
	E	5158	6060	3.0					24.29		
B4138-022[4]	A	0	1667	2.0	5.0	N	N	60	26.31	0.0	E, S, W
	B	1667	2837	3.0					25.60		
	C	2837	3870	4.0					24.93		
	D	3870	4107	5.0					24.51		
B4138-023	A	0	1620	1.0	5.0	N	N	60	26.82	0.0	E, S, W
	B	1620	2765	2.0					25.13		
	C	2765	3665	3.0					23.03		
B4138-024[5]	A	0	819	2.0	5.0	N	N	12	4.69	0.0	None
	B	819	1422					24	9.46		
	C	1422	2033					36	14.62		
	D	2033	2644					48	19.26		
	E	2644	3840					60	24.73		
B4138-025	A	0	994	1.0	5.0	N	N	30	13.09	0.0	None
	B	994	1440	1.0				60	26.04		
	C	1440	2142	2.0				60	24.79		
B4138-026	A	0	1950	1.5	5.0	N	N	60	24.73	0.0	None
B4138-027	A	0	2780	1.5	5.0	N	N	60	25.23	0.0	None
B4138-028	A	0	1284	0.5	NA	NA	NA	60	27.29	0.0	None
B4138-030	A	0	880	1.0	5.0	N	Y	12	5.38	0.0	None
	B	880	1480					24	10.79		
	C	1480	2080					36	15.89		
	D	2080	2680					48	21.16		
	E	2680	3280					60	26.55		
B4138-031	A	0	870	0.5	5.0	N	Y	12	5.35	0.0	None
	B	870	1492					24	11.26		
	C	1492	2090					36	16.65		
	D	2090	2670					48	22.16		
	E	2670	3270					60	27.50		
B4138-032	A	0	837	2.0	5.0	N	Y	12	3.97	0.0	None
	B	837	1442					24	23.51		
	C	1442	2042					36	24.48		
	D	2042	2640					48	24.54		
	E	2640	3240					60	24.57		
B4138-033	A	0	3600	2.0	5.0	N	Y	60	27.79	0.0	None
B4138-034	A	0	3600	2.0	5.0	N	Y	0	0.80	0.9	All
B4138-035	A	0	3600	2.0	5.0	N	Y	0	0.56	0.2	All
B4138-036	A	0	2390	2.0	5.0	N	Y	0	0.43	0.2	Lab

Test	Step	Start time (s)	End time (s)	Fire size (MW)	Comp. open. width (m)	Comp. open. fascia	Draft curtains	Exhaust fan speed (Hz)	Exhaust system mass flow rate (kg/s)	Curtain opening depth (m)	Louvers
B4138-036	B	2390	4170	2.0	5.0	N	Y	60	26.22	0.2	Lab
B4138-037	A	0	1089	2.0	5.0	N	Y	0	0.57	0.2	Lab
	B	1089	1989					12	4.90		
	C	1989	2889					24	10.42		
	D	2889	3789					36	15.73		
	E	3789	4689					48	20.94		
	F	4689	5590					60	26.14		
B4138-038	A	0	1126	1.0	5.0	N	Y	0	0.57	0.2	Lab
	B	1126	2026					12	5.39		
	C	2026	2926					24	10.95		
	D	2926	3826					36	16.48		
	E	3826	4726					48	22.11		
	F	4726	5626					60	27.09		
B4138-039	A	0	1053	0.5	5.0	N	Y	0	0.55	0.2	Lab
	B	1053	1953					12	5.77		
	C	1953	2853					24	11.48		
	D	2853	3753					36	17.25		
	E	3753	4653					48	23.26		
	F	4653	5553					60	28.07		
B4138-040	A	0	1341	3.0	5.0	N	Y	0	1.53	0.2	Lab
	B	1341	2241					12	0.70		
	C	2241	3141					24	4.18		
	D	3141	4041					36	9.61		
	E	4041	4941					48	14.69		
	F	4941	5841					60	19.97		
B4138-041	A	0	2030	4.0	5.0	N	Y	0	1.31	0.2	Lab
	B	2030	2930					12	3.52		
	C	2930	3830					24	9.18		
	D	3830	4730					36	14.15		
	E	4730	5630					48	19.06		
	F	5630	6540					60	24.45		
B4138-042	A	0	914	5.0	5.0	N	Y	0	0.59	0.6	Lab
	B	914	1620					36	13.90		
	C	1620	2520					60	24.45		
B4138-043	A	0	1488	5.0	5.0	N	Y	12	3.59	0.6	Lab
	B	1488	2359					24	9.38		
	C	2359	3254					48	18.26		
B4138-044	A	0	1124	0.5	5.0	Y	Y	0	1.22	0.2	Lab
	B	1124	2022					12	6.02		
	C	2022	2895					24	11.88		
	D	2895	3800					36	17.80		
	E	3600	4700					48	23.85		
	F	4700	5600					60	29.31		
B4138-045	A	0	1130	1.0	5.0	Y	Y	0	0.44	0.2	Lab
	B	1130	2000					12	5.36		
	C	2000	2900					24	10.46		
	D	2900	3800					36	16.27		
	E	3800	4700					48	22.69		
	F	4700	5600					60	28.90		
B4138-046	A	0	1120	2.0	5.0	Y	Y	0	1.23	0.2	Lab
	B	1120	2020					12	4.79		
	C	2020	2920					24	10.23		
	D	2920	3805					36	15.96		

Test	Step	Start time (s)	End time (s)	Fire size (MW)	Comp. open. width (m)	Comp. open. fascia	Draft curtains	Exhaust fan speed (Hz)	Exhaust system mass flow rate (kg/s)	Curtain opening depth (m)	Louvers
B4138-046	E	3805	4705	2.0	5.0	Y	Y	48	21.58	0.2	Lab
	F	4705	5605					60	26.38		
B4138-047	A	0	1240	3.0	5.0	Y	Y	0	0.49	0.9	Lab
	B	1240	2150					12	5.80		
	C	2150	3060					24	10.73		
	D	3060	3960					36	16.27		
	E	3960	4260					48	22.12		
	F	4260	5770					60	27.09		
B4138-048	A	0	1364	4.0	5.0	Y	Y	0	1.52	0.4	Lab
	B	1364	2264					12	5.19		
	C	2264	3206					24	10.62		
	D	3206	4030					36	15.48		
	E	4030	4330					48	21.06		
	F	4330	5820					60	26.28		
B4138-049	A	0	1343	5.0	5.0	Y	Y	0	0.81	0.6	Lab
	B	1343	2240					12	9.13		
	C	2240	3140					24	24.40		
B4138-050	A	0	1200	5.0	5.0	Y	Y	0		0.6	Lab
	B	1200	2100					36			
	C	2100	3000					48			
	D	3000	3900					60			
B4138-051	A	0	1200	1.0	10.0	Y	Y	0	1.02	0.2	E, W @ 0.9 m
	B	1200	2100					12	5.20		
	C	2100	3020					24	11.50		
	D	3020	3900					36	17.67		
	E	3900	4800					48	23.95		
	F	4800	5700					60	29.19		
B4138-052	A	0	1140	2.0	10.0	Y	Y	0	1.07	0.2	E, W @ 0.9 m
	B	1140	2070					12	4.81		
	C	2070	2940					24	11.05		
	D	2940	3855					36	16.87		
	E	3855	4740					48	22.12		
	F	4740	5640					60	27.97		
B4138-053	A	0	1170	3.0	10.0	Y	Y	0	0.57	0.2	E, W @ 0.9 m
	B	1170	2100					12	3.75		
	C	2100	3050					24	9.94		
	D	3050	3900					36	14.10		
	E	3900	4800					48	20.68		
	F	4800	5700					60	25.47		
B4138-054	A	0	1590	4.0	10.0	Y	Y	0	0.50	0.4	E, W @ 0.9 m
	B	1590	2520					12	3.54		
	C	2520	3420					24	9.50		
	D	3420	4320					36	14.59		
	E	4320	5220					48	18.66		
	F	5220	6120					60	24.53		
B4138-055	A	0	1422	5.0	10.0	Y	Y	0	0.44	0.4	2E, 2W @ 0.9 m
	B	1422	2320					12	3.03		
	C	2320	3260					24	8.82		
	D	3260	4140					36	13.78		
	E	4140	5040					48	18.68		
	F	5040	5880					60	23.45		
B4138-056	A	0	1270	4.0	10.0	N	Y	0	0.64	0.4	E, W @ 0.9 m
	B	1270	2160					12	3.80		

Test	Step	Start time (s)	End time (s)	Fire size (MW)	Comp. open. width (m)	Comp. open. fascia	Draft curtains	Exhaust fan speed (Hz)	Exhaust system mass flow rate (kg/s)	Curtain opening depth (m)	Louvers
B4138-056	C	2160	3080	4.0	10.0	N	Y	24	9.77	0.4	E, W @ 0.9 m
	D	3080	3970					36	14.99		
	E	3970	4860					48	19.81		
	F	4860	5760					60	25.62		
B4138-057	A	0	1160	1.0	10.0	N	Y	0	0.80	0.2	E, W @ 0.9 m
	B	1160	2060					12	5.35		
	C	2060	2960					24	11.76		
	D	2960	3860					36	17.57		
	E	3860	4780					48	23.99		
	F	4780	5680					60	29.60		
B4138-058	A	0	1140	1.0	10.0	N	Y	0	0.64	0.4	E, W @ 0.9 m
	B	1140	2040					12	5.63		
	C	2040	3240					24	11.69		
	D	3240	4140					36	17.25		
	E	4140	4440					48	23.46		
	F	4440	5940					60	29.23		
B4138-059	A	0	1140	2.0	10.0	N	Y	0	0.64	0.6	E, W @ 0.9 m
	B	1140	2040					12	4.78		
	C	2040	2940					24	9.93		
	D	2940	3840					36	16.65		
	E	3840	4740					48	22.18		
	F	4740	5640					60	26.16		
B4138-060	A	0	1293	3.0	10.0	N	Y	0	0.58	0.9	E, W @ 0.9 m
	B	1293	2193					12	2.70		
	C	2193	3093					24	8.96		
	D	3093	3993					36	13.74		
	E	3993	4893					48	19.63		
	F	4893	5795					60	25.20		
B4138-061	A	0	1333	3.0	10.0	N	Y	0	0.13	0.9	E, W @ 0.9 m
	B	1333	2173					12	3.69		
	C	2173	3105					24	9.94		
	D	3105	4005					36	15.35		
	E	4005	4905					48	20.88		
	F	4905	5805					60	26.20		
B4138-062	A	0	1260	5.0	10.0	N	Y	0	0.75	0.9	E, W @ 0.9 m
	B	1260	2160					12	4.08		
	C	2160	3060					24	9.40		
	D	3060	3960					36	15.10		
	E	3960	4860					48	21.56		
	F	4860	5760					60	25.09		
B4138-063	A	0	1290	3.0	10.0	N	Y	0	0.56	0.6	E, W @ 0.9 m
	B	1290	2160					12	4.32		
	C	2160	3060					24	10.43		
	D	3060	3960					36	15.97		
	E	3960	5145					48	21.45		
	F	5145	6045					60	26.90		
B4138-064	A	0	1200	3.0	10.0	N	N	0	0.68	0.6	E, W @ 0.9 m
	B	1200	2100					12	4.26		
	C	2100	3000					24	9.98		
	D	3000	3900					36	16.33		
	E	3900	4800					48	22.21		
	F	4800	5700					60	28.81		
B4138-065	A	0	1125	2.0	10.0	N	N	0	0.81	0.6	E, W @ 0.9 m

Test	Step	Start time (s)	End time (s)	Fire size (MW)	Comp. open. width (m)	Comp. open. fascia	Draft curtains	Exhaust fan speed (Hz)	Exhaust system mass flow rate (kg/s)	Curtain opening depth (m)	Louvers
B4138-065	B	1125	2010	2.0	10.0	N	N	12	4.58	0.6	E, W @ 0.9 m
	C	2010	2910					24	10.95		
	D	2910	3810					36	16.77		
	E	3810	4710					48	22.37		
	F	4710	5610					60	27.94		
B4138-066	A	0	1170	3.0	10.0	N	N	0	0.70	0.9	E, W @ 0.9 m
	B	1170	2070					12	3.73		
	C	2070	2970					24	10.18		
	D	2970	3870					36	15.85		
	E	3870	4770					48	20.77		
	F	4770	5670					60	26.42		
B4138-067	A	0	1200	4.0	10.0	N	N	0	0.72	0.9	E, W @ 0.9 m
	B	1200	2100					12	4.49		
	C	2100	3000					24	9.95		
	D	3000	3900					36	15.20		
	E	3900	4800					48	20.52		
	F	4800	5700					60			
B4138-068	A	0	1260	5.0	10.0	N	N	0	0.24	0.9	E, W @ 0.9 m
	B	1260	2160					12	3.44		
	C	2160	3060					24	9.43		
	D	3060	3960					36	14.72		
	E	3960	4860					48	19.85		
	F	4860	5760					60	25.13		
B4138-069	A	0	1080	1.0	10.0	N	N	0	0.52	0.4	E, W @ 0.9 m
	B	1080	1980					12	5.77		
	C	1980	2880					24	11.56		
	D	2880	3780					36	17.84		
	E	3780	4680					48	23.78		
	F	4680	5580					60	29.04		
B4138-070	A	0	1140	1.0	10.0	N	N	0	0.69	0.4	E, W @ 0.9 m
	B	1140	2040					12	5.72		
	C	2040	2940					36	17.97		
	D	2940	3840					60	29.71		
B4138-071	A	0	1080	1.0	10.0	Y	N	0	0.67	0.4	E, W @ 0.9 m
	B	1080	1980					12	5.41		
	C	1980	2880					24	11.81		
	D	2880	3780					36	18.13		
	E	3780	4680					48	23.98		
	F	4680	5580					60	29.37		
B4138-072	A	0	1080	2.0	10.0	Y	N	0	0.84	0.4	E, W @ 0.9 m
	B	1080	1980					12	4.76		
	C	1980	3000					24	10.74		
	D	3000	3900					36	16.34		
	E	3900	4800					48	22.14		
	F	4800	5700					60	27.43		
B4138-073	A	0	1140	3.0	10.0	Y	N	0	0.64	0.6	E, W @ 0.9 m
	B	1140	2040					12	4.07		
	C	2040	2940					24	9.86		
	D	2940	3840					36	15.50		
	E	3840	4740					48	21.30		
	F	4740	5640					60	26.08		
B4138-074	A	0	1230	4.0	10.0	Y	N	0	0.53	0.9	E, W @ 0.9 m
	B	1230	2130					12	3.61		

Test	Step	Start time (s)	End time (s)	Fire size (MW)	Comp. open. width (m)	Comp. open. fascia	Draft curtains	Exhaust fan speed (Hz)	Exhaust system mass flow rate (kg/s)	Curtain opening depth (m)	Louvers
B4138-074	C	2130	3030	4.0	10.0	Y	N	24	9.61	0.9	E, W @ 0.9 m
	D	3030	3930					36	14.93		
	E	3930	4830					48	20.40		
	F	4830	5730					60	23.96		
B4138-075	A	0	1105	3.0	10.0	Y	N	0	0.71	0.9	E, W @ 0.9 m
	B	1105	2005					12	4.36		
	C	2005	2905					24	9.73		
	D	2905	3805					36	15.24		
	E	3805	4705					48	20.60		
	F	4705	5605					60	26.10		
B4138-076	A	0	1260	5.0	12.0	Y	Y	0	0.40	0.9	E, W @ 0.9 m
	B	1260	2160					12	4.13		
	C	2160	3060					24	9.70		
	D	3060	3960					36	14.35		
	E	3960	4860					48	20.33		
	F	4860	5760					60	25.20		
B4138-077	A	0	1080	1.0	12.0	Y	Y	0	0.89	0.2	E, W @ 0.9 m
	B	1080	1980					12	5.67		
	C	1980	2880					24	11.54		
	D	2880	3780					36	16.91		
	E	3780	4680					48	23.06		
	F	4680	5580					60	28.64		
B4138-078	A	0	1050	2.0	12.0	Y	Y	0	0.70	0.2	E, W @ 0.9 m
	B	1050	1950					12	4.24		
	C	1950	2910					24	15.53		
	D	2910	3780					36	15.34		
	E	3780	4680					48	20.94		
	F	4680	5580					60	26.48		
B4138-079	A	0	1110	3.0	12.0	Y	Y	0	0.24	0.2	E, W @ 0.9 m
	B	1110	2010					12	3.26		
	C	2010	2910					24	9.43		
	D	2910	3810					36	14.88		
	E	3810	4710					48	19.91		
	F	4710	5610					60	23.71		
B4138-080	A	0	1230	4.0	12.0	Y	Y	0	0.29	0.6	2E, 2W @ 0.9 m
	B	1230	2130					12	3.95		
	C	2130	3030					24	9.63		
	D	3030	3930					36	14.76		
	E	3930	4830					48	20.06		
	F	4830	5730					60	26.75		
B4138-081	A	0	1230	4.0	12.0	Y	N	0	3.51	0.6	2E, 2W @ 0.9 m
	B	1230	2130					12	3.53		
	C	2130	3030					24	9.44		
	D	3030	3930					36	14.51		
	E	3930	4830					48	19.62		
	F	4830	5730					60	24.70		
B4138-082	A	0	1200	5.0	12.0	Y	N	0	2.00	0.6	2E, 2W @ 0.9 m
	B	1200	2100					12	3.08		
	C	2100	3000					24	8.84		
	D	3000	3900					36	13.94		
	E	3900	4800					48	17.66		
	F	4800	5700					60	23.77		
B4138-083	A	0	1080	1.0	12.0	Y	N	0	0.67	0.2	2E, 2W @ 0.9 m

Test	Step	Start time (s)	End time (s)	Fire size (MW)	Comp. open. width (m)	Comp. open. fascia	Draft curtains	Exhaust fan speed (Hz)	Exhaust system mass flow rate (kg/s)	Curtain opening depth (m)	Louvers
B4138-083	B	1080	1980	1.0	12.0	Y	N	12	5.22	0.2	2E, 2W @ 0.9 m
	C	1980	2880					24	10.69		
	D	2880	3780					36	16.79		
	E	3780	4680					48	22.41		
	F	4680	5580					60	28.24		
B4138-084	A	0	1080	2.0	12.0	Y	N	0	0.45	0.2	2E, 2W @ 0.9 m
	B	1080	1980					12	4.78		
	C	1980	2880					24	10.20		
	D	2880	3780					36	15.76		
	E	3780	4680					48	19.77		
	F	4680	5580					60	26.09		
B4138-085	A	0	1080	3.0	12.0	Y	N	0	0.69	0.4	2E, 2W @ 0.9 m
	B	1080	1980					12	3.81		
	C	1980	2880					24	9.59		
	D	2880	3780					36	14.87		
	E	3780	4680					48	19.87		
	F	4680	5580					60	23.69		

Notes:

1. B4138-016: 3240 s: SW atrium fan on @ 3240 s
2. B4138-017: 1500 s: SW atrium fan on @ 1500 s.
3. B4138-018: 3420 s: SW atrium fan on @ 3420 s.
4. B4138-022: Partial burner blowout during 5.0 MW fire.
5. B4138-024: SW and SE atrium fans on @ 3237 s.

Appendix B Full-Scale Experimental Fire Compartment CFD Simulations

Simulation	Comp. open. width (W)	Burner elevation (m)	Burner surfaces	Compartment surfaces	Grid design	Control volume size Δx, Δy, Δz (m, m, m)
B4138-C01	13.844	0.000	Burner	Inert	Single	0.180,0.173,0.185
B4138-C02	13.844	0.000	Burner	Inert	Single	0.0997,0.0961,0.0997
B4138-C03	13.844	0.000	Burner	Inert	Single transformed	Burner: 0.100,0.100,0.0997 Comp.: 0.169,0.197,0.0997
B4138-C04	Invalid simulation					
B4138-C05	12.000	0.457	Burner, inert, inert	Inert	Single transformed	Burner: 0.100,0.100,0.0997 Comp.: 0.169,0.197,0.0997
B4138-C06	12.000	0.457	Burner, inert, inert	Inert	Single transformed	Burner: 0.0500,0.0500,0.0498 Comp.: 0.0846,0.0987,0.0498
B4138-C07	12.000	0.457	Burner, inert, inert	Inert	Single	0.538,0.461,0.498
B4138-C08	12.000	0.457	Burner, inert, inert	Inert	Single	0.269,0.256,0.249
B4138-C09	12.000	0.457	Burner, inert, inert	Inert	Single	0.0997,0.0961,0.0997
B4138-C10	12.000	0.457*	Burner, inert, inert	Inert	Single	0.269, 0.256,0.249
B4138-C11	12.000	0.457	Burner, concrete, concrete	Concrete	Single	0.269, 0.256,0.249
B4138-C12	12.000	0.457*	Burner, concrete, concrete	Concrete	Single	0.269, 0.256,0.249

Simulation	Comp. open. width (W)	Burner elevation (m)	Burner surfaces	Compartment surfaces	Grid design	Control volume size Δx, Δy, Δz (m, m, m)
B4138-C13	12.000	0.457	Burner, inert, inert	Inert	Single	0.0748,0.0721,0.0779
B4138-C14	12.000	0.457	Burner, inert, inert	Inert	Double embedded	Grid 1: 0.240, 0.240,0.249 Grid 2: 0.538,0.461,0.498
B4138-C15	12.000	0.457	Burner, inert, inert	Inert	Double embedded	Grid 1: 0.100,0.100,0.0997 Grid 2: 0.269,0.256,0.249
B4138-C16	12.000	0.457	Burner, inert, inert	Inert	Triple overlapped	Grid 1: 0.0748,0.0781,0.0779 Grid 2: 0.269,0.250,0.249 Grid 3: 0.269,0.250,0.249
B4138-C17	12.000	0.457	Burner, inert, inert	Inert	Triple overlapped	Grid 1: 0.0748,0.0781,0.0779 Grid 2: 0.0997,0.100,0.0997 Grid 3: 0.0997,0.100,0.0997

Notes:

1. All simulations were conducted with a fire size of Q = 2.0 MW and burner dimensions of 2.0 by 2.0 m.
2. Asterisks (*) indicates simulations where the burner was modeled as a rectangular volume extending from z = 0.000 to 0.457 m.

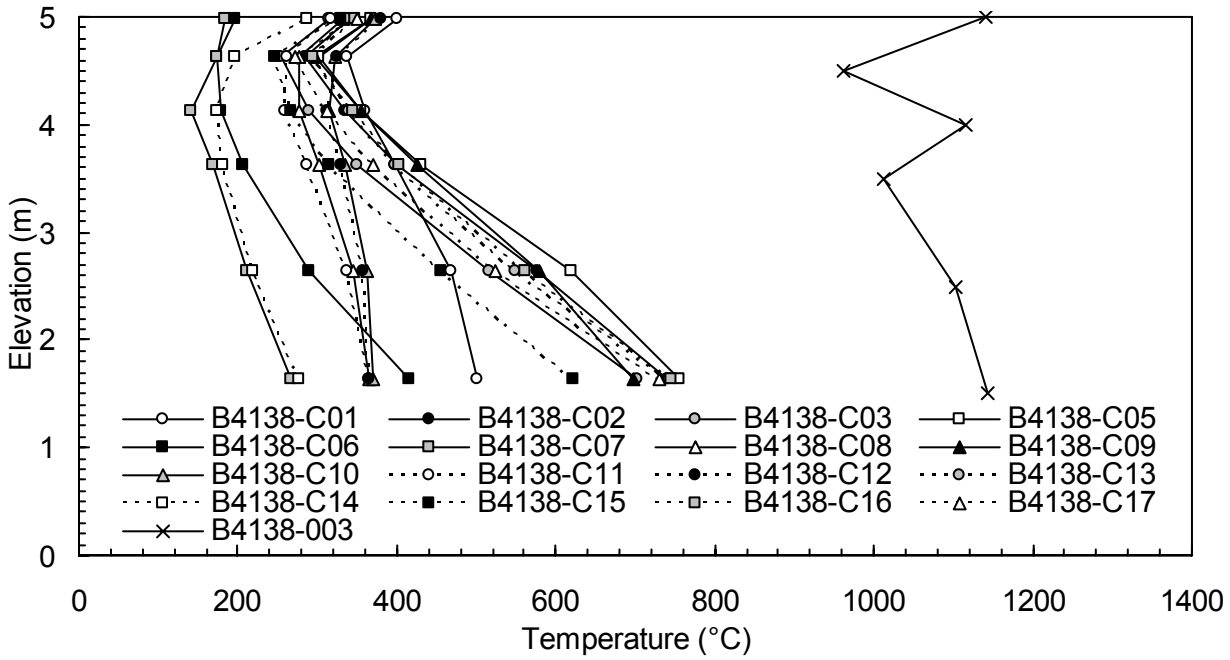

Figure 55. Fire compartment CL temperature profiles from CFD simulations and experiment B4138-003.

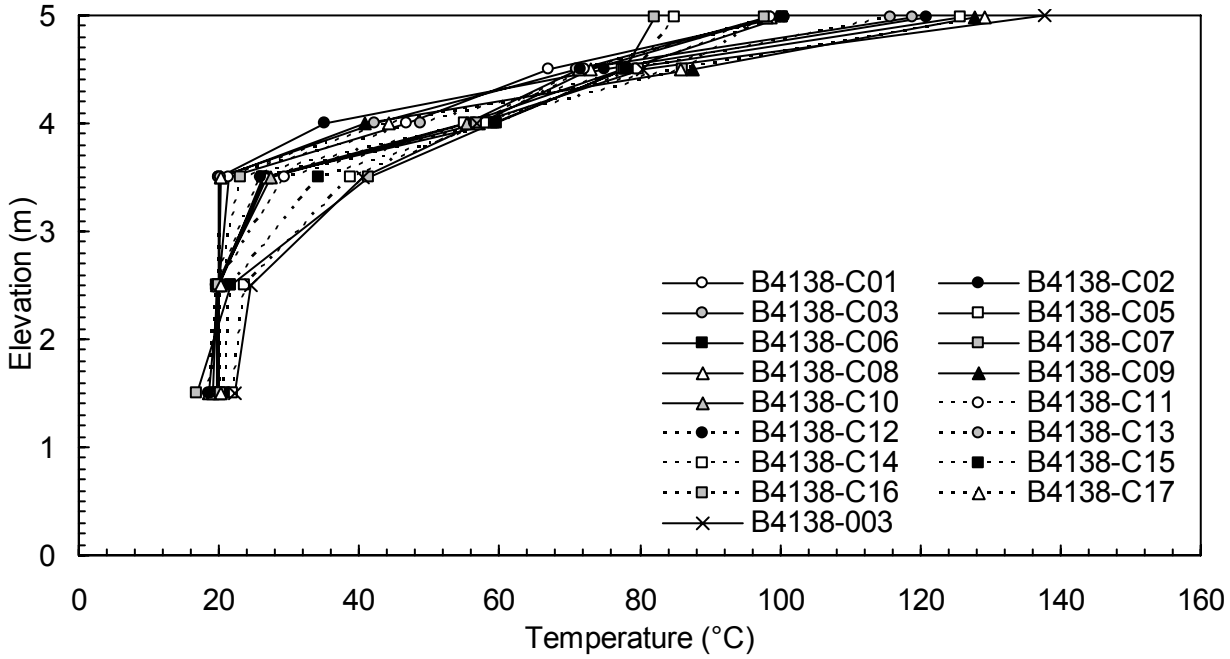

Figure 56. Fire compartment N temperature profiles from CFD simulations and experiment B4138-003.

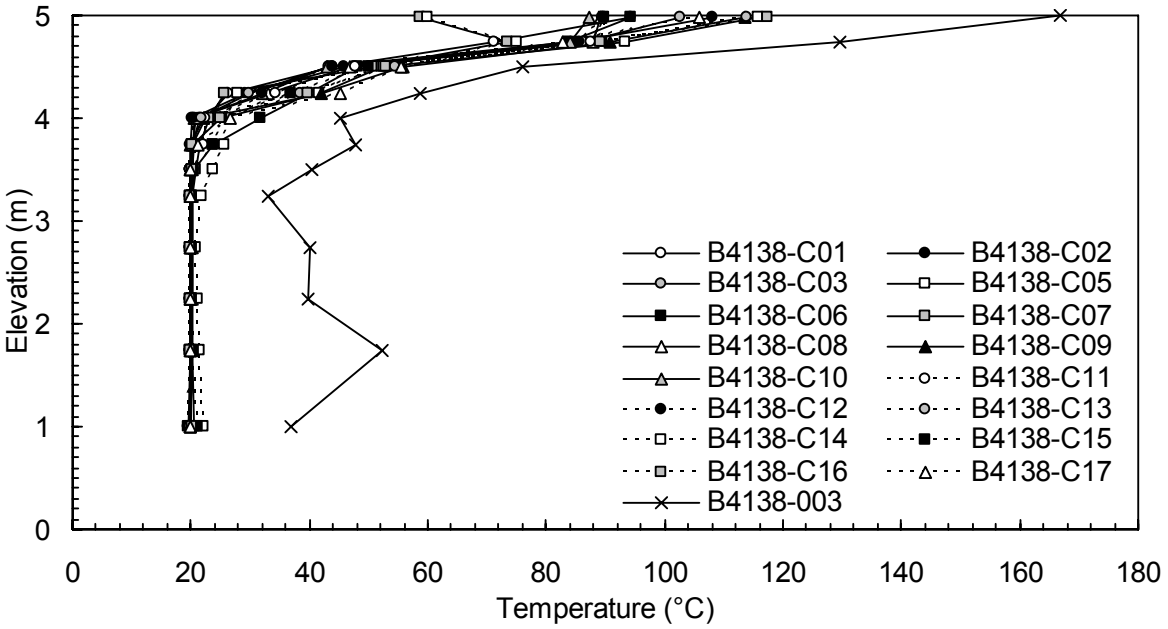

Figure 57. Compartment opening CL temperature profiles from CFD simulations and experiment B4138-003.

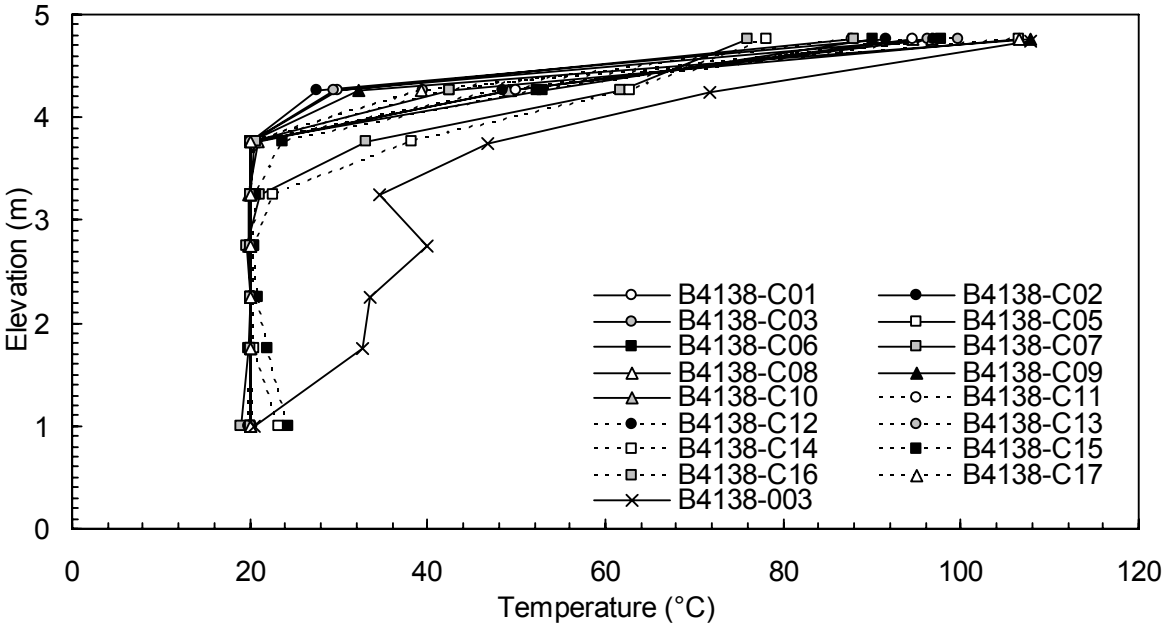

Figure 58. Compartment opening N temperature profiles from CFD simulations and experiment B4138-003.

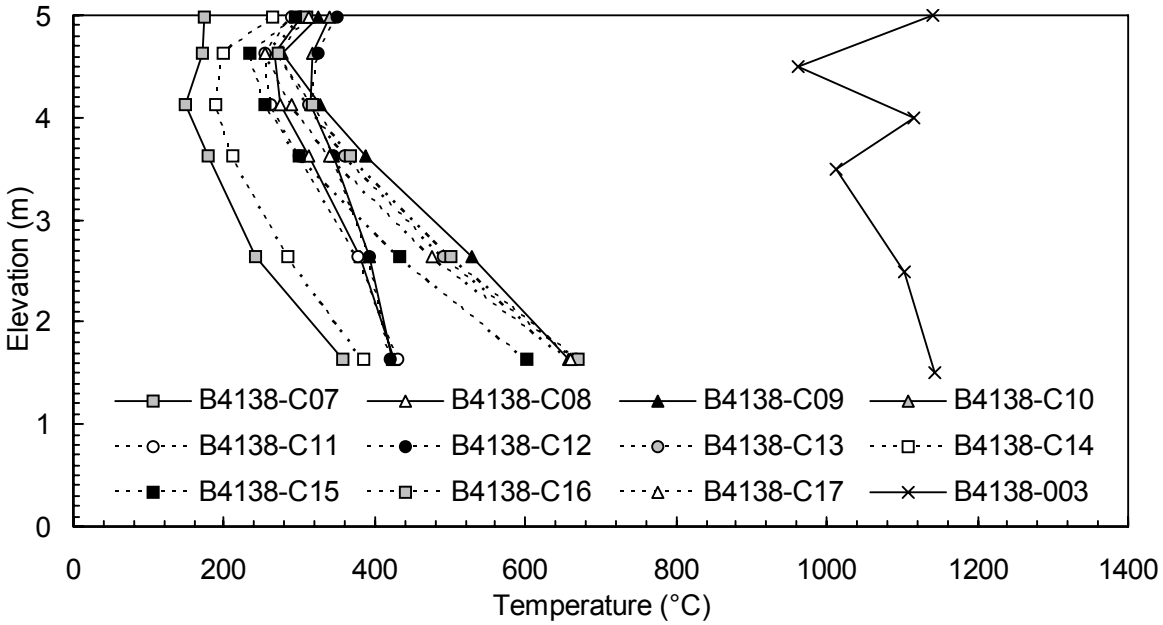

Figure 59. Fire compartment CL temperature profiles from CFD simulations with radiation correction.

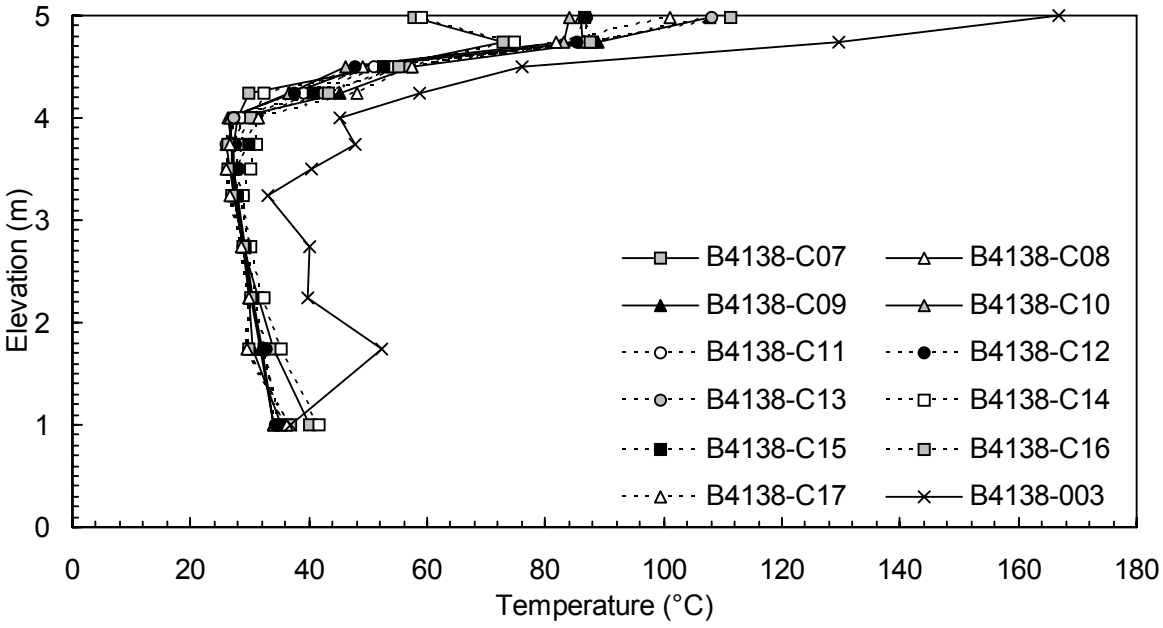

Figure 60. Compartment opening CL temperature profiles from CFD simulations with radiation correction.

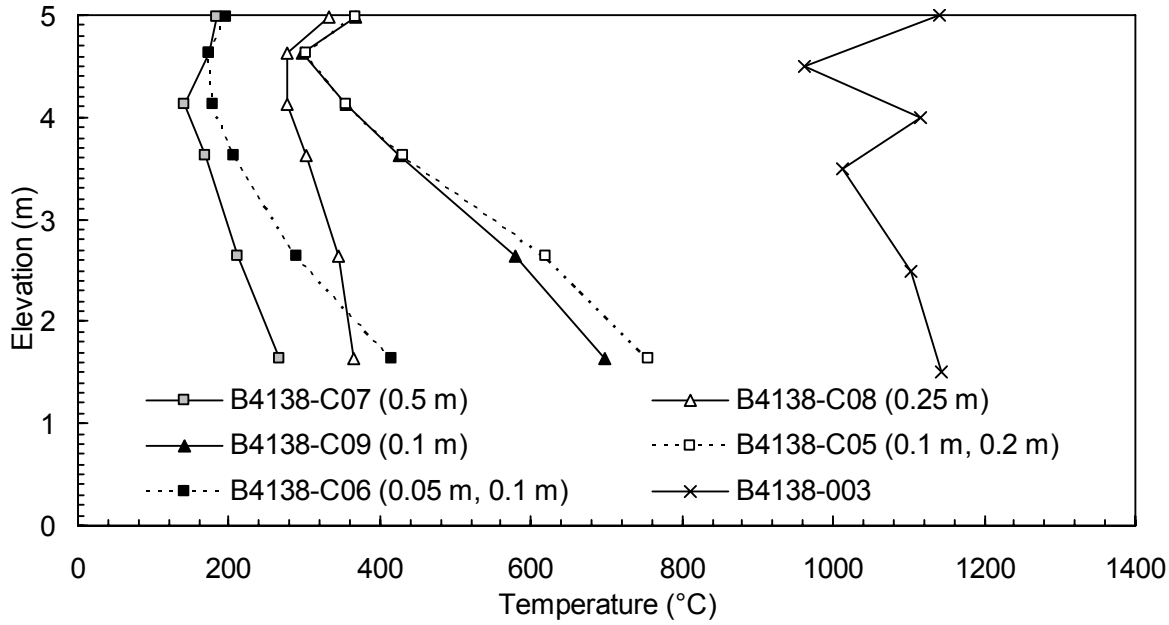

Figure 61. Fire compartment CL temperature profiles from CFD simulations with single and single transformed grid designs.

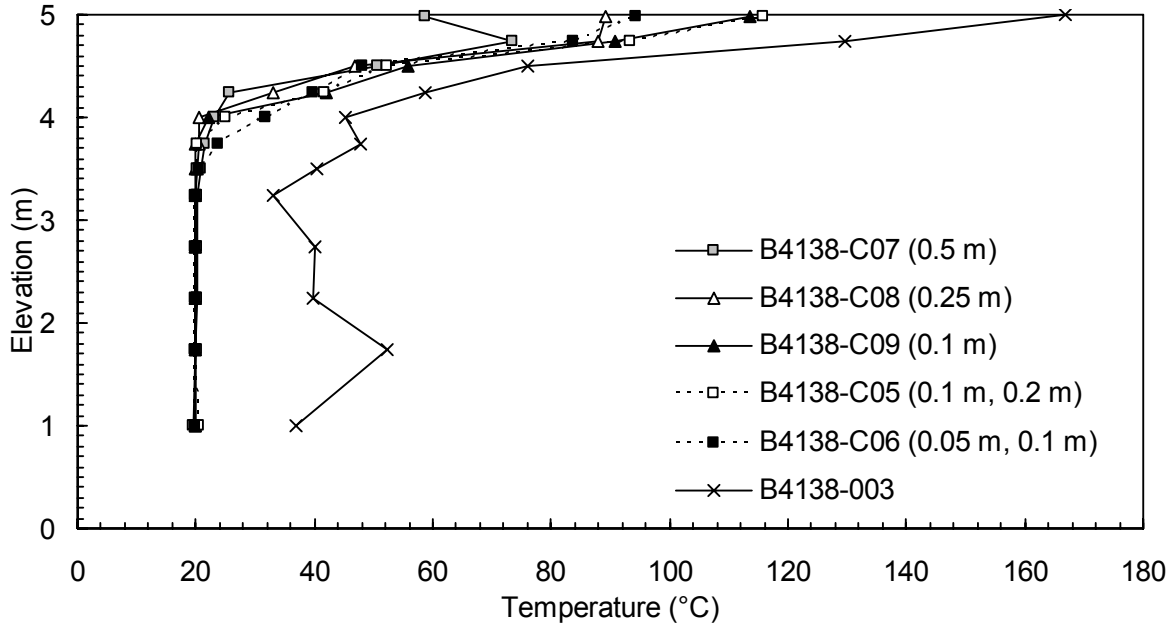

Figure 62. Compartment opening CL temperature profiles from CFD simulations with single and single transformed grid designs.

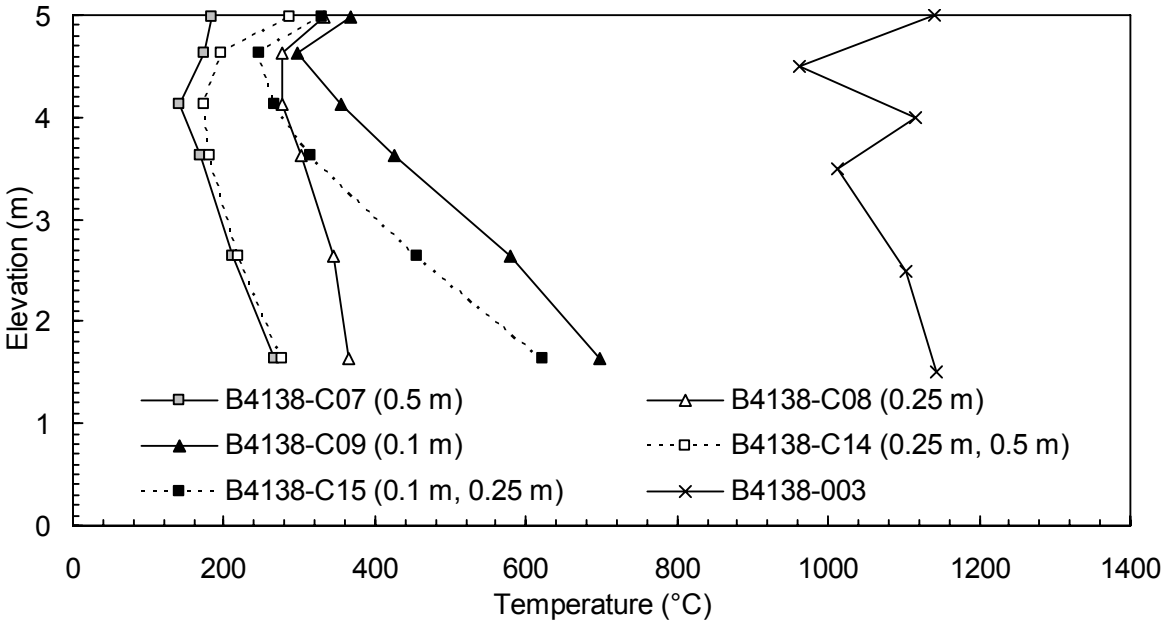

Figure 63. Fire compartment CL temperature profiles from CFD simulations with single and double embedded grid designs.

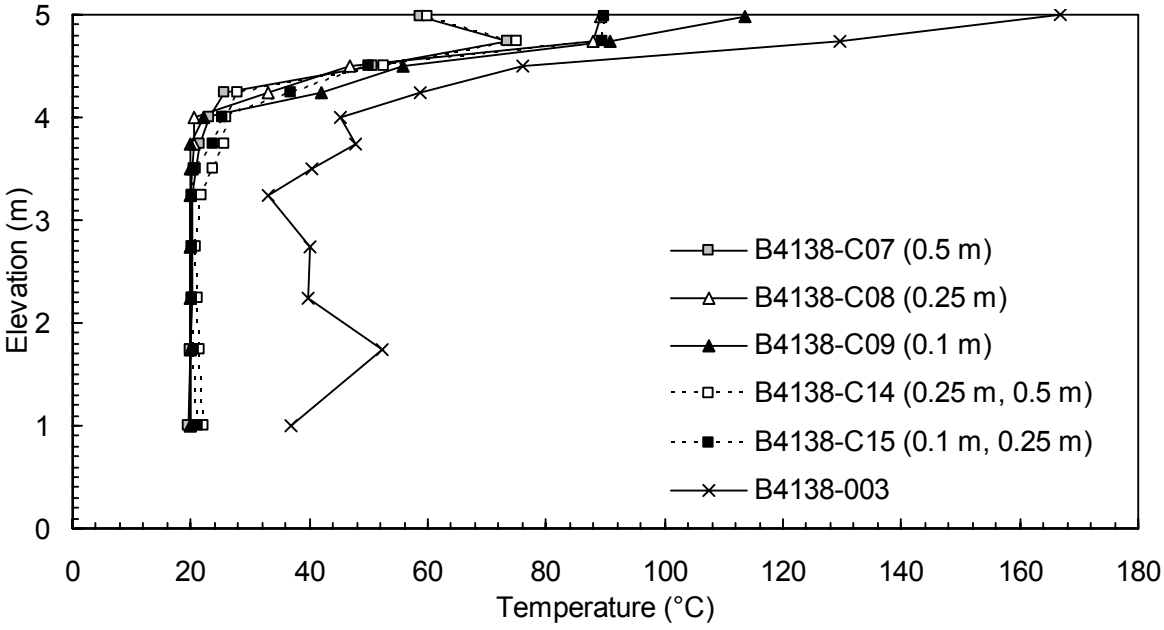

Figure 64. Compartment opening CL temperature profiles from CFD simulations with single and double embedded grid designs.

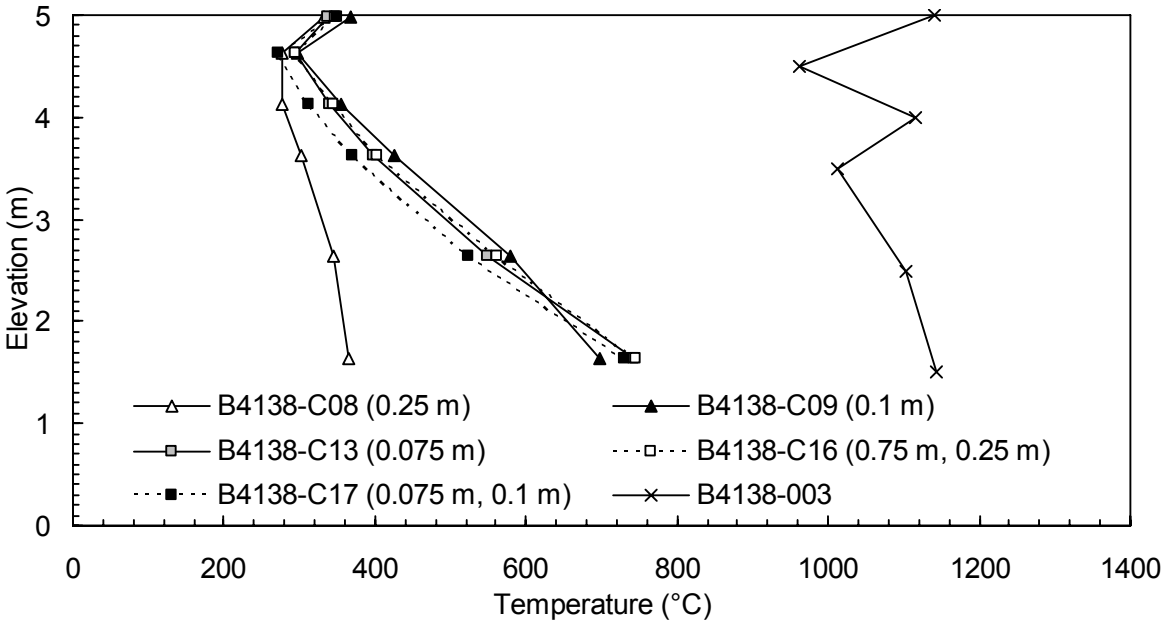

Figure 65. Fire compartment CL temperature profiles from CFD simulations with single and triple overlapping grid designs.

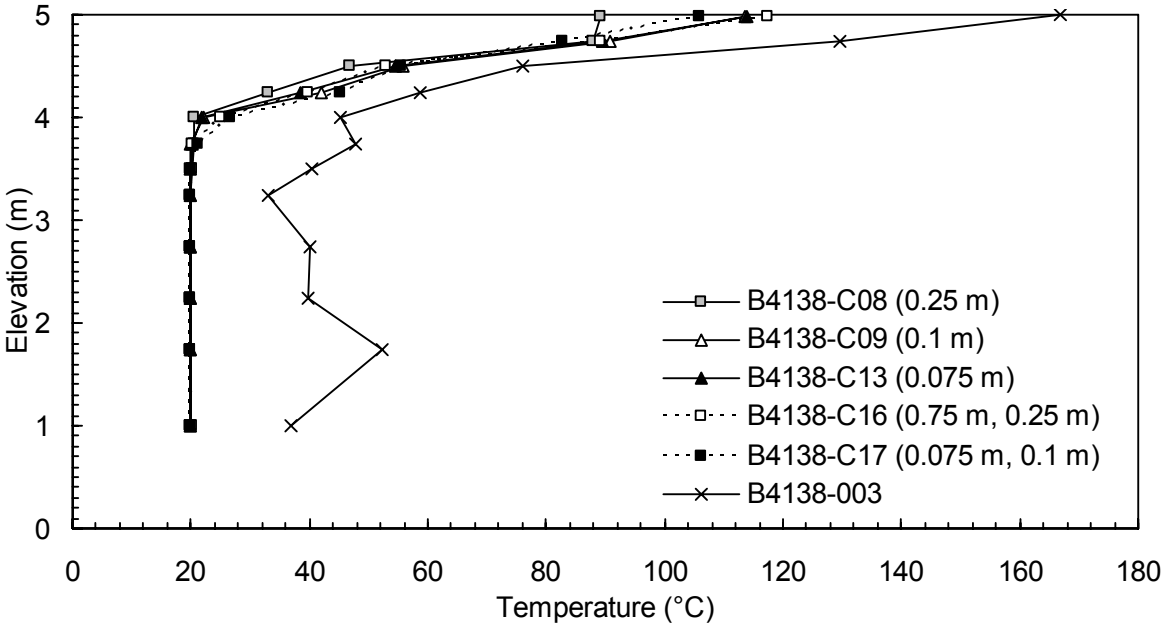

Figure 66. Compartment opening CL temperature profiles from CFD simulations with single and triple overlapping grid designs.

Appendix C CFD Simulations of BSP Behaviour at High Elevations

Simulation	Fire size, Q (MW)	Opening width, W (m)	Draft curtain depth, h_{draft} (m)	Compartment opening fascia depth, h_{fasc} (m)	Flow domain dimensions (m, m, m)	Control volume size, Δ (m)	Symmetry boundary condition
B4138-0066	2.0	10.0	0.0	0.0	50.0, 30.0, 50.0	0.5	No
B4138-0067	2.0	10.0	2.5	0.0	50.0, 30.0, 50.0	0.5	No
B4138-0068	2.0	10.0	2.5	1.0	50.0, 30.0, 50.0	0.5	No
B4138-0069	2.0	10.0	0.0	0.0	50.0, 15.0, 50.0	0.5	Yes
B4138-0070	2.0	10.0	2.0	0.0	50.0, 30.0, 50.0	1.0	No
B4138-0071	2.0	10.0	2.0	0.0	50.0, 30.0, 50.0	0.5	No
B4138-0072	2.0	10.0	2.0	0.0	50.0, 30.0, 50.0	0.25	No
B4138-0073	2.0	10.0	2.0	0.0	50.0, 30.0, 25.0	1.0	No
B4138-0074	2.0	10.0	2.0	0.0	50.0, 30.0, 25.0	0.5	No
B4138-0075	2.0	10.0	2.0	0.0	50.0, 30.0, 100.0	0.5	No
B4138-0076	2.0	10.0	2.0	0.0	50.0, 50.0, 50.0	0.5	No
B4138-0077	1.0	10.0	2.0	0.0	50.0, 50.0, 50.0	0.5	No
B4138-0078	5.0	10.0	2.0	0.0	50.0, 50.0, 50.0	0.5	No
B4138-0079	2.0	5.0	2.0	0.0	50.0, 50.0, 50.0	0.5	No
B4138-0080	1.0	5.0	2.0	0.0	50.0, 50.0, 50.0	0.5	No
B4138-0081	5.0	5.0	2.0	0.0	50.0, 50.0, 50.0	0.5	No
B4138-0082	2.0	8.0	2.0	0.0	50.0, 50.0, 50.0	0.5	No
B4138-0083	1.0	8.0	2.0	0.0	50.0, 50.0, 50.0	0.5	No
B4138-0084	5.0	8.0	2.0	0.0	50.0, 50.0, 50.0	0.5	No
B4138-0086	5.0	8.0	0.0	0.0	50.0, 50.0, 50.0	0.5	No
B4138-0087	5.0	5.0	0.0	0.0	50.0, 50.0, 50.0	0.5	No
B4138-0089	5.0	10.0	0.0	0.0	50.0, 50.0, 50.0	0.5	No
B4138-0090	5.0	5.0	0.0	1.5	50.0, 50.0, 50.0	0.5	No
B4138-0091	5.0	5.0	2.0	1.5	50.0, 50.0, 50.0	0.5	No